Dissertation

Fatty acid species-dependent hepatic cellular lipotoxicity

Submitted by
Juergen Gindlhuber
BSc, MSc

for the Academic Degree of
Doctor of Philosophy
(PhD)

at the
Medical University of Graz

Division of Pathology,
Diagnostic and Research Institute of Pathology

under the supervision of
Prof. Ruth Birner-Gruenberger

2022

Statutory Declaration

I hereby declare that this thesis is my own original work and that I fully acknowledged by name all of those individuals and organisations that have contributed to the research for this thesis. Due acknowledgement has been made in the text to all other material used. Throughout this thesis and in all related publications I followed the guidelines of “Good Scientific Practice and Ombuds Committee at the Medical University of Graz”.

Graz, June 2022 Juergen Gindlhuber

Disclosures

Part of this thesis has been published in Gindlhuber J, et al. “Hepatocyte proteome alterations induced by individual and combinations of common free fatty acids.” Int J Mol Sci. 2022 Mar 20;23(6):3356. doi: 10.3390/ijms23063356. (1)

Co-authors who contributed to this thesis and the publication and agreed to the use of their data in the thesis:

Diagnostic and Research Institute of Pathology, Medical University of Graz, Graz, Austria
Maximilian Schinagl, Laura Liesinger, Barbara Darnhofer

Institute of Chemical Technologies and Analytics, Technische Universität Wien, Vienna, Austria
Tamara Tomin, Matthias Schittmayer, Ruth Birner-Gruenberger

Acknowledgements

PhD student, Juergen Gindlhuber, received funding support from the Medical University of Graz, TU Wien and the Austrian Science Fund FWF (grant numbers F73 (SFB “Lipid hydrolysis”), KLI645 and W1226 (Doctoral School “DK-Metabolic and Cardiovascular Disease”).

First and foremost, I sincerely express my gratitude to my supervisor Ruth Birner-Gruenberger. I am grateful for all the advice and guidance I received in every aspect. She has been supporting of my work from the first day five years ago when I came for my master’s degree, until now. Throughout that time, she gave me the opportunity to make my own mistakes and learn from them, allowing me to grow into an independent scientist and communicative team member.

I am very grateful for my mentor Matthias Schittmayer, who not only provided extensive theoretical and practical knowledge about everything mass spec related but was an invaluable conversation partner and friend.

I am also thankful to the members of my thesis committee, Guenter Haemmerle and Roland Malli, for their continuous help and input during the course of my studies.

I am grateful to every member of the Proteomics Pirates for creating an exceptional work environment all these years.

Finally, I need to acknowledge my partner, who is always trying to push me out of my comfort zone, our child, who patiently listened to all presentations and my family, which gave me the opportunity to focus on my research.

Table of contents

List of abbreviations	1
Zusammenfassung	3
Abstract	5
1. Introduction	6
1.1. Lipids, the lubricant of evolution	6
1.2. Lipids	8
1.2.1. Fatty acids	8
1.2.2. Glycerolipids	9
1.2.3. Glycerophospholipids	10
1.2.4. Sphingolipids	12
1.2.5. Sterols	13
1.2.6. Prenols	14
1.2.7. Saccharolipids	15
1.2.8. Polyketides	15
1.3. The liver	16
1.4. Lipids as nutrition	18
1.5. Lipotoxicity	21
1.5.1 Tissue specific differences	22
1.5.1.1. Brain	22
1.5.1.2. Heart	22
1.5.1.3. Endothelium	23
1.5.1.4. Pancreas & lipid induced insulin resistance	23
1.5.1.5. Skeletal muscle	24
1.6. Hepatic lipotoxicity & NAFLD	25
1.7. Study questions	28
2. Material and methods	30
2.1. Experimental design and statistical rational	30
2.2. Reagents	30

2.3. Cell culture 30
2.4. BSA fatty acid conjugates and treatment regime 30
2.5. Growth analysis 31
2.6. LD imaging and volume analysis 31
2.7. Cell cycle and apoptosis analysis 32
2.8. Proteomics sample preparation 32
2.9. Peptide prefractionation 33
2.10. LC MS/MS proteomics measurement 34
2.11. Proteomics data analyses 34
2.12. Lipidomics sample preparation 35
2.13. LC-MS/MS lipidomics measurement 35
2.14. Lipidomics data analysis 36
2.15. FAME sample preparation and measurement 36
2.16. FAME data analysis 40
3. Results 41
3.1. Impact of fatty acids on cell growth 41
3.2. Impact of fatty acids on LD formation 41
3.3. Fatty acid specific proteome changes 42
3.4. Fatty acid specific effects on cell cycle and viability 46
3.5. Correlation of potential cellular lipotoxicity protein biomarkers to hepatic cellular carcinoma gene expression and survival 47
3.6. Fatty acid specific changes to the lipidome 49
3.7. Fatty acid uptake 52
4. Discussion 56
4.1. Conclusion 65
4.2. Study limitations 66
5. References 67
6. Appendix 81

Abbreviations*

AA	amino acid
APO	apolipoprotein
ATP	adenosine triphosphate
BCA	bicinchoninic acid assay
BSA	bovine serum albumin
CER	ceramide
CerS	ceramide synthase
CGI-58	comparative gene identification 58
CoA	coenzyme A
DG	diglycerides
DGAT	diacylglycerol acyltransferase
EA	elaidic acid
ER	endoplasmic reticulum
FA	fatty acid
FFA	free fatty acid
GSL	glycosphingolipid
HCC	hepatocellular carcininoma
HDL	high-density lipoprotein
HPLC	high performance liquid chromatography
IDL	intermediate-density lipoprotein
LD	lipid droplet
LDA	Lipid Data Analyzer
LDL	low-density lipoprotein
LFQ	label free quantitation
LPL	lipoprotein lipase
LPS	lipopolysaccharide
LUCA	last universal cellular ancestor
MA	myristic acid
MG	monoacylglycerol
MGAT	monoacylglycerol acyltransferase
MGL	monoacylglycerol lipase
MRM	multi reaction monitoring
MS	mass spectrometry
MUFA	mono unsaturated fatty acid
NAFLD	non-alcoholic fatty liver disease
NASH	non-alcoholic steatohepatitis
OA	oleic acid
PA	palmitic acid
PBS	phosphate-buffered saline

PC	phosphatidylcholine
PE	phospahteidylethanolamine
PI	phosphatidylinositol
PL	phospholipid
PS	Phosphatidylethanolamine
PT	prevention treatment
PUFA	poly unsaturated fatty acid
SA	stearic acid
SL	sphingolipid
SM	sphingomyelins
TG	triglyceride
VLDL	very-low density lipoprotein

*Abbreviations are arranged in alphabetical order

Zusammenfassung

Die nicht-alkoholische Fettleber beschreibt ein Krankheitsbild, das in etwa eine von vier Personen während ihres Erwachsenenlebens betrifft. Die Bestimmung exakter Zahlen fällt schwer, da die Diagnose eines erhöhten Fettgehaltes anfänglich nur mithilfe einer magnetresonanztomographischen Untersuchung möglich ist, und weder erhöhte Entzündungswerte noch andere diagnostische Marker über diesen transienten Zustand Auskunft geben. Auch wenn all dies nun nach einem nur geringfügig veränderten Stoffwechsel der Leber klingen mag, würde man mit einer solchen Einschätzung sehr falsch liegen, da davon auszugehen ist, dass die Mehrheit der unidentifizierten Leberzirrhosen darauf zurückzuführen ist. Auch wenn die Leber auf periodische Fettaufnahme spezialisiert ist, entweder nach der Nahrungsaufnahme oder durch die Freisetzung während Fastens aus dem Fettgewebe, kann es zu pathologischen Veränderungen in deren Stoffwechsel und Erscheinungsbild kommen. Diese Veränderungen gehen meist mit einer beginnenden Gewebsentzündung, Aktivierung von Lebersternzellen und der Einwanderung von Fibroblasten einher. Im weiteren Verlauf führen diese Prozesse zur vermehrten Vernarbung des Lebergewebes, welches letztendlich die Organfunktion einschränkt und als Leberzirrhose bezeichnet wird. Ist dieser Punkt erst einmal erreicht, kann dem Patienten nur mehr mit einem Organtransplantat geholfen werden, wobei im Falle einer rechtzeitigen Diagnose der Grunderkrankung eine Veränderung des Lebensstiles wahrscheinlich ausgereicht hätte, um eine Verschlechterung zu verhindern.

Eben deswegen stellen sich diese ersten Veränderungen im Stoffwechsel der Leberzelle als Schlüssel für unser Verständnis der pathologischen Mechanismen heraus, welche dazu führen, dass eine scheinbar gesunde Leber irreversiblen Schaden nimmt.

Der Fokus dieser Studie lag darin, Veränderungen in Leberzellen nachzuweisen, welche aufgrund einer veränderten Fettkomposition im Plasma zustande kommen. Zu diesem Zweck wurden hochauflösende Massenspektrometer verwendet, mit welchen Proteom und Lipidom der Zellen genauestens untersucht wurden. Mikroskopie und Durchflusszytometrie wurden herangezogen, um dynamische Veränderungen, des Stoffwechsels oder Erscheinungsbildes der Zellen zu dokumentieren.

Obwohl eine erhöhte Fettaufnahme weitgehende Änderungen im Proteinmuster zur Folge hat, gelang es uns im Rahmen der Studie, jene Proteine zu identifizieren welche nur in lipotoxischen

Konzentrationen verändert waren. Des Weiteren gelang es uns die Akkumulation von Diglyceriden und Ceramiden nachzuweisen, welche in der Literatur als toxisch für andere Gewebsarten beschrieben sind. Schlussendlich konnte auch zum ersten Mal nachgewiesen werden, dass verschiedene langkettige gesättigte Fettsäuren, trotz struktureller Gemeinsamkeiten, deutliche Unterschiede auf das Überleben der Zelle haben.

Abstract

Non-alcoholic fatty liver disease (NAFLD) is a ubiquitous condition affecting, on average, one out of four people throughout their adult life. Accurate numbers are hard to determine as only specialized diagnostic methods, like magnet resonance imaging, can detect elevated lipid content in the liver. Early stages of NAFLD most often not being accompanied by inflammation or other easily measured biomarkers and the disease occurs transiently. All of these facts belittle the reality that the majority of cryptic cirrhosis cases might originate from this seemingly mild alteration of the liver's metabolic state, becoming chronic. At a certain point, following an initial accumulation of lipids in the liver originating from either overabundant food intake or release from the adipose tissue, alteration in the hepatocytes' morphology and physiology can be encountered. These alterations go hand in hand with mild lobular inflammation in the beginning and fibroblast recruitment, progressing over time into severe scarification due to increased fibrin deposition in the tissue and ending with the loss of liver function, at this point termed cirrhosis. At this final stage, the only possible treatment is a liver transplant, whilst a change in lifestyle could have likely prevented any further progression at an earlier stage.

Thus, key to improving our understanding of hepatic lipotoxicity is resolving these first steps of hepatocyte alteration which occurs when the liver is seemingly still healthy, before inflammation and irreversible fibrosis takes place.

This study focused on investigating alterations introduced to hepatocytes with artificial shifts in abundance of individual and mixed fatty acids in the medium. We employed high resolution mass spectrometry approaches to investigate proteome and lipidome of cultured hepatocytes as well as microscopy and flow cytometry techniques to examine their phenotypical and physiological changes.

Results from this study suggest that despite the fatty acid treatment causing major changes to the proteome, only a few of them are unique for lipotoxic fatty acids concentrations. In addition, we were able to identify ectopic accumulation diglycerides and ceramides previously described to cause lipotoxic effects in other tissues. Finally, we were able to show for the first time that different long chained fatty acids can influence the cellular fate in divergent ways within the same cell system.

1. Introduction

1.1. Lipids, the lubricant of evolution

When we think about the beginning of life itself on earth, we tend to immediately focus on DNA or amino acids (AA) and peptides, in other words either the blueprint or machinery of live. In the Miller-Urey experiment of 1952 for the first-time people tried to recreate atmospheric conditions present at ancient earth adding energy in the form of electric sparks simulating lighting (2). They succeeded in creating 5 AAs of which 4 were proteinogenic, organic compounds like urea and several mono and dicarboxylic acids (3). After Miller´s death in the year 2007 several sealed flasks originating from his volcanic spark experiments, a slight modification of the original array with a steam jet added to simulate volcanic activity, were analysed with modern high-performance liquid chromatography (HPLC) mass spectrometry (MS) and it was unveiled that actually 22 amino acids were present of which 7 were proteinogenic (4). Follow up experiments showed also that purines and pyrimidines, the fundamental building blocks for the formation of DNA or RNA, can form under similar conditions (5). These results further gain significance through an analysis of AA usage in ancient organisms and or ancient genes that, conserved to this day, predominantly code for AAs found to be generated under the conditions simulated by Miller and Urey. Based on these results, the theory known as last universal cellular ancestor (LUCA) was formed and is essential to the concept of evolution (6). What is a key assumption for the theory, is that all these biomolecules would have no or almost no impact swimming in the ancient oceans, just randomly getting into contact with each other once in a while. They needed an enclosed space, a container, to form what later on will be referred to as a cell (7). This was made possible by the phospholipid membrane, since it offers an enclosed environment in which these biomolecules can be enriched so that interactions were much more likely, reaction conditions could be controlled and most importantly, organisation could be established. This generation of order in a system, a drive against entropy, is fundamental to all life as we know it and would not be possible without lipids.

In addition, lipids were key in allowing life to become more complex as organisms slowly evolved from the state of a prokaryotic to eukaryotic cell. Prokaryotes lack, as the name indicates, a nucleus, and most other forms of organelles such as mitochondria or the endoplasmic reticulum (ER), essentially, everything is found floating in the cytoplasm of the cell only enclosed by the cellular membrane. The exception to this is the presence of thylakoid membranes for photosynthesis in cyanobacteria and it was exactly this feature that led to the formation of the endosymbiont theory. This theory in short postulates that the complexity of eukaryotic cells was attained via prokaryotic cells, verbatim, enveloping each other (8). Thus, explaining why mitochondria and chloroplasts possess a double membrane, the original cell membrane and the one they were enclosed in from the host, and why they, to this day, have their own residual genome and 70s ribosomes instead the 80s ribosomes of eukaryotes. This evolutional step forward, from archaea and bacteria to eukaryotes, was accompanied by the increasing complexity of the cells lipid system and entailed compartmentalisation of the cell to providing task specific local environments for essential processes such as protein folding, oxidative phosphorylation or gene transcription (Fig. 1). All of this resulted in improved performance of eukaryotic organisms outcompeting prokaryotes. Which in turn, a few million years later, led to the formation of primitive sessile cell accumulations specialising in individual tasks, alike to modern sponges, before developing real tissues and gaining mobility, like recent cnidaria or placozoa. The process of evolution might be driven by complexification of the genetic code allowing adaptions of the metabolism to settle in new ecological niches but would never have happened without lipids providing the scaffold for life as we know it (9).

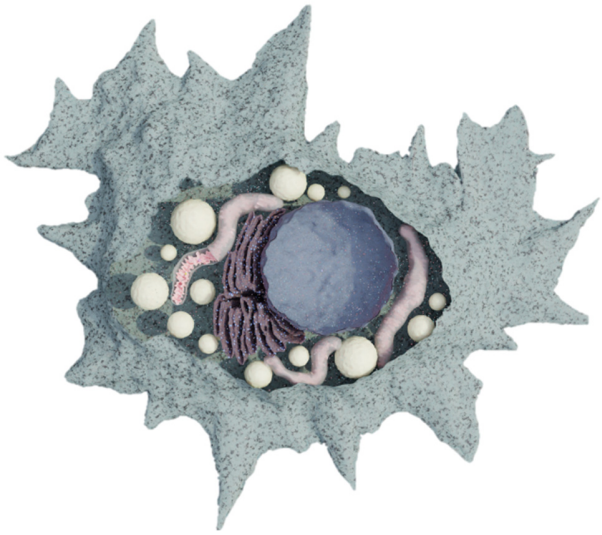

Figure 1 Shown above is an artistic representation of a eukaryotic cell, highlighting its different organelles, each one providing a unique microenvironment. Every organelle is defined via a specific lipid membrane and enclosed in the phospholipid bilayer around the cell.

1.2. Lipids

Lipids, from the Greek word λίπος, meaning fat, are a group of small biomolecules defined by their full or partial insolubility in water. This hydrophobicity is the result of long hydrocarbon chains most lipids possess. Nowadays lipids are subdivided into eight classes following the International Lipid Classification and Nomenclature Committee guidelines (10).

1.2.1. Fatty acids

Fatty acids (FA) are molecules consisting of a hydrocarbon chain of varying length and a carboxylic acid headgroup (Fig. 2). These molecules can be generated by organisms via fatty acid synthesis, a process in which an acetyl coenzyme A (CoA) primer is elongated with malonyl-CoA building blocks. Their structure infers an amphiphilic character to the molecule, due to a hydrophilic carboxylic acid and a hydrophobic hydrocarbon chain. FAs can be further subcategorized into saturated and unsaturated FAs. One FA is considered saturated when no double bonds are present in the hydrocarbon chain. Double bonds found in the hydrocarbon chains have predominantly cis configuration, introducing a bend into the chain, and can vary in number, generally subdividing the group further into mono unsaturated fatty acids (MUFA) and poly unsaturated fatty acids (PUFA).

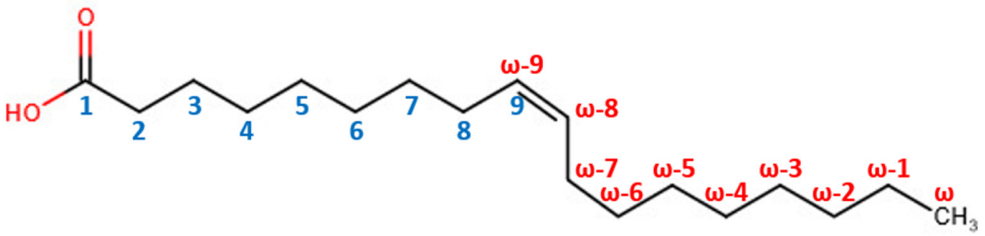

Figure 2 The structural formula of the C18:1 cis-9 FA, commonly refered to as oleic acid. In blue is indicated the number of the C atoms, in red with the greek symbol ω in front an alternative counting method most often used to indicate the position of of the double bonds. The figure was generated with the online drawing tool for chemical formulas provided by Chem-Space.com.

There are multiple methods in use to indicate the position of the double bond. The displayed molecule in Fig.2 has the trivial name of oleic acid (OA) and the IUPAC name of (9Z)-Octadec-9-enoic acid. Common abbreviations found are 18:1 FA, 18 indicating the carbon chain length and 1 the number of double bonds. As this short annotation is still lacking the position and orientation of

the double bond the suffix cis-9 or cis-Δ^9 is added with the number or Δ^n indicating the C atom at which the double bond is positioned. Alternatively, the small Greek letter ω can be used to indicate the C atom position of the double bond but starting counting from the terminal end of the molecule which makes oleic acid an ω-9 18:1 FA. FAs produced in eukaryotes in general have an even number chain length, nevertheless odd chain lengths can be observed in adipocytes and in ruminants as a byproduct of their fermentative digestive system, which can also influence in vitro experiments (11). Several functional groups may be found attached to the hydrocarbon chain as well as fatty esters and fatty amides also notably belonging to the group of FAs. A subgroup of FAs of biological importance because of their signaling function are the eicosanoids, originating from the degradational pathway of PUFAs, most notably of arachidonic acid (AA). Eicosanoids are important mediators of the inflammation, influence asthma and allergies, can activate nuclear transcription factors or induce the sensation of pain to an individual.

1.2.2. Glycerolipids

Glycerolipids are formally formed by the esterification of the hydroxyl group of glycerol with a FA and followingly classified as mono-, di- and triglycerides (MG, DG, TG) (Fig. 3).

TGs (Fig.3) are the primary form of storage lipid in the human body, stored in intracellular lipid droplets (LD) of varying sizes depending on the tissue (12). Cells of white adipose tissue, which are specialized on storing fat, are dominated by one central LD which fills the whole cell. MGs and DGs are only found transiently in low amounts due to their strong emulsifying character. TG synthesis can occur in two tissue specific ways, starting with DGs generated in the Kennedy pathway, present in most cell types, or from recycling MGs into DGs via the enzyme monoacylglycerol acyltransferase (MGAT), found in enterocytes and adipocytes (13,14). The final step is catalyzed by diacylglycerol transferase (DGAT) 1/2 for either of those pathways. DGAT 1 and 2 are initially located on the ER membrane and are thought to release the newly formed TGs between the leaflets of the ER membrane. After the so-called lipid lens reaches a certain size, the protein seipin facilitates the budding of the LD from the outer ER membrane, explaining why this organelle only has a single phospholipid layer (15). Subsequently, DGAT2 can transfer onto the newly formed LD.

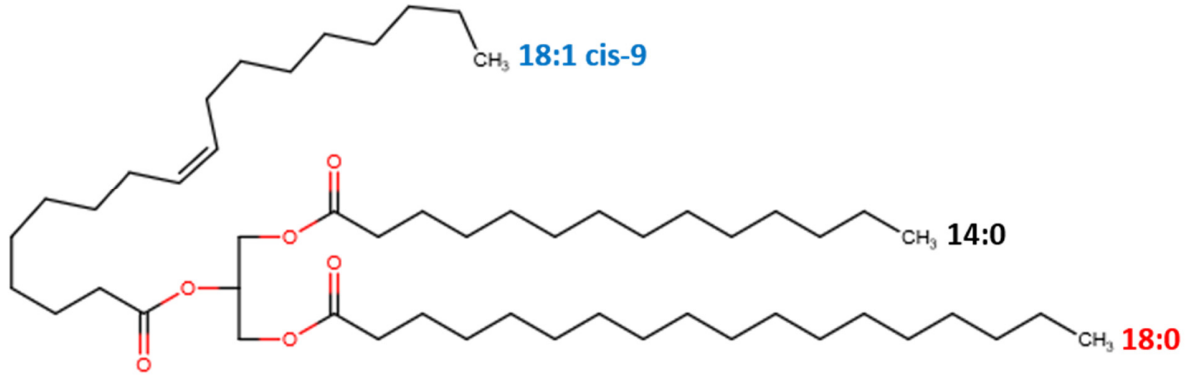

Figure 3 Structural formula of a triglyceride with the sum formula of C50:1. However this short annotation does not contain information about the three different substitutents found on sn 1/2 and 3 position of the glyreol backbone. From top to bottom the fatty acid esters present are myristic acid C14:0, oleic acid C18:1 cis-9 and Stearic acid C18:0. The figure was generated with the online drawing tool for chemical formulas provided by Chem-Space.com.

The reversal of this process is called lipolysis. During lipolysis acyl groups are consequently removed from the TG first via adipose triglyceride lipase (ATGL), forming a DG + FA, followed by hormone sensitive lipase (HSL), forming a MG + FA, and finally by monoacylglycerol lipase (MGL), forming glycerol + FA. This process is strictly regulated via phosphorylation of perilipins and comparative gene identification 58 (CGI-58) (16).

1.2.3. Glycerophospholipids

This lipid family, often referred to shortly as phospholipids, forms the main constituents of the lipid bilayer by nature of their amphiphilic character. They contain a glycerol esterified with two FAs and a phosphate group on the 3rd terminal hydroxyl, which can be further esterified by serine, ethanolamine, choline or inositol (Fig. 4).

Phosphatidylserine (PS) is generated in mammals via headgroup exchange reactions catalyzed by phosphatidylserine synthase from phosphatidylethanolamine (PE) or phosphatidylcholine (PC). In a healthy cell, PS is mainly localized on the cytosolic side of the phospholipid bilayer, and externalization is a sign of apoptosis, the programmed cell death (17). PE is important for the regulation of curvature and fluidity of cellular membranes, displaying higher melting points as PCs with the same acyl groups (18). PE plays an important role during membrane fusion of dividing cells, in lipoprotein secretion as well as the proper functioning of mitochondria. In humans, PE can

be synthesized via the cytidine diphosphate-ethanolamine pathway in the cytoplasm or via phosphatidylserine decarboxylase in the inner mitochondrial membrane. PCs, sometimes also referred to as lecithin, are predominantly found on the extracellular side of the cellular membrane, form the micelles for lipid digestion in the intestine and are used as surfactants in the lung. The main pathway of synthesis is the condensation of a DG with cytidine 5'-diphosphocholine via the enzyme diacylglycerol choline-phosphotransferase, although the liver also can generate it from methylation of PE with S-adenosyl methionine. Phosphatidylinositol (PI) is only found to a minor degree in membranes of mammals, nevertheless, it plays a significant role in lipid trafficking and signaling.

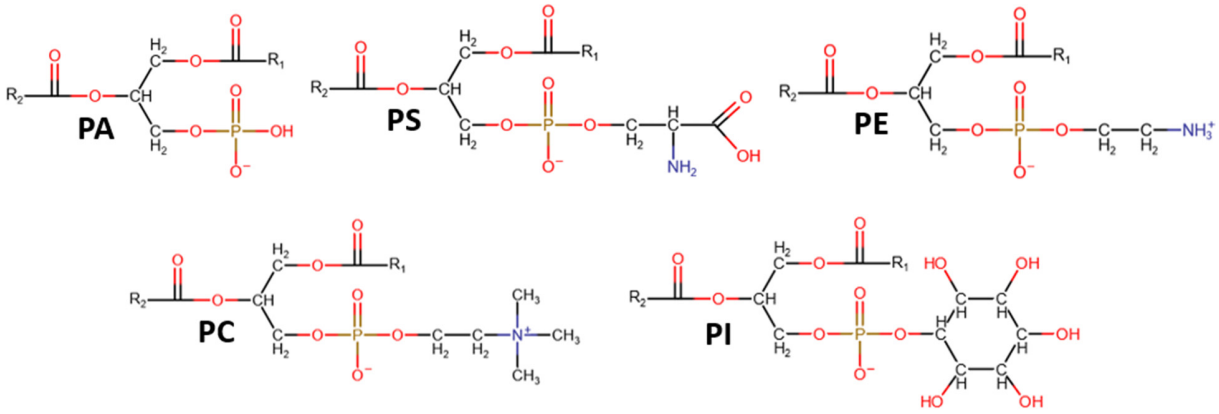

Figure 4 Headgroups of the phospholipid family. R1 and R2 are acyl chains of varying length and saturation state; however, some subgroups might prefer certain fatty acids on specific positions. PA) phosphatidic acid; PS) phosphatidylserine; PE) phosphatidylethanolamine; PC) phosphatidylcholine, PI) phosphatidylinositol. The figure was generated with the online drawing tool for chemical formulas provided by Chem-Space.com.

The biosynthesis of PI takes place in the ER, where it is formed from phosphatidic acid (PA) via the intermediate cytidine diphosphate diacylglycerol (19). Most of the PI found in the cell shows very little structural diversity, with R1 being stearic acid (SA) and R2 being arachidonic acid in the majority of cases, which is believed to be due to the substrate specificity of diacylglycerol kinase epsilon (20). This structural rigidity makes PI the dominant source of AA for the production of eicosanoids through phospholipase A_2 cleavage. Further, PIs can be mono-, bis- or tris-phosphorylated on the 3,4 and 5 position of the inositol ring via specific kinases, and the resulting phosphatidylinositol phosphates play a role in membrane trafficking, recognition and signaling (21–23).

1.2.4. Sphingolipids

Sphingolipids (SL) consist of various subgroups with sphingosine being the common structural element. Sphingosine is formed from the amino acid serine and palmityl CoA via serine-palmitoyl transferase, resulting in dehydrosphingosine which is subsequently reduced and oxidized to sphingosine (24) (Fig. 5).

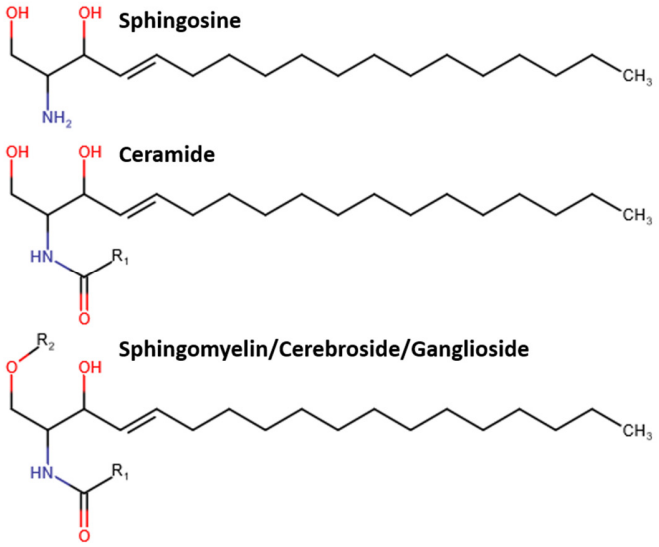

Figure 5 Structural formulas of important steps during the sphingolipid de novo synthesis. R1 is a fatty acid acyl chain added by the ceramide synthase. Different ceramide synthases have specific substrate preferences. R2 can be a phosphoethanolamine or phosphocholine in the case of Sphingomyelins. If R2 is a single sugar residue it is a Cerebroside and in the case of Gangliosides R2 is a sialic acid containing oligosaccharide. The figure was generated with the online drawing tool for chemical formulas provided by Chem-Space.com.

The first derivative of the basal sphingosine structure are ceramides, formed by sphingosine N-acyltransferases, also called ceramide synthases (CerS), via addition of a FA-CoA to a sphingosine base. Ceramides together with sterols and FAs make up the stratum corneum, the body's protective outer layer (25), providing protection from invading microorganisms and prevention of excessive evaporation and water loss. The other way ceramides can be formed is through SM hydrolysis, via the enzyme sphingomyelinase. This process is tightly linked with the initiation of apoptosis and other related signaling functions (26–29). SMs have either a phosphocholine or phosphoethanolamine group added to the first hydroxyl group of ceramides via sphingomyelin synthase in the Golgi apparatus (30). Whilst SMs are a general component of the cell membrane, they are the dominant constituents of the myelin sheath of nerve cell axons. Their role in

intracellular signaling is not limited to their degradation, also a role through signaling via synthesis, which releases DGs as possible second messengers, has been postulated (31). Glycosphingolipids (GSL) are a subgroup of SLs, mainly located at the extracellular side of the cellular membrane, and essential for cell adhesion and cellular interactions. GSLs are formed from a ceramide and a carbohydrate, either galactose or glucose, via the enzyme glycosyl transferase. These GSLs with only a single sugar residue are referred to as cerebrosides, with galactosyl ceramide found predominantly in the brain, in the myelin sheath, and glucosylceramide found predominantly in the stratum corneum. If it contains an oligosaccharide the GSL is referred to as a globoside and if one of the sugar residues is a sialic acid, as gangliosides. These oligosaccharide residues reach far into the intercellular space and are essential for cell recognition but are sometimes used by viruses and bacteria as a way of entry into the cell.

1.2.5. Sterols

Sterol, the C-3 alcohol of gonane, is the structural basis for the group of sterols and its derivatives are called steroids (Fig. 6). Cholesterol is a major component of the cell membrane, regulating its fluidity, and is a precursor for bile acids (32,33).

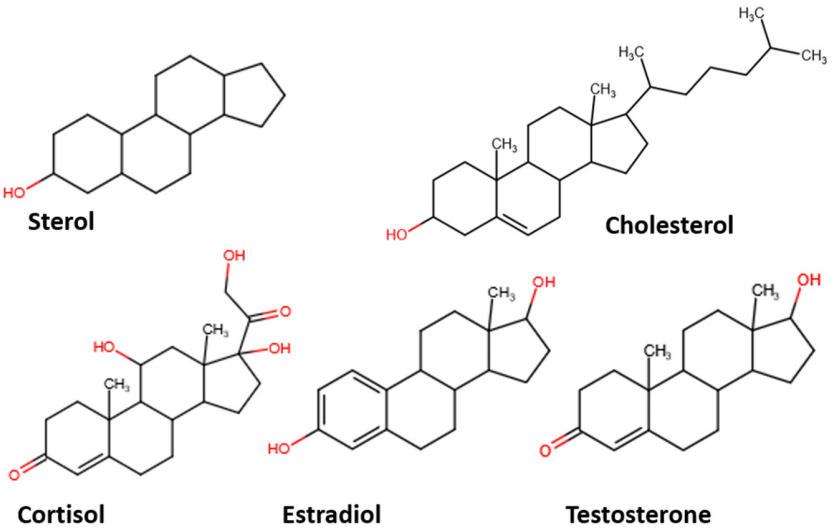

Figure 6 Structural formulas of selected steroids. The sterol backbone acts as the namesake for this family of lipids. Cholesterol is an important lipid for the regulation of membrane fluidity. Cortisol is a steroid hormone released in stress response situations. Estradiol is a steroid hormone and the major female sex hormone. Testosterone is also a steroid hormone and the major male sex hormone. The figure was generated with the online drawing tool for chemical formulas provided by Chem-Space.com.

The de novo formation encompasses 37 elaborate steps from acetyl-CoA, via mevalonate and squalene to cholesterol. This process as well as the formation of bile acids occurs predominantly in the liver. Bile acids are derivatives of cholic acid and form the bile salts when conjugated with either glycine or taurine (34). They are secreted via the bile duct into the intestine and are surfactants essential for the formation of micelles during lipid digestion. Another group of important steroids are steroid hormones roughly grouped into corticosteroids, like cortisol, and sex steroids, like estradiol and testosterone. Cortisol, belonging to the glucocorticoids, is produced in the adrenal glands and released in a diurnal cycle and as a response to stress. A short term rise in cortisol levels increases blood sugar due to increased gluconeogenesis and increased lipolysis (35,36), while long term elevation leads to protein degradation and atrophy. Of pharmacological importance is the ability of cortisol to suppress the release of certain immune mediators. It does not lead to a complete suppression of the immune response, but rather favors a shift from the cell-mediated to the humoral immune response (37–39). The primary female sex hormone estradiol as well as the male sex hormone testosterone are important for the function of the respective reproductive system and formation of secondary sexual characteristics.

1.2.6. Prenols

Prenols consist of five-carbon subunits either isopentenyl pyrophosphate or dimethylallyl pyrophosphate linked together, forming geranyl pyrophosphate via the enzyme geranyl pyrophosphate synthase (40) (Fig. 7).

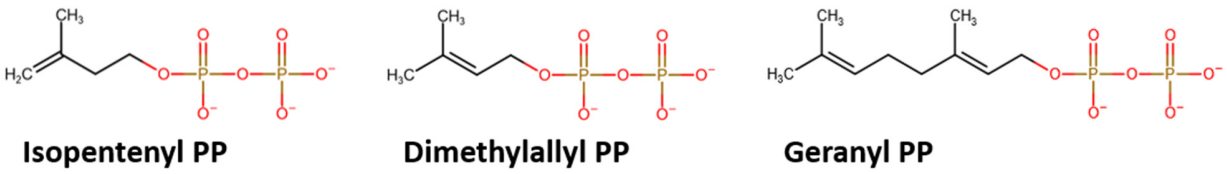

Figure 7 Structural formulas of the building blocks of prenols. Isopentenyl and dimethylallyl pyrophosphate form geranyl pyrophosphate via the enzyme geranyl pyrophosphate synthase. The figure was generated with the online drawing tool for chemical formulas provided by Chem-Space.com.

Nomenclature of the group is derived from the number of the fused units, where geranyl pyrophosphate, is referred to as a mono terpene. Whilst the highest diversity of this group is found in plants, especially as constituents of essential oils, they are still synthesized in humans through

the mevalonate pathway; i.e., squalene, an intermediate of cholesterol biosynthesis is a triterpene (41). A distinct feature of fat-soluble vitamins A, E and K as well as ubiquinones is their isoprenoid tail.

1.2.7. Saccharolipids

Saccharolipids, not to be confused with glycolipids, are formed from FAs bound to a sugar backbone, not glycerol. They are the constituents of the Lipid A, which itself is the membrane anchoring part of the Gram-negative bacterial lipopolysaccharides (LPS) (42). Whilst humans do not produce saccharolipids, LPS of bacterial origin is recognized by the immune system and causes an inflammatory response.

1.2.8. Polyketides

Polyketides include a huge variety of secondary metabolites originating from all trees of life formed by an enzyme complex called polyketide synthase (43). Not unlike FA synthase, it uses a primer of acetyl- or propionyl-CoA followed by elongation with malonyl- or methylmalonyl-CoA. Further complexity and variety are introduced by post tailoring enzymes generating often cyclic end products with a plethora of medical uses such as antibiotics (doxycycline and erythromycin), statins (lovastatin), anthelmintics (ivermectin) and antifungals (nystatin).

1.3. The Liver

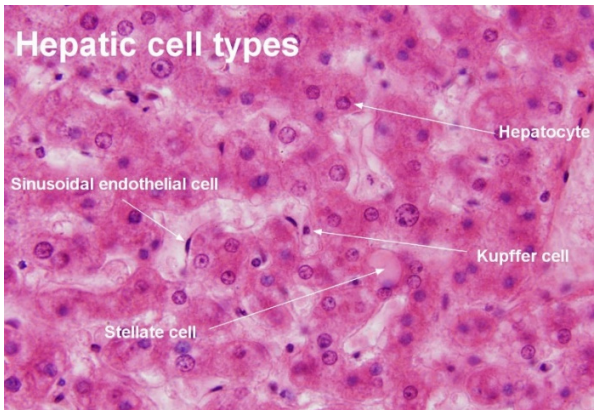

Figure 8 Microscopic image of an haematoxylin eosin stained hepatic tissue section taken at 400x magnification. Hepatocytes are arranged inbetween the sinusoids in cords. Sinusoidal endothelial cells can be identified via their elongated nucleus lining the sinusoidal wall. Kupffer cells represent themselves with a round dense nucleus inside the sinusoids. Stellate cell are located in between the hepatocytes but can be differentiated due to their lipid droplet taking up most of the cytoplasmic space as well as their dense marginal nucleus.

Found in all vertebrates, the liver serves as a major metabolic organ of the body, performing tasks ranging from detoxification, digestion and resource distribution to protein and hormone synthesis. Whilst the evolutionary origins of the liver are still debated to date, we know that the closest living relative to all vertebrates, the cephalochordate *amphioxus*, possesses a liver analog in the hepatic caecum. Thus far studies have shown that even in this early evolutional stage, next to the secretion of hormones, proteins and detoxification, regulation of the acute phase response is a key task of the liver. It is the largest visceral organ and consists of four major cell types: first hepatocytes, the main liver cells; second hepatic stellate cells (quiescent resident antigen presenting cells); third Kupffer cells, hepatic macrophages; and fourth liver sinusoidal endothelial cells (endothelial lining of the microvasculature) (Fig.8). Microscopically, hepatocytes organize into hexagonal lobules, with the hepatic triad in the peripheral region and a central drainage through the hepatic vein (Fig. 9). The hepatic triad consists of branches from the hepatic artery and portal vein as well as a leaving bile duct (Fig. 10). Macroscopically the liver divides into four lobes, with the right lobe being the largest and the smaller left lobe being the only ones visible anteriorly. The smaller caudate and quadrate lobe, separated from the right lobe by the inferior vena cava and gall bladder respectively, are only visible dorsally. In humans the liver forms out of the distal foregut during the 4th week of embryonal development, with hepatocytes and the bile duct epithelium deriving from endodermal origins. The later migration of mesodermal cells into the liver provides it with hematopoietic capabilities during prenatal development (44). Though the hematopoietic potential of the liver is lost after birth, hematopoietic stem cells have been shown to migrate into the liver as a response to hepatic damage

and help in specific regeneration without scarification (45). During weeks four to six the afferent venous structure is established from the vitelline and the umbilical vein, which at this fetal age is the source of oxygen rich blood (46). Whilst efferent veins are formed during the same time and also originate from the vitelline veins, the formation of the hepatic artery only starts during the 8th week of fetal development, and branching into the peripheral regions only happens between the 10th and 15th week. In adults, approximately 25% of the cardiac output is attributed to the liver, with a third of the supply coming from the hepatic artery and two thirds from the portal vein (47). These two afferent blood supplies, high pressure and oxygen rich arterial and low pressure but nutrient rich venous blood, mix in the hepatic sinusoids and exit through lobular central veins combining into the efferent hepatic vein. The biliary tract is the second efferent transport system, in which the bile, consisting primarily of bile acids, phospholipids and cholesterol is transported to the duodenum. From the bile ducts in the hepatic triads the bile is transported via intrahepatic ducts to the common hepatic duct. When the gall bladder, which serves as a storage compartment for the bile, interlaces via the cystic duct, it henceforth is referred to as the common bile duct. After joining with the pancreatic duct and

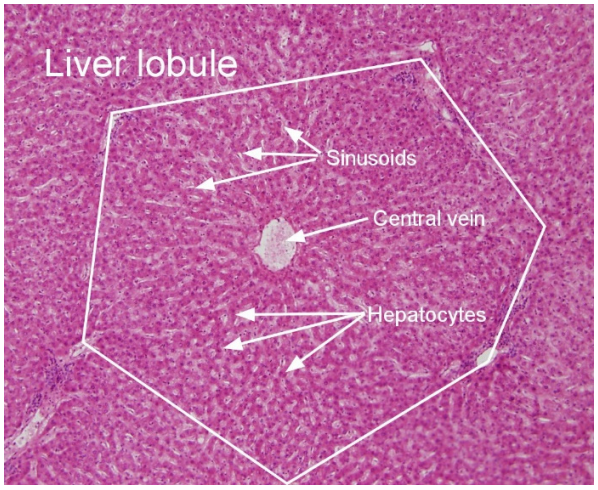

Figure 9 Microscopic image of an haematoxylin and eosin stained liver lobule taken at 100x magnification. As indicated by the overlay the liver lobules organize in hexagonal structures. Indicated with arrows are the sinusoids, the micovasculature surrounding the hepatocytes on two sites. The afferent flow, originating from the hepatic triads is drained through the central vein.

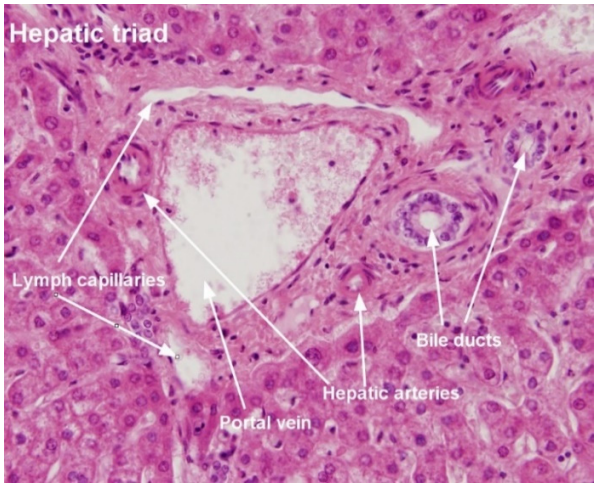

Figure 10 Haematoxylin eosin stain of the hepatic triad taken at 200x magnification. Positioned on each corner of the liver lobule the triad consists of the hepatic vein, hepatic arteries and the bile ducts. Often they are accompanied by lymphatic capillaries. The triad entails two afferent vascular systems in form of the hepatic artery, bringing oxygenated blood, and the portal vein, delivering nutrient rich blood directly from the intestines. The bile ducts collect bile, a mix of bile acids, phospholipids and cholesterol.

forming the hepatopancreatic ampulla, or ampulla of Vater, they empty into the duodenum at the major duodenal papilla. or papilla of Vater. The specimen used to generate figures 8,9 and 10 was kindly provided by Prof. Dr. Astrid Hammer.

1.4. Lipids as nutrition

Whilst the human body possesses the ability to synthesise FAs *de novo*, the lack of specific desaturases $\Delta^{12/15}$ results in the two FAs, linoleic (C18:2 *cis*-9,12) and α-linolenic acid (C18:3 cis-9,12,15) being essential nutritional supplements (48,49). Linoleic acid is primarily converted via desaturases $\Delta^{5/6}$ and elongation to arachidonic acid, and thus is key to eicosanoid mediated lipid signaling(50,51). α-Linolenic acid can be used as precursor for longer chained PUFAs, but due to low conversion rates uptake from different nutritional sources is more prevalent (52). Studies focusing on α-linolenic acid supplement have overall shown an improvement to lipid metabolism but reported various disadvantageous side effects (53,54).

The majority of dietary lipid uptake happens in the form of TGs as fats and oils. As only cholesterol and FFAs can pass unhindered through cellular membranes, enzyme mediated cleavage during digestion is necessary. Enzymes mediating the cleavage of TGs are called lipases, and a number of them, evolutionary tuned to work in the specific environment, can be found spatially distributed in the gastrointestinal tract (55). Already in the oral cavity the lingual lipase starts the breakdown of medium and long chained TGs into FFAs and DGs (56). The lingual lipase has a pH optimum of around 5, which is lower than the pH of average human saliva, but allows for the enzyme to pass the stomach and remain active in the duodenum and jejunum(57). Gastric lipase, secreted from gastric chief cells located in the mucosa of the fundus, is the second acidic lipase, with a pH optimum of around 4.5 (58). Long chained FFAs inhibit gastric lipase, a mechanism called feedback inhibition, thus suggesting that the main task of this lipase is not mere hydrolysis of TGs but digestion of milk fat globule membranes (59,60). In the duodenum, after the digestive mix has left the stomach and pH levels return to more neutral levels, pancreatic lipase and bile-salt dependent lipase are added to the chyme (61,62). These two lipases originate from the exocrine section of the pancreas and are in their function dependent on bile salts and, in the case of the pancreatic lipase, colipase (63). Whilst colipase acts as a true coenzyme, itself being activated by trypsin, bile salts act as surfactants, enclosing bigger fat droplets in the chyme and breaking them

down with the peristalsis movement of the intestines into smaller droplets, also referred to as micelles. This increases their surface to volume ratio and allows better access for the lipases. Both pancreatic lipases catalyse the complete lysis of TGs to two FFAs and MG. These MGs and FFAs as well as cholesterol can leave the digestive micelles and permeate into the epithelium of the small intestine wherein the FFAs become re-esterified to TGs and stored in LDs. The enterocyte can also take these TGs and cholesterol esters to form chylomicrons at the ER and pass them into the lacteals through their basolateral membrane (64). Chylomicrons, sometimes referred to as ultra-low-density lipoproteins, consist like LDs of a TG and cholesterol esters core and a phospholipid monolayer hull but contain specific apolipoproteins (APO) differentiating them from other lipoproteins (65). Whilst lipoproteins are present on all lipoprotein particles in varying amounts, the APOB45 isoform is specific for the small intestine and identifies these particles as nascent chylomicrons. The lacteals, collecting the chylomicrons from the villi of the small intestine, fuse with larger lymphatic vessels until combining in the thoracic duct and emptying into the subclavian vein. In the blood, interactions between high-density lipoproteins (HDL) and nascent chylomicrons result in the transfer of APOC2 and APOE onto the chylomicron. The addition of APOC2 leads to its maturation as it allows for lipoprotein lipase to become active and to distribute the FAs in the body (66,67). When the TG storage of the mature chylomicron becomes depleted it becomes a chylomicron remnant and gets reabsorbed into the liver after returning the APOC2 to HDL particles. The plasma half-life of a chylomicron is very short, about 15- 20 minutes, thus the liver produces the lipoprotein particle referred to as very low-density lipoprotein (VLDL), to distribute lipids throughout the body (68,69). Besides a difference in size, nascent VLDL particles differ from nascent chylomicrons only in the presence of the liver specific isoform APOB100, but they also depend on the uptake of APOC2 from HDL particles for maturation. The mature VLDL particle circulates through the bloodstream whilst LPL cleaves the stored TG, thus emptying the VLDL particle. When the majority of the TGs have been transferred to tissues in the periphery and the particle is mainly made up of cholesteryl esters it has become an intermediate-density lipoprotein (IDL). These IDLs can now either be taken up by the liver or experience further TG hydrolysis via the hepatic lipase if they stay in circulation. Following this further depletion of the particle TGs, the particle reaches now its final state as a low-density lipoprotein (LDL). If a cell experiences a need for cholesterol, which cannot be satisfied via de novo synthesis, most often occurring in

steroid synthesising tissues, they express an LDL receptor. This receptor is expressed on specific patches on the extracellular membrane and binds a passing LDL particle leading to its uptake by endocytosis.

The liver also produces HDL, lipoprotein particles which facilitate the return of unneeded cholesterol from the periphery to the liver, and which are the smallest of the five most important lipoprotein particles. Nascent HDL particles are characterized by the presence of APOA1 and APOA2 as well as a flattened disc shape. HDL particles interact with cells via the adenosine triphosphate (ATP) binding cassette transporter A1 to take up excess cholesterol; and the plasmatic enzyme lecithin- cholesterol acyltransferase converts the freshly taken up cholesterol back into hydrophobic cholesteryl esters (70,71). This full, round HDL particle can now either transport the cholesterol to the liver, where it would be excreted via the bile or exchange it for TGs with VLDL or IDL particles with help of the cholesteryl ester transfer protein. The second pathway results in the formation of LDL particles, due to a decrease of TGs and an increase of the cholesteryl ester content, which will be taken up by different cells and thus will be removed from the circulation, and after degradation of the TGs transferred to the HDL particle, via hepatic lipase, it is empty and can start with the reuptake of cholesterol (72).

1.5. Lipotoxicity

Lipotoxicity is a term used to sum up pathological processes involving lipids in a direct or indirect way, and while there is no unanimous conclusion it is considered a primarily metabolic disease. Fundamental to all occurrences of observed lipotoxicity is an imbalance of availability and demand of FFAs. The human body has a dedicated long-term storage for fat in form of the white adipose tissue. Cells of the white adipose tissue are well adapted to handle an excess amount of lipids, as they contain a dominant giant LD taking up most of the intracellular space. However, this phenotype cannot be reproduced *in vitro* (Fig. 11). The main constituent of LDs are TGs, which are generally considered safe for the cell. Short term fluctuations of the FFA load in the plasma, either following nutritional uptake or release from white adipose tissue in case of starvation, are buffered by the liver. Problems arise when the storage capacities in the liver or the adipose tissue are overwhelmed, and spill over to different tissues occurs. In these unspecialised tissues most often an accumulation of lipid metabolism intermediates, such as DGs and CERs, are causal for derailing the homeostatic equilibrium; but also increased ROS production or changes to the cell membrane composition have been observed and reported. The differential impact of various FFAs is poorly understood and appears to be tissue specific, with the exception being, that toxicity decreases with the degree of desaturation (73).

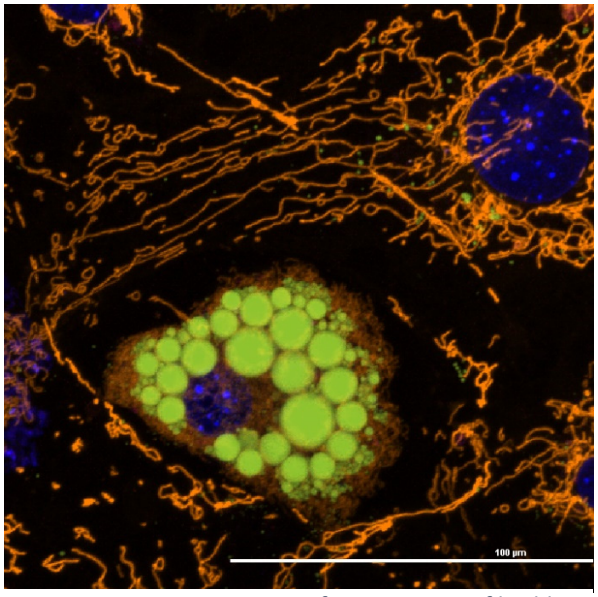

Figure11 Microscopic image of 3T3-L1 mouse fibroblasts aquired with a 63x objective with a confocal laser scanning microscope. Cells were differentiated into adipocytes, displaying a plethora of intracellular lipid droplets. Vissible in the upper part of the image is an undifferenciated cell, having an elongated interconnected mitochondrial network and almost no recognizable lipid droplets. Nuclei= blue; lipid droplets= green, mitochondria= orange

1.5.1. Tissue specific differences

The following subchapters report on selected mechanisms encountered in different tissues which are all summed up under the term lipotoxicity.

1.5.1.1. Brain

Sixty percent of the brain and central nervous systems dry mass are lipids and, despite only making up 2% of the average total body mass, the brain consumes a fifth of the resting body's energy (74). So, it might be surprising that the brain relies on a continuous supply of glucose instead of the more energy rich FAs (75). Of all the different cells in the brain neurons have the highest energy demand but almost exclusively metabolise glucose while the astrocytes, cells that traffic nutrients in the brain, metabolise almost all of the FAs (76,77). In experiments with cultured SH-SY5Y cells, a neuronal cell model, low doses of palmitic acid led to a cell cycle arrest due to accumulation of phosphorylated eIF-2, a marker protein for ER stress, and the release of proinflammatory cytokines (78,79). *In vivo* models demonstrate that the impact of elevated FFA serum levels seems to be mitigated by astrocytes which display the ability to safely store the FAs as TGs in LDs which also has been found to happen during pathological processes or ischemia (80).

1.5.1.2. Heart

The heart is the organ with the highest energy demand in the body and displays a high grade of metabolic flexibility (81). About 60% of the energy is generated from beta oxidation while most of the remaining demand is satiated via glycolysis. Heart failure has long been linked to metabolic syndrome, which in turn is linked to excessive fat accumulation not only in white adipose tissue but also in the heart (82). Thus, cardiomyocytes have been extensively studied in animal models and cell culture systems, and their vivid LD dynamics have been documented (83). In all these models a plethora of pathophysiological alterations with varying severity have been detected, ranging from lipid induced apoptosis, ceramide accumulation to ROS overproduction and ER stress (84). Only recently a complex model has been proposed, in which ROS generated during beta oxidation leads to post translational modification of proteins involved in mitochondrial dynamics, resulting in a fragmented mitochondrial state which no longer can meet the energy demand resulting in the observed cardiomyopathy (85).

1.5.1.3. Endothelium

As the lining of all blood vessels the endothelium is always in contact with nutrients transported in the blood and experiences elevated lipid levels first hand. A hallmark of the majority of cardiovascular pathologies is an altered endothelial phenotype referred to as endothelial dysfunction (86). Endothelial dysfunction is characterized by a reduced capability of vasorelaxation in response to pharmacological or physical stimuli despite a healthy vascular musculature (87). Crucial for unimpaired endothelial function is the bioavailability of nitric oxide, which not only regulates vasorelaxation but also inflammation, coagulation and proliferation (88). It has been corroborated that the key enzyme, endothelial nitric oxide synthase, has severely decreased turnover rates in the presence of ceramides, as these lipids downregulate activating kinases of NO-synthase (89–91). Incubation with palmitic acid and ceramides resulted in decreased vasorelaxation, increased vasoconstriction and overall decreased NO levels in cell models as well as isolated arteries (92–94).

1.5.1.4. Pancreas & lipid induced insulin resistance

Divided into an exocrine and endocrine part, the pancreas is one of the most prominent glands of the human body, and pathologies associated with it are of immediate concern. A ubiquitous disease, which is becoming more and more prevalent in the human population, associated with the pancreas is diabetes. Though it is believed to be the oldest ever described disease in history, researchers have been working on improving our understanding relentlessly for the past decades (95). Specialized cells within the pancreas, referred to as β cells, release insulin into the blood stream in an effort to reduce elevated blood glucose levels by increasing cellular uptake. What happens to people suffering from type 2 diabetes, acquired diabetes, is a combination of reduced insulin secretion and reduced cellular response, both of which are linked to elevated FA serum levels (96). Whilst in the short-term FAs improve insulin secretion, due to being part of the glucose- stimulated insulin secretion cascade, a shift from beta oxidation towards glycolysis under high glucose conditions in β cells might prove fundamental for the pathological process (97). With the ensuing accumulation of fatty acyl coenzyme A (CoA) in the cytoplasm, alternate pathways such as TG, PL and SL synthesis are used at increased rates accumulating lipotoxic intermediates like DGs and CERs and disrupting the membrane fluidity with increased PL levels. But in the case of β cells especially the

unesterified forms of saturated long to very long chained FAs have proven integral for reduced insulin synthesis and secretion, and even shown to induce apoptosis (98–100). The second important component of the diabetes phenotype is the reduced insulin sensitivity, especially in the muscle and liver. For both of these tissues a unifying theory exists how the before mentioned intermediate of TG synthesis, DG, can activate protein kinase C isoforms θ in muscles & ε in the liver (101). The signalling cascade after insulin binds to the insulin receptor entails phosphorylation of the insulin-receptor substrate, which in turn activates 1-phosphatidylinositol 3-kinase, and ends after several further steps with the translocation of the glucose transporter 4 to the cell membrane (102). However, active protein kinase C in turn leads to an inactivating phosphorylation of the insulin receptor blocking the insulin signal transduction in the very first step (103).

1.5.1.5. Skeletal muscle

The skeletal muscle consumes up to 80% of the postprandial glucose, highlighting that the previously described insulin resistance, due to intramyocellular lipid accumulation of DGs, will have severe metabolic consequences (104). Skeletal muscle can be divided into two types of fibres, type one (red slow oxidative low pitch fibres) and type 2 fibres (lighter coloured fast oxidative high pitch fibres) (105). Studies have shown that muscle specific insulin resistance occurs mainly following lipid accumulation in type 1 fibres (106). However, this matter might not be as straight forward as presented due to the existence of what is referred to as the athlete's paradox (107). This phenomenon describes how the type 1 muscles fibres of trained endurance athletes have greatly increased lipid content but display enhanced insulin sensitivity. Moreover, following prolonged intermediate exercise up to 70% of the intramuscular TG content is used in oxidative phosphorylation (108). Studies indicate that the difference in the insulin sensitive athlete's muscle and an insulin resistant sarcopenic patient is a different answer to the ROS originating from beta oxidation in the FA oversaturated muscle (109). Athletes respond with an upregulation of the peroxisome proliferator-activated receptor-γ coactivator-1α which stimulates mitochondrial biogenesis, regulates oxygen consumption and over all drives the differentiation of type 1 muscle fibres (110,111); whilst in non-athletes, ROS shuts down further mitochondrial beta oxidation resulting in elevated ectopic lipid accumulation, reduced insulin sensitivity and initiation of muscle fibres' death (112).

1.6. Hepatic lipotoxicity & NAFLD

During the last years a push has been made to rename and revaluate the term NAFLD, as the definition of a pathology via a "non-condition" should be avoided (113,114). Thus, the term metabolic associated fatty liver disease (MAFLD) was created and defined by the presence of liver steatosis in addition to either obesity, type 2 diabetes or metabolic dysregulation. Metabolic dysregulation has itself been defined by the presence of two of the following factors: increased waist circumference, arterial hypertension, hypertriglyceridemia, low HDL-C, prediabetes, insulin resistance and subclinical inflammation (115). While this new definition would include occasional drinkers, and has a significant overlap with NAFLD diagnosed patients, it excludes most patients with a lower BMI and better metabolic profile (116). As this study focuses on the influence of lipids without alcohol as a cofactor and NAFLD is the established term in science and medicine, this will be the terminology used in this thesis.

Hepatic lipotoxicity is inseparably linked to the development of NALFD, a disease which is on the rise worldwide (117). Models suggest that with the end of this decade the numbers of NAFLD patients will rise over 100 million in the United States alone (118). NAFLD can be divided into two subgroups: non-alcoholic fatty liver (NAFL) and non-alcoholic steatohepatitis (NASH). Established clinical practice for the diagnosis of NAFL is the presence of elevated hepatic lipid content (≥5%) in the absence of causal factors like alcohol abuse, drugs, inflammation or auto-immune diseases (119). However, detecting this 5% threshold is only possible with magnetic resonance imaging; sonography and computer tomography only offer an accurate estimation of lipid content above 20% (120). About a fourth of NAFL patients will progress into NASH, a disease without a unified treatment plan, which increases the risk to develop type two diabetes and hepatocellular carcinoma (121). The accurate diagnosis of NASH is more challenging since it differs from NAFL in the presence of lobular inflammation, hepatocellular ballooning and onset of fibrosis, parameters which necessitate a biopsy (122). Every second patient with NASH will develop a fibrotic liver, which is likely to progress into cirrhosis, necessitating the need of a liver transplant (123). Whilst comorbidities, like obesity and type two diabetes, or a polymorphism in the patatin-like phospholipase domain-containing 3 protein (I148M), are huge risk factors for the

progression of the disease, knowledge about its early developmental stage is still lacking (124–126).

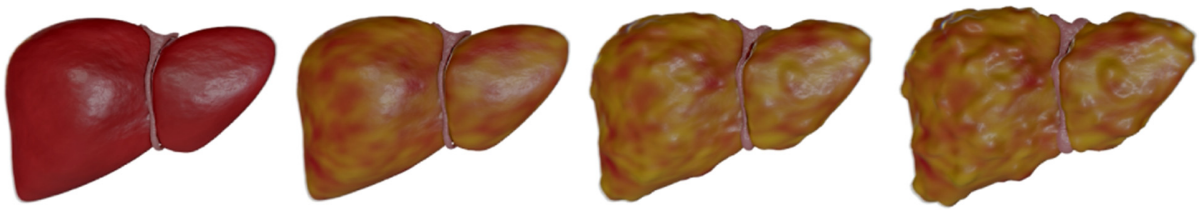

Figure 12 Schematic progression of non-alcoholic fatty liver disease from left to right: Healthy liver; non-alcoholic fatty liver; non-alcoholic steatohepatitis; advanced fibrosis/cirrhosis. The transition to non-alcoholic fatty liver is marked by the lipid content of the liver surpassing 5%. With the onset of lobular inflammation and fibrosis as well as the presence of ballooning cells the patient has transitioned into non-alcoholic steatohepatitis. Terminal stage of non-alcoholic fatty liver disease is advanced tissue scarification, inhibiting proper liver function being referred to as cirrhosis. Hepatocellular carcinoma also occurs with increased frequency in these cirrhosis patients.

Indeed, western lifestyle leads to an overabundance of FFAs in the plasma, increasing their bioavailability. However, the high percentage of Asians considered lean, with their respective BMI cutoff being even lower at 23, but diagnosed with NAFLD, stresses the fact that diet and lifestyle are not the only factors important for development of the disease (127). Recent studies increasingly note that, while there is a link between intrahepatic lipid accumulation and dietary uptake, the amount incorporated might vary drastically with the composition of dietary fats (128). In most cases the increased intrahepatic lipid content which constitutes NAFL recedes on its own. However, the consensus is, independent of the source, that if the steatosis becomes chronic the disease will progress (129). Nuclear factor kappa β has been found to be increased in steatotic livers, promoting pro inflammatory signaling, leading to the recruitment and activation of hepatic stellate and Kupffer cells (130–133). These changes fit the progression from NAFL to NASH, but do not improve the understanding of the conditions necessary for this disease to occur in the first place. Scientists tend to perform these fundamental studies in animal models, due to the possibility to meticulously control all the environmental parameters. Rodents are commonly used worldwide as test animals, due to their availability, defined genetic background and relatively low cost compared to other animals. The various established models can be broadly separated into two groups: genetic or diet based NAFLD development. Genetic models either target the leptin

signaling pathway, thus disrupting the feeding habit due to the mice never feeling satiated, or the lipoprotein metabolism (134–136).

Whilst mice who are leptin deficient tend to get obese, they only develop NASH and fibrosis on special diets; whereas mice with altered lipoprotein metabolism remain lean and show no signs of insulin resistance (137–139). Diet induced models manage to mimic overall more of the desired pathological traits, such as ballooning cells and the development of fibrosis and HCC. Interestingly, no one single model combines all desirable characteristics (140,141). Of note, the development of ballooning cells should be a trait sought after in models, as it marks the point of no return in the pathophysiological development. Ballooned Hepatocytes present themselves as enlarged cells (≥30µm diameter), with microvesicular LDs, a rarefied cytoplasm and Mallory-Denk bodies (142). Mallory-Denk bodies are composed of the remnants of cytoplasmic keratin 8/18 which is lost in ballooned cells. The presence of these cells is used to grade the development and progression of NASH itself and is caused by localized pro-fibrogenic signaling due to their expression of sonic hedgehog (143,144). Henceforth, understanding the conditions which lead to the alteration of these hepatocytes might be mandatory to comprehend and treat NAFLD.

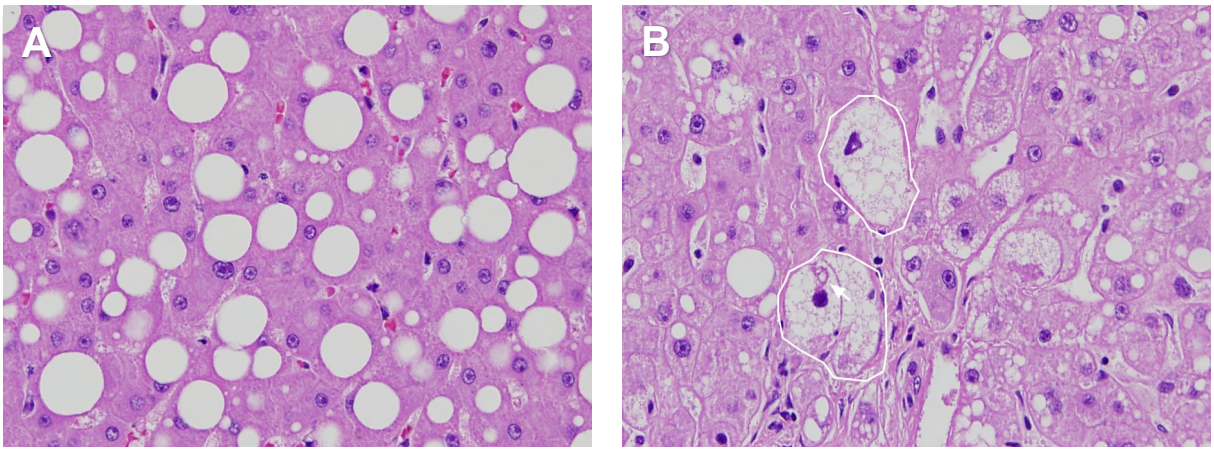

Figure 13 Microscopic images of hematoxylin and eosin stains of formalin fixed paraffin embedded human tissue sections taken at 400x magnification. A) Steatotic liver with macro vesicular lipid droplets. Despite the elevated fat content, the cells are not enlarged and cytoplasm has still the original dark pinkish coloration. B) Indicated in white are ballooned hepatocytes and a possible Mallory-Denk body with an arrow. They differentiate themselves from healthy hepatocytes due to their 2-3 times increase in size, multiple microvesicular lipid droplets and rarified cytoplasm. Mallory-Denk bodies are the remnants of the cytoskeleton component keratin 8/18. Careful observation of these cells reveals a remodeled extracellular matrix around them due to habit of inducing fibrogenesis through activated sonic hedgehog signaling. The Specimens used to generate Figure 13 were kindly provided by Prof. Dr. Karoline Lackner.

1.7 Study questions

We stipulated that a deregulated hepatic lipid environment is fundamental for the development of NAFLD marked by pathological and morphological alterations of the hepatocytes prior to inflammation and fibrosis. Thus, we employed a human hepatocyte cell line model exposed to a controlled lipid environment to address the following questions within this thesis (Fig. 14).

1. What is the impact of different FFAs and FFA combinations on the viability of the hepatocytes? Can these effects be prevented?
2. What morphological changes can be observed following the treatment?
3. What are the changes in the proteome composition following lipid treatment?
4. What are the changes in the lipidome following FFA uptake?
5. Do combinations of FAs change the uptake dynamics?

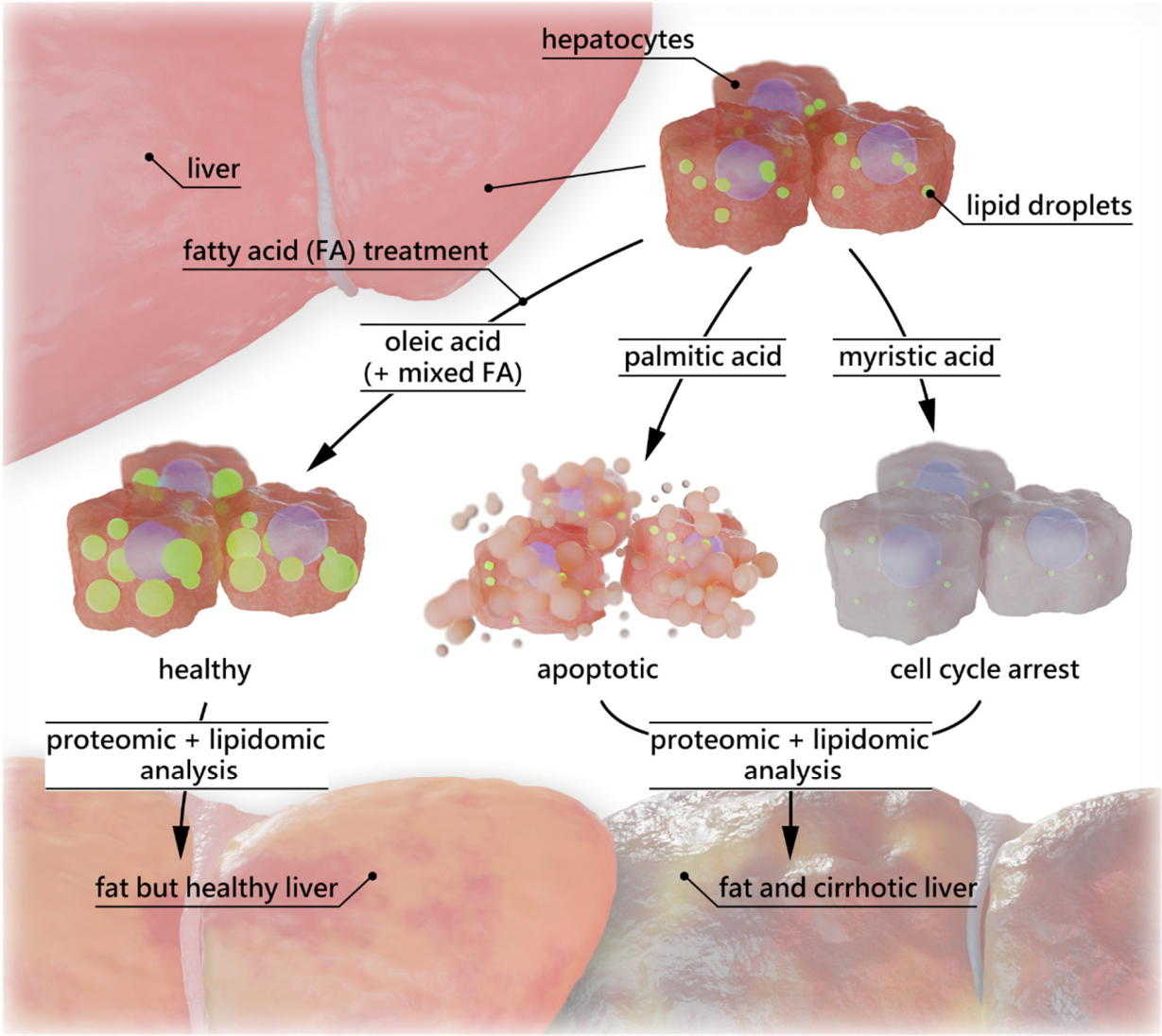

Figure 14 Graphical abstract of the study design. Figure adapted from Gindlhuber et al. 2022 with permission from the publisher.

2. Materials and methods

2.1. Experimental design and statistical rationale

Data are presented as mean ± standard deviation error bars of n biological replicates (n number always indicated in graph). Experimental data were analysed with a two-sided unpaired Student's t-test for two groups or ANOVA with Dunnett's multiple comparisons test for more than two groups. The Mantel-Cox test was employed for comparison of survival curves. Differences were considered significant below a threshold of 0.05 ($p < 0.05$ (*); $p < 0.01$ (**); $p < 0.001$ (***)). If not stated otherwise in the dedicated method section statistical analysis and generation of graphs was performed with GraphPad Prism (version 8.0).

2.2. Reagents

If not stated otherwise reagents were purchased from Sigma-Aldrich, Austria.

2.3. Cell culture

We used the immortal hepatocellular carcinoma cell line HepG2 in our experiments. Cells were obtained from the CellBank Graz, and cultured at 37°C and 5% CO_2 in RPMI-1640 medium supplemented with 10% foetal bovine serum and 584 mg/L glutamine.

2.4. BSA fatty acid conjugates and treatment regime

To increase solubility of the hydrophobic free FAs and thus improve cellular uptake, they were used as bovine serum albumin (BSA) conjugates. The FA: BSA ratio was 6:1. A heated magnetic stirrer was used to dissolve FA free lyophilized BSA in a 150 mM NaCl solution at approximately 37 °C under continuous motion. Myristic (MA; 14:0), palmitic (PA; 16:0) and oleic acid (OA; 18:1 cis-9) sodium salts were slowly heated in 150 mM NaCl solution, also employing a water bath on a heated magnetic stirrer, until the solution turned completely clear at approximately 70°C. The clear FA solution was transferred, using a preheated glass pipet to prevent precipitation of the FA due to cooling of the liquid, only in tiny amounts so that the BSA solution never surpassed 40 °C. If the temperature of the BSA solution surpassed 39°C ice chips were added to the water bath. The conjugate solution was then stirred for one hour, afterwards Volume and pH were adjusted to obtain a 5 mM stock solution. FA-BSA conjugates were added to the growth media after the cells had

reached desired confluency and left on them for 24 hours. Treatments only employing a single FA are abbreviated in this thesis with the shorthand form of the FA with the concentration in µM in the numeral suffix (e.g., MA125 = myristic acid 125 µM). Mixed treatments are labelled as either MO (indicating a mix of MA and OA) or PO (indicating a mix of PA and OA), followed by a number suffix indicating the ratio 11 (equal mix of 125 µM of either fatty acid) or 21 (unequal mix of 250 µM of the saturated FAs MA or PA and 125 µM of OA). Which concentrations of fatty acids were used in our experiments were determined by their observed impact on cell growth. The final upper limit, 500 µM, was the lowest concentration at which a negative effect on cell growth following OA treatment could be observed, as well as being the concentration when growth for saturated FFAs was no longer detectable whilst still being within reported FFA serum levels (145).

2.5. Growth analysis

To determine cellular growth rates, 80,000 cells were seeded into each well of a 12-well plate 24 hours prior to the start of image acquisition and lipid treatment. Growth was analysed through observation of the cells for up to 120 hours with a Zeiss Cell Observer microscope with a 5x objective. Phase contrast images were taken hourly from seven positions in each well. Gathered images were subjected to an automated confluency analysis in FIJI (version 1.51h) and the mean out of all positions in one well was calculated and plotted per hour. An equation was fitted over the plotted data points and analysed for the maximum inclination during their exponential growth phase.

2.6. LD imaging and volume analysis

100,000 cells were seeded onto KOH treated cover slips put into the bottom of 6 well plates 24 hours prior to lipid loading. Following a 24-hour lipid treatment period, cells were incubated with a 1:1000 dilution of a 10 mg/ml BODIPY™ 493/503 stock (Thermo Fisher Scientific, Waltham, USA) for 10 minutes at 37°C in a dark environment, to stain intracellular LDs, and fixed for 10 minutes with 3.7 % formaldehyde in phosphate buffered saline (PBS) at room temperature. After fixation two washing steps with PBS were performed prior to the mounting with VECTASHIELD® antifade mounting medium containing DAPI (Szabo-Scandic, Wien Austria). Images were acquired using a Nikon A1+ confocal laser scanning microscope with a 405 nm diode

laser and 450/50 BP filter for DAPI, a 488 nm argon laser with a 525/50 BP filter for BODIPY™ and a 60x CFI Plan Apochromat λ oil immersion objective with a numerical aperture of 1.4. The settings for x, y and z were chosen to fit the Nyquist criterion for the 488 nm channel as it contained the desired LD information. A minimum of ten images for each condition were acquired. The analysis was performed with FIJI (version 1.51h) (146). For each image a maximum intensity projection of the BODIPY™ channel was generated and thresholded using the Kapur-Sahoo-Wong (Maximum Entropy) method (147). The calculated thresholding values were thereafter used on the whole z-stack for lipid droplet volume quantification. The information of the DAPI stain was used to perform a nucleus count so an average LD volume per cell for each image could be calculated and compared across conditions.

2.7. Cell cycle and apoptosis analysis

300,000 HepG2 cells were seeded into 6 well plates and grown for 48 h to approximately 80% confluency. Lipid loading was performed 24 hours prior to analysis on a CytoFLEX LX (Beckman Coulter, Brea, USA) flow cytometer. To determine if the FAs influence the cell cycle, cells were treated with the cell permeable DNA intercalating dye Hoechst 33342 (Thermo Fisher, Germany) for 10 minutes at 37 °C. This was followed by a washing step with PBS and detaching with trypsin. Trypsin was neutralized with 5 volumes of full media and cells were stored on ice until measurement. To perform necrosis and apoptosis analysis, cells were first washed with PBS and detached with trypsin. Cells were pelleted by centrifugation at 220 g for 5 minutes and incubated with Annexin V FITC (BioLegend, San Diego, USA) and propidium iodide for 15 minutes prior to analysis. In each case unstained controls and single stained controls, were analysed to determine auto fluorescence levels and perform necessary compensation for channel cross talk. The obtained data were analysed with Cytexpert software (version 2.4).

2.8. Proteomics sample preparation

300,000 HepG2 cells were seeded into 6 well plates and grown for 48 h to approximately 80% confluency prior to lipid loading. Following a treatment period of 24 hours the cells were washed 3 times with ice cold PBS and collected in 300 µL lysis buffer (100 mM Tris pH = 8, 1% sodium dodecyl sulphate (SDS), 10 mM tris(2-carboxyethyl) phosphine, 40 mM chloroacetamide). To lyse

the cell suspension, a microtip sonication probe at 90% amplitude (counting to 1500 J for each sample) was used, followed immediately by a reduction and alkylation step. Insoluble debris was precipitated via a 30-minute centrifugation step at 3500 g. The individual protein content of each sample was estimated using the bicinchoninic acid assay (BCA; Thermo Fisher Scientific). Subsequently, 100 µg protein of each sample were precipitated overnight by adding 3 volumes of acetone. The following day, the obtained protein pellets were re-dissolved in 25% trifluoroethanol (in 100 mM Tris pH 8.5), which had to be diluted to 10% trifluoroethanol with ammonium bicarbonate prior to the overnight digestion with trypsin (Thermo Fisher Scientific) at 37°C in a thermal shaker.

2.9. Peptide prefractionation

To perform a peptide prefractionation, we employed a high-pH reversed-phase C18 column from Waters (Xbridge Peptide BEH 186008979, inner diameter 2.1 mm; length 50 mm; 2.5 µm particle size) on an Agilent 1100 & 1200 series HPLC system. 20 µg of the digested protein solution were dissolved in solvent A (0.1% triethylamine (N,N-diethylethanamine), pH 10) and loaded onto the column. A gradient starting with 3% solvent B (100% acetonitrile) rising to 30% B within 30 minutes was utilized with a constant flow rate of 300 µl/min with a column temperature of 50°C. The gradient rose to 60% B at minute 41.3 of the run, reaching 95% B at 44.6 minutes and staying at 95% B for another 2 minutes followed by a final descend to 3% B at 54 minutes. In total 54 fractions (300 µl each) were collected and pooled in an online fashion into 8 combined fractions using the Agilent 1200 fraction collector system (148). Fraction 1 was combined with fractions 9, 17, 25, 33, 41 and 49; fraction 2 was combined with fractions 10, 18, 26, 34, 42 and 50, etc., into Eppendorf low-bind 96 deep well plates. These deep plates were subsequently dried in a Thermo Fisher vacuum concentrator for 24 hours at room temperature. Samples were re-dissolved in 200 µl of a ddH2O: acetonitrile 1:1 (vol: vol) mixture with 0.1% formic acid added and further combined to a total of 4 fractions (fraction 1+5, 2+6, etc.) for measurement. Finally, samples were transferred to glass vials (Bruckner Analysentechnik GmbH, Linz, Austria), dried down for approximately another 6 hours at 30°C and dissolved in 10 µl 3% acetonitrile, + 0.1% formic acid and kept at -20°C until measurement.

2.10. LC-MS/MS proteomics measurement

Obtained peptide fractions were analysed by nano-HPLC (Dionex Ultimate 3000) equipped with an Aurora (IonOpticks, Australia) nanocolumn (C18, 1.6 µm, 250 x 0.075 mm). Separation was carried out at 50°C at a constant flow rate of 300 nl/min using the following gradient, where solvent A was 0.1% formic acid in water and solvent B was acetonitrile containing 0.1% formic acid: 0-18 minutes: 2% B; 18-100 minutes: 2-25% B; 100-107 minutes: 25-35% B, 107-108 minutes: 35-95% B; 108-118 minutes: 95% B, 118-118.1 minutes: 95-2% B; 118.1-133 minutes: equilibration at 2% B. The maXis II ETD mass spectrometer (Bruker) was operated with the captive source in positive mode with following settings: mass range: 200 - 2000 m/z, 4 Hz, capillary 1600 V, dry gas flow 3 L/min with 150°C, nano Booster 0.2 bar, precursor acquisition control top20 (CID).

2.11. Proteomics data analysis

MaxQuant (v1.6.1.0) software was used to perform database search and quantitation (149). The database used was obtained from SwissProt (human fasta file downloaded on 06.04.2019 containing 20467 sequences) with the most common protein contaminants added. The allowed false discovery rate for peptide identification, via peptide spectrum matching as well as peptide protein matches was set to 1%. Peptide tolerance was ± 20 and ± 4.5 parts per million for the first and main peptide search, respectively. The allowed product mass tolerance was set to ± 0.5 Dalton. Cysteine carbamidomethylation was set as static modification and whilst methionine oxidation was set as dynamic. The minimum required peptide length was set to six amino acids and maximum number of allowed missed tryptic cleavages was set to two. Match between runs was enabled within a retention time window of 3 minutes and an alignment window of 20 minutes. No intensity threshold for individual spectra was defined in the software. For the statistical analysis of the proteomics data we employed Perseus software (v1.6.15.0) (150). Protein quantitation was based on label free quantitation (LFQ), with a minimum of 2 peptides per protein (unique and razor) defined as quantitation requirement. This resulted in a list of 5548 proteins with their corresponding LFQ values. Identified common contaminants were removed and the resulting matrix was filtered to only contain hits with at least 3 valid values in at least one group (every concentration of each individual FA was considered a group). This reduced the matrix to 3432 proteins. Partial or full missing values inside groups were imputed from normal distribution (downshift 1.8, width 0.5).

Consequently, ANOVA, for the comparison of more than two groups, and Student t-tests, for the comparison of two groups, were performed with the following criteria: p-value of at least 0.05, an S0 of 0.1 and permutation-based FDR set to 5% to correct for multitesting. Venn diagrams shown in this thesis were generated using the BioVenn webtool (151).

2.12. Lipidomics sample preparation

800.000 HepG2 cells were seeded in 6 cm dishes and grown to approximately 80% confluency prior to lipid loading. Following 24h of lipid treatment, cells were washed 3 times with ice cold PBS, scraped off and collected in a glass vials for mass spectrometry samples (Bruckner Analysentechnik GmbH, Austria). Cells were pelleted via centrifugation for 5 minutes with 4000g at 4°C. The PBS supernatant was discarded and 600µL of a 2:1 (vol:vol) chloroform/methanol mix were added. After lysis with a sonication probe at 90% amplitude the internal standard, EquiSPLASH was added, mixed and left on ice for 15 min. After vortexing again, 150µL water added and a Folch extraction with a final chloroform/methanol/water ratio of 8:4:3 (vol:vol:vol) was performed (152,153). Samples were centrifuged for 15min with 7197g at 4°C to induce phase separation. The lower chloroform phase was collected and samples were re-extracted by adding 400µl of a chloroform/methanol/water 2:1:1 (vol:vol:vol) mix. After collecting and merging the chloroform phases, the residual methanol/water phase was collected and dried to perform a protein content estimation via bicinchoninic acid assay (Thermo Fisher Scientific). The dried down lipids were resuspended in 60µL of a 90:5:5 (vol:vol:vol) isopropanol/ethanol/water mixture and were kept at -80°C until measurement.

2.13. LC-MS/MS lipidomics measurement

Lipid samples were analysed by LC/MS. Chromatography was performed with a Dionex Ultimate 3000 (Thermo Fischer Scientific) HPLC equipped with a C8 Waters ACQUITY UPLC BEH column, (pore size 130 Å, particle size 1.7 µm, length 100mm, diameter 2.1 mm, Waters, USA). Separation was carried out at 50°C at a flow rate of 150 µl/min using the gradient: 50-100% B in 42 minutes, hold at 100%B for 8 minutes and equilibration of column for 7 min at 50%B, where solvent A was water with 10mM ammonium formate and 0.1% formic acid and solvent B was a 5:2 mix (vol:vol) of acetonitrile/isopropanol with 10mM ammonium formate and 0.1% formic acid.

The OrbiTrap Velos Pro (Thermo Fisher Scientific) was operated with the ESI source in positive mode and the 10 most abundant ions being selected for CID (154).

2.14. Lipidomics data analysis

The data was analysed employing the Lipid Data Analyser (vers. 2.7.0) in OrbiTrap Velos Pro settings with CID set to +30 eV corresponding to the acquisition settings (155). The complete positive sample table, distributed with the software, was used for identifications. Results were normalized on internal standard as well as on the protein content of the individual samples to compensate for differences in cell amount following the lipid treatment.

2.15. FAME sample preparation and measurement

Lipids from cells and media were extracted as previously described in the section 2.12. lipidomics sample preparation with the exception of the internal standard being pentadecanoic acid (C15:0). In the case of cell culture media samples, a time series was measured to monitor the uptake by the cells, with the individual time points being 0, 3, 6, 12, and 24 hours. The media were used instead of water during the first extraction, and the extraction mix was shaken for an hour at room temperature. 1 µl of a 1mg/ml pentadecanoic acid (C15:0) stock solution was used as internal standard for all FAME samples. The organic phases were collected and dried under a nitrogen stream. Dried samples were re-dissolved in 100 µL MTBE (Methyl tertiary-butyl ether), and 50 µL TMSH (trimethylsulfonium hydroxide) were added for transesterification. Samples were analysed via GC-MS/MS (GCMS-QP2010 SE Shimadzu) equipped with a Zebron ZB-FAME (30 m x 0.25 mm I.D., 0.2 µm film thickness, Phenomenex LTD, Germany) column. Helium was used as the carrier gas at a column flow rate of 1.0 mL/min and constant flow compensation. GC injection temperature and MS transfer lines were set to 250°C. From each sample 1 µL was injected, injection was done splitless. The temperature gradient started at 60 °C which was held for 1 min followed by a temperature increase to 140 °C at a rate of 50 °C/min. Followed by an 8 °C/min increase from 140 to 172 °C, and an increase from 172 to 173.4 °C at a rate of 0.2 °C/min, which again was held for a 1 min. These steps were followed by an increase from 173.4 to 188 °C at a rate of 5 °C/min and an increase from 188 to 191 °C at a rate of 0.2 °C /min, again performing a hold for 1 min. The last step started with an increase from 191 to 220 °C at a rate of 5 °C/min and

a final increase from 220 to 260 °C with a rate of 50 °C/min, resulting in a total analysis time of 40.12 minutes. GC–MS was carried out using 70 eV EI in multiple reaction monitoring (MRM) simultaneously with full scan acquisition in the mass range 45 - 500 m/z. All ions acquired during MRM are listed in the subsequent table.

Compound	RT start	RT end	Ch1 m/z	Ch2 m/z	Ch3 m/z	Ch4 m/z
Methyl octanoate	2.80	4.07	87.00>55.00	87.00>59.00	74.00>59.10	55.00>53.00
Methyl decanoate	4.07	6.06	87.00>55.00	143.00>55.10	143.00>83.10	143.00>101.10
Methyl undecanoate	4.07	6.06	87.00>55.00	169.00>57.00	169.00>71.10	169.00>95.10
Methyl laurate	4.07	6.06	87.00>55.00	183.00>57.10	183.00>71.20	87.00>59.00
Methyl tridecanoate	4.07	6.06	87.00>55.00	143.00>83.10	143.00>55.10	143.00>101.10
Methyl myristate	4.07	6.06	87.00>55.00	143.00>55.10	143.00>83.10	199.00>101.10
Methyl myristoleate	6.06	7.68	208.00>97.10	208.00>111.10	55.00>53.10	208.00>55.10
Methyl pentadecanoate	6.06	7.68	87.00>55.00	213.00>101.10	213.00>73.10	213.00>55.10
Methyl cis-10-pentadecenoate	6.06	7.68	222.00>98.10	55.00>53.10	222.00>111.10	222.00>55.20
Methyl palmitate	7.68	9.77	87.00>55.00	143.00>55.10	143.00>83.10	143.00>101.10
Methyl palmitoleate	7.68	9.77	236.00>97.10	236.00>67.10	236.00>111.00	55.00>53.10
Methyl heptadecanoate	7.68	9.77	87.00>55.00	143.00>83.10	143.00>55.10	143.00>101.10
cis-10-heptadecanoic acid methyl ester	7.68	9.77	55.00>53.00	250.00>111.00	250.00>98.10	250.00>55.00
Methyl stearate	9.77	10.99	87.00>55.00	143.00>55.10	143.00>83.10	143.00>101.10
trans-9-elaidic acid methyl ester	9.77	10.99	83.00>55.10	55.00>53.10	83.00>68.10	296.00>213.00
cis-9-oleic acid methyl ester	9.77	10.99	83.00>55.10	264.00>79.00	55.00>53.10	264.00>97.20
Methyl linolelaidate	10.99	12.28	82.00>67.10	95.00>67.10	81.00>79.10	95.00>55.10
Methyl linolenate	13.13	14.29	79.00>77.10	93.00>77.00	95.00>67.10	79.00>51.10
Methyl arachidate	13.13	14.29	87.00>55.00	283.00>101.10	283.00>73.20	87.00>59.00
cis-11-Eicosenoic acid methyl ester	14.29	15.46	83.00>55.10	292.00>67.00	292.00>98.00	292.00>95.00
cis-11,14-Eicosadienoic acid methyl ester	15.46	16.78	82.00>67.10	95.00>67.10	81.00>79.10	95.00>55.10
Methyl heneicosanoate	15.46	16.78	87.00>55.00	143.00>55.10	143.00>83.20	143.00>101.10
cis-8,11,14-Eicosatrienoic acid methyl ester	16.78	17.51	79.00>77.10	79.00>51.10	81.00>79.10	80.00>77.00
Methyl arachidonate	17.51	18.25	79.00>77.10	79.00>51.10	91.05>65.10	119.05>91.10
cis-11,14,17-Eicosatrienoic acid methyl ester	17.51	18.25	79.00>77.10	93.00>77.10	79.00>51.10	93.00>91.10
Methyl behenate	18.25	18.89	87.00>55.00	354.00>101.00	354.00>73.10	354.00>55.10
Methyl erucate	18.89	19.54	83.00>55.10	320.00>79.00	320.00>95.00	320.00>98.00
cis-5,8,11,14,17-Eicosapentaenoic acid methyl ester	19.54	20.33	79.00>77.10	91.00>65.10	93.00>77.10	79.00>51.10

cis-13,16-Docosadienoic acid methyl ester	20.33	40.00	95.00>67.10	81.00>79.10	95.00>55.10	81.00>53.10
Methyl tricosanoate	20.33	40.00	87.00>55.00	325.00>101.10	325.00>73.00	87.00>59.10

Table 1 GC/MS multi reaction monitoring settings of fatty acid methyl esters. Channels 1-3 refer to different precursor product ion transitions.

2.16. FAME data analysis

Due to the instability of Shimadzu's provided outdated GC/MS software on modern computers, data analysis was performed in Skyline 64-bit (vers. 21.2.0.369) utilizing the data table of the MRM setup for compound classification (156). Automated peak picking and separation of isomers only defined by retention time shift and not individual fragments, such as the 18:1 isomers oleic and elaidic acid, was controlled manually prior to data export. A dilution series of the Supelco 37-Component Fame Mix (Sigma, Vienna, Austria) was used to determine absolute concentrations of individual FAs.

3. Results

3.1. Impact of fatty acids on cell growth

The performed growth assay with HepG2 cells revealed a strikingly similar dose dependent decline of growth rates following treatment with either MA or PA, compared to cells receiving only BSA serving as negative control (Fig. 15). OA influenced the cellular growth rates only at the highest concentration used in our setup, being 500 µM. Prevention treatments (PTs), were our mixed treatments of MA or PA with OA at ratios of 1:1 (125 µM: 125 µM) or 2:1 (250 µM: 125 µM) respectively, resulted in restoration of the growth rate, abolishing completely the negative impact of the saturated FFAs on cell growth. This preservative feature of OA has been previously reported in Chinese hamster ovary cells (157).

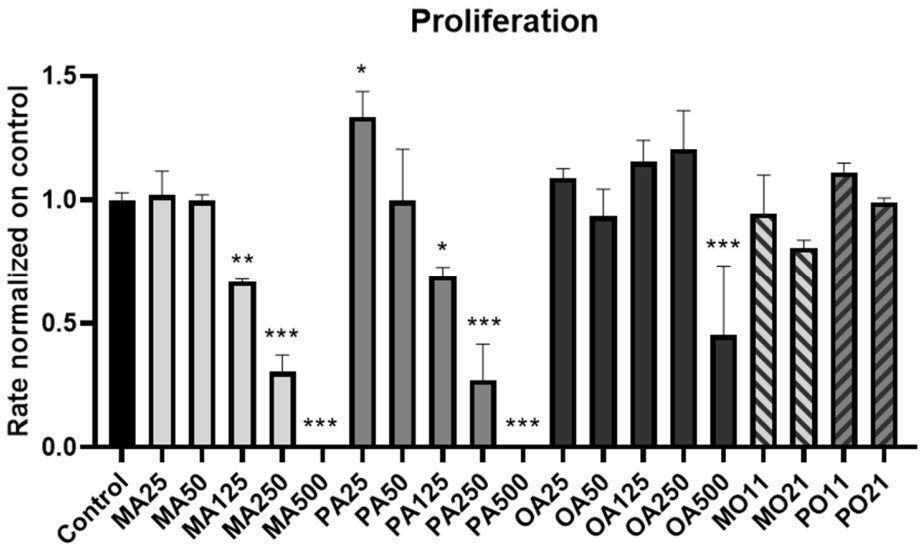

Figure 15 Growth analysis of HepG2 cells treated with FFAs and imaged every hour for 120 hours total. Conditions are labelled as fatty acid and concentration used in µM (MA myristic acid; PA palmitic acid; OA oleic acid) The prevention treatments indicate both fatty acids and the ratio (MO myristic and oleic acid; PO palmitic and oleic acid; 11 125 µM:125 µM; 21 250 µM:125 µM). The confluency was calculated and plotted over time. The maximum inclination of the resulting function was determined as growth rate readout. Rates presented are a mean out of 7 random positions per well of at least 3 biological replicates. Figure adapted from Gindlhuber et al. 2022 with permission from the publisher. ($p < 0.05$ (*); $p < 0.01$ (**); $p < 0.001$ (***) compared to control)

3.2. Impact of fatty acids on LD formation

We measured the LD content of HepG2 cells 24 hours after the FA treatment to assess their amount of stored neutral fats. Supplementation with OA induced an increase in the average LD volume per cell in a concentration-dependent manner (Fig. 16). Both saturated FAs led to an increased number

of LDs per cell compared to control but failed to significantly increase LD volume (Fig. 16). Most of the PTs showed an increase in LD volume compared to treatments with any FA alone with the exception of PO11.The respective LD volume levels of the combined treatments were comparable to a 250 µM OA (OA250) treatment, which is double the amount we would expect from the OA present in the PTs (125 µM). The only exception as mentioned is the 1:1 mixture of PA and OA (PO11) treatment, where no increase above the LD volume expected from 125 µM OA (OA125) alone could be observed.

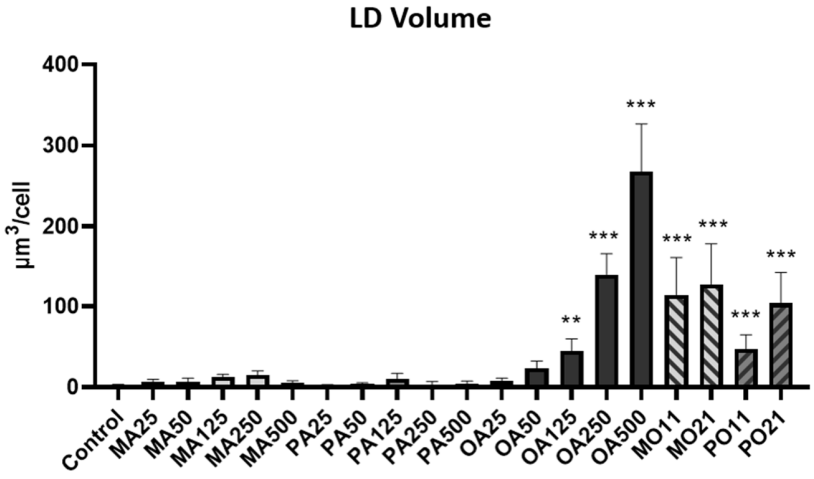

Figure 16 Lipid droplet volume analysis of HepG2 cells treated with FA-BSA conjugates for 24 hours. Conditions are labelled as fatty acid and concentration used in µM (MA myristic acid; PA palmitic acid; OA oleic acid) The prevention treatments indicate both fatty acids and the ratio (MO myristic and oleic acid; PO palmitic and oleic acid; 11 125 µM:125 µM; 21 250 µM:125 µM). LD volume per cell was calculated from at least 10 randomly chosen positions for each condition with a total of 1793 cells been analyzed. Figure adapted from Gindlhuber et al. 2022 with permission from the publisher. ($p < 0.05$ (*); $p < 0.01$ (**); $p < 0.001$ (***) compared to control)

3.3. Fatty acid specific proteome changes

We performed an LFQ proteomics LC/MS analysis to determine changes to the proteome composition, introduced following the treatment of HepG2 cells with different concentrations of varying FAs or combinations for 24 hours. Tested groups and concentrations for the setup included MA, PA and OA at 125 µM, 250 µM and 500 µM concentration as single FA treatments and combinations of MA or PA with OA at a 1:1 (125 µM each) or 2:1 (250 µM: 125 µM) ratio termed PTs (n=3 biological replicates in each group). After removal of contaminants and filtering for 3

valid values in at least one group, each group represents one concentration of any FA single or prevention treatment, 5,322 proteins were reliably identified in our dataset (FDR of 0.01).

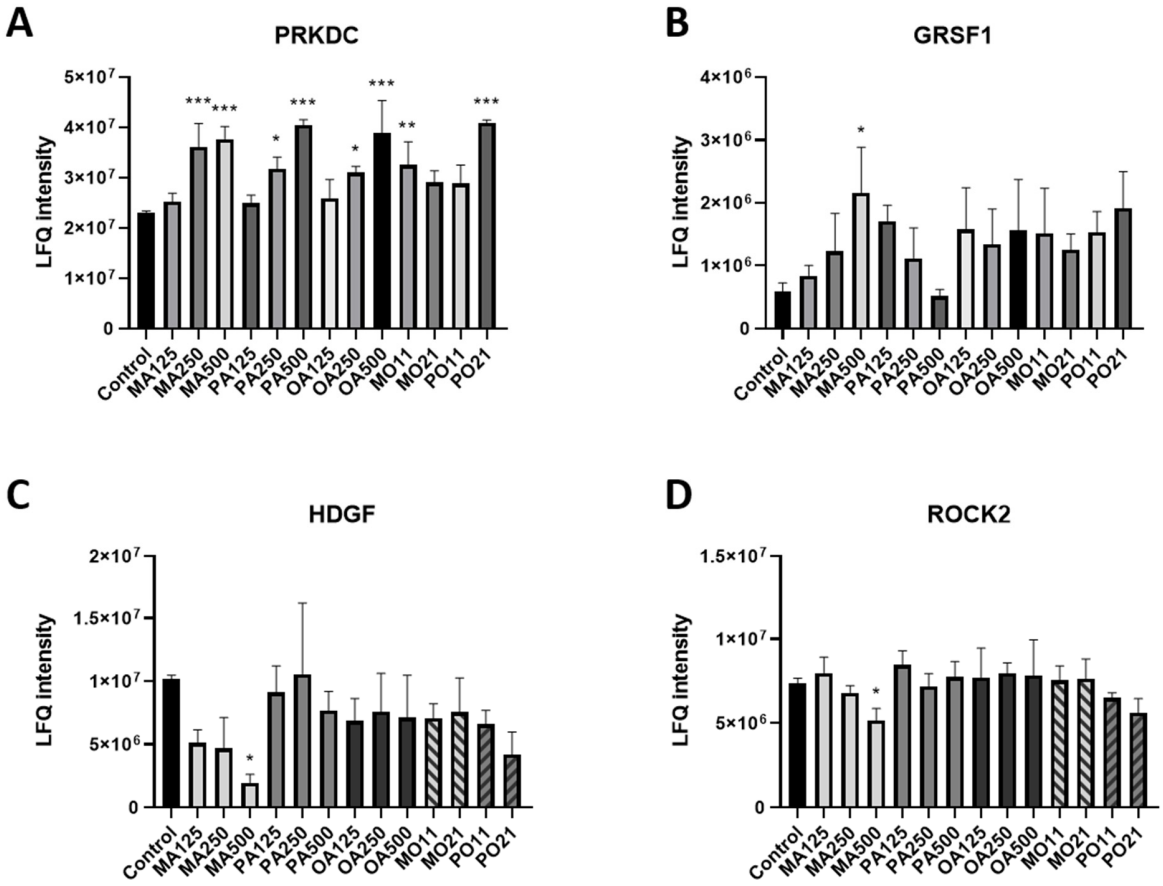

Figure 17 Observed proteome abundance changes following a 24-hour treatment period with either single free fatty acids or prevention treatments. A) PRKDC protein levels B) GRSF1 protein levels C) HDGF protein levels D) ROCK2 protein levels. ($p < 0.05$ (*); $p < 0.01$ (**); $p < 0.001$ (***) compared to control)

Single FFA treatments were compared to the BSA control and statistically significant protein abundance alterations were determined via ANOVA analysis with S0 set to 0.1 and employing a permutation-based FDR of 0.05 with 250 randomizations. The PTs were compared to their corresponding saturated FFA concentration using a two-sided Student t-test, again with S0 set to 0.1 and a permutation-based FDR of 0.05 with 250 randomizations. This resulted in an overall list containing only 38 significantly altered proteins. Most of the proteins which displayed a significantly altered expression, did so following saturated FA treatment. 23 after MA, 10

following PA treatment as well as 6 in the PTs. And only a single protein was significantly altered in all of the different treatments and this was PRKDC, a protein associated with sensing DNA damage and required for double strand break repair (Fig. 17A). Moreover, the two saturated FAs appeared to regulate GRSF1, a regulator of mitochondrial gene expression, in opposite directions. MA led to a dose dependent increase, whereas protein levels for PA peaked at 125 µM with a 2.9-fold upregulation compared to the control, followed by a dose dependent reduction at higher concentrations (Fig. 17B). Interestingly, HDGF and ROCK2, two proteins involved in cell cycle progression, exhibited a dose dependent decline only following MA treatment (Fig. 17 C, D). To create an overview, Venn diagrams including proteins with a fold change of $\geq \pm 1.5$ were generated and the results compared (Fig. 18). To identify potential significantly altered protein networks and or biological processes, String and GO analysis were performed for the 500 µM treatments of single FFAs loading all proteins with a $\geq \pm 1.5$-fold change compared to control. The same was done for the 21 PTs using proteins which exhibited a $\geq \pm 1.5$-fold change compared to the respective single FFA treatments. Data was loaded into the STRING webtool and analyses was performed with the minimum required interaction score set to 0.7 (high confidence) and unconnected nodes removed. MA treatment showed upregulated protein clusters connected to mitochondrial biogenesis and cellular respiration whilst down-regulated cytoplasmic translation (App. 2, 3). These results were similar to PA treatment, except that the latter lacked the cluster with GO terms indicating increased oxidative phosphorylation (App. 4, 5). OA induced overall less changes indicating increased mitochondrial biogenesis and diminished cytosolic translation (App. 6, 7). PTs containing MA and OA did not only recover cytoplasmic translation but even indicated a further increase in oxidative phosphorylation (App. 8, 9). PTs containing PA and OA did not display a cluster for cytoplasmic translation but indicated an increase in the mitochondrial electron transport chain (App. 10, 11).

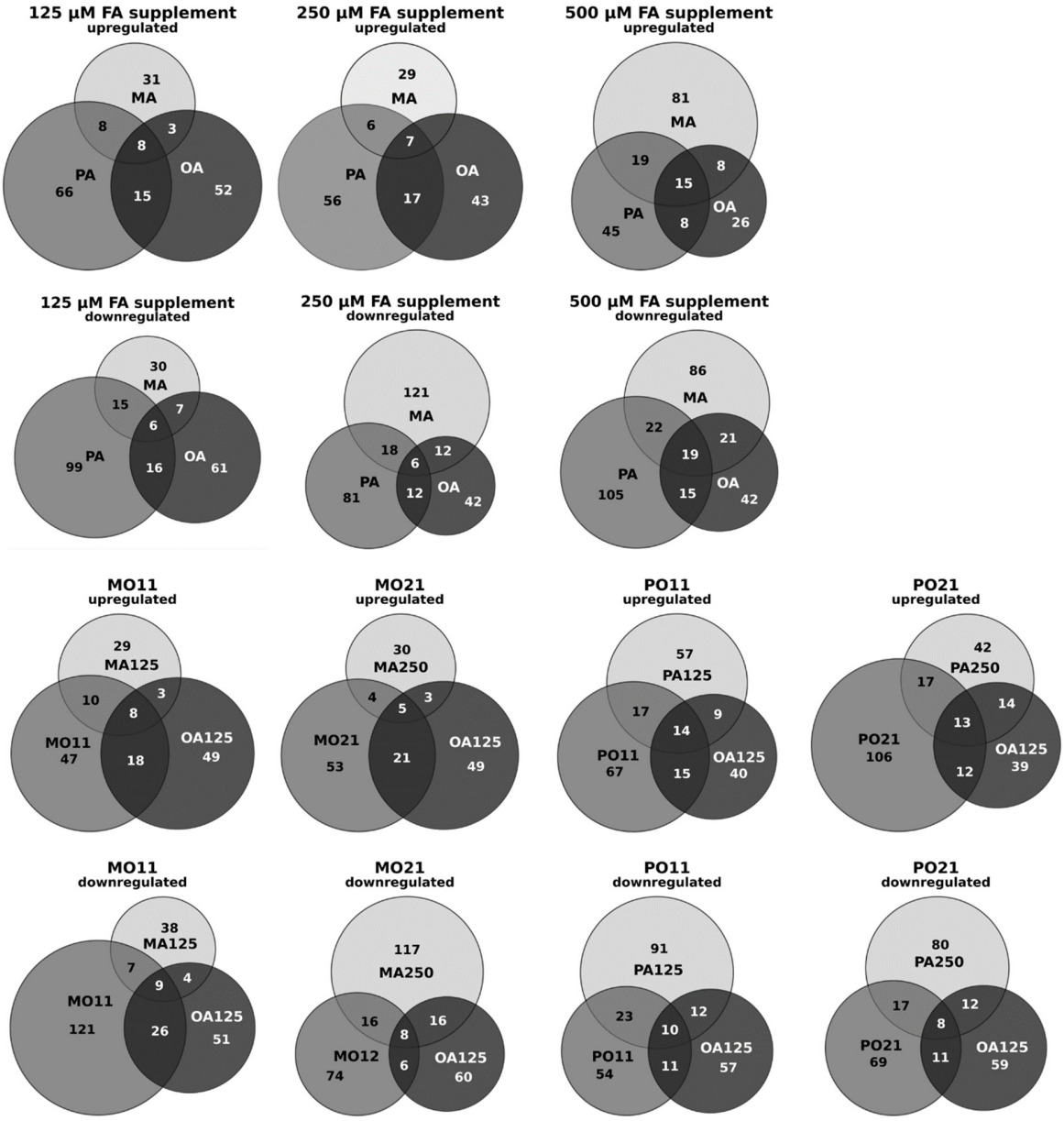

Figure 18 Comparison of fatty acid treatment specific proteome changes. Conditions are labelled as fatty acid and concentration used in µM (MA myristic acid; PA palmitic acid; OA oleic acid, MO myristic and oleic acid; PO palmitic and oleic acid; 11 125:125 µM; 21 250:125µM). Venn diagrams displaying the overlap of proteins with a fold change of ≥ ± 1.5 compared to control after single FFA or PTs for 24 hours. Figure adapted from Gindlhuber et al. 2022 with permission from the publisher.

3.4. Fatty acid specific effects on cell cycle and viability

As a follow up on the observed MA specific alteration of regulatory cell cycle proteins we performed a flow cytometry analysis-based cell cycle and viability analysis of all FFA treatments. It was found that cell cycle progression was impaired throughout all single FFA treatments at the highest tested concentration of 500 µM. But we could corroborate that the only FA displaying an effect on cell cycle progression at lower concentrations was MA. The number of cells in G2 phase was found to be reduced from 22.1% to 13.5% already at a concentration of 125 µM (Fig.19 A).

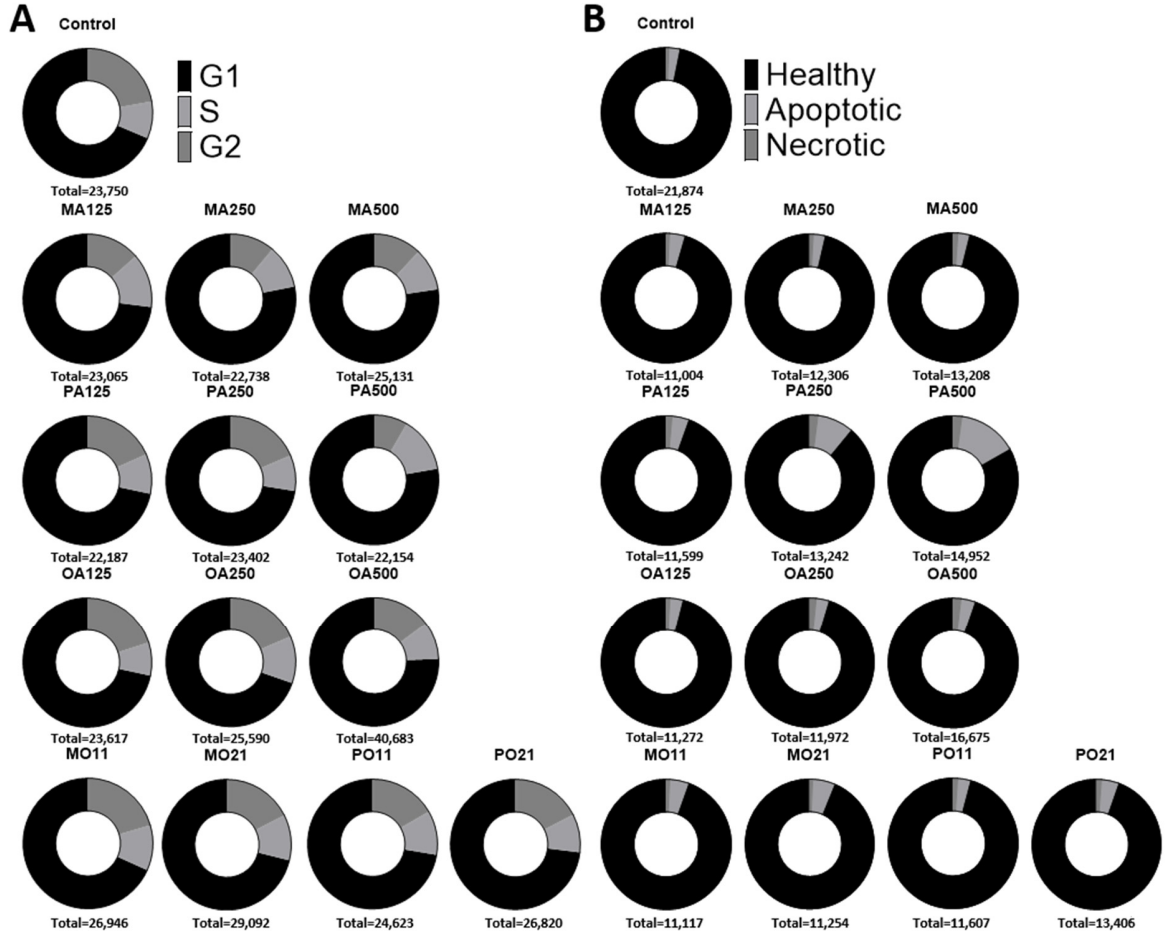

Figure 19 Cell cycle and apoptosis/necrosis assay of HepG2 cells after 24 hour of lipid loading. A) For the cell cycle analysis cells were stained with Hoechst 33342.Only cells treated with myristic acid display a decrease of cells in G2 phase at low concentrations. B) For the apoptosis/necrosis analysis cells were stained with propidium iodide and Annexin V FITC 24 to examine the integrity of the cell wall as well as possible externalization of phosphatidylserine. An increase of apoptotic cells can be observed following the treatment with palmitic acid. Figure adapted from Gindlhuber et al. 2022 with permission from the publisher.

In addition, a propidium iodide and annexin V staining was used to differentiate between necrotic cells, which are only positive for propidium iodide marking the cell membrane as compromised, and apoptotic cells, which have externalised PS. Opposite to their effect on cell cycle progression no general impact of higher doses of FFAs on the viability could be observed. Exclusively treatment with PA resulted in an increase of apoptotic not necrotic cells (Fig. 19B). Compared to 2.5% in the BSA control, the percentage of apoptotic cells following PA treatment rose to 4.0, 9.0 and 14.6% for the respective concentrations 125, 250 and 500 µM. Both, MA´s suppression of cell cycle progression and PA's induction of apoptosis, were observed to be fully abolished in the PTs.

3.5. Correlation of potential cellular lipotoxicity protein biomarkers to hepatic cellular carcinoma gene expression and survival

All proteins which were found to be significantly altered following a single FA treatment in at least one condition were manually examined if a dose depend effect could be observed or not. If either an increase or decrease in protein abundance was present, the levels of corresponding PTs were checked for their behaviour. If they rose or sank in tandem to the single FA, the protein was determined to not be of interest. However, if the PTs kept the protein levels comparable to the control treatments, the protein was considered a possible readout for lipotoxicity. This process revealed six proteins of interest (Fig. 20 A). Namely A2M, a mediator of acute phase response and SERPINA3, an acute phase protein itself, which are of high importance on tissue level and possibly mediating the local inflammatory response, but should not influence the cultured hepatocytes themselves. The other four identified proteins had in common that they are involved in transcriptional activity and one of them H2AFY, has recently been described as a promising biomarker candidate for HCC patients. Since HCC is a potential terminal outcome of NAFLD, we compared mRNA expression levels of healthy against HCC tissue for the three remaining identified proteins, DNTTIP2, ZNF326 and LMO7, next to the published HCC biomarker candidate H2AFY in data from the cancer genome atlas liver hepatocellular carcinoma database (n = 50; Fig. 20 B, last accessed Nov. 29, 2021). For DNTTIP2 no difference in expression between HCC and healthy liver tissue could be found, although its expression correlated with the survival rate of HCC

patients. On the other hand, the 3-year survival rate for ZNF326 was not affected despite

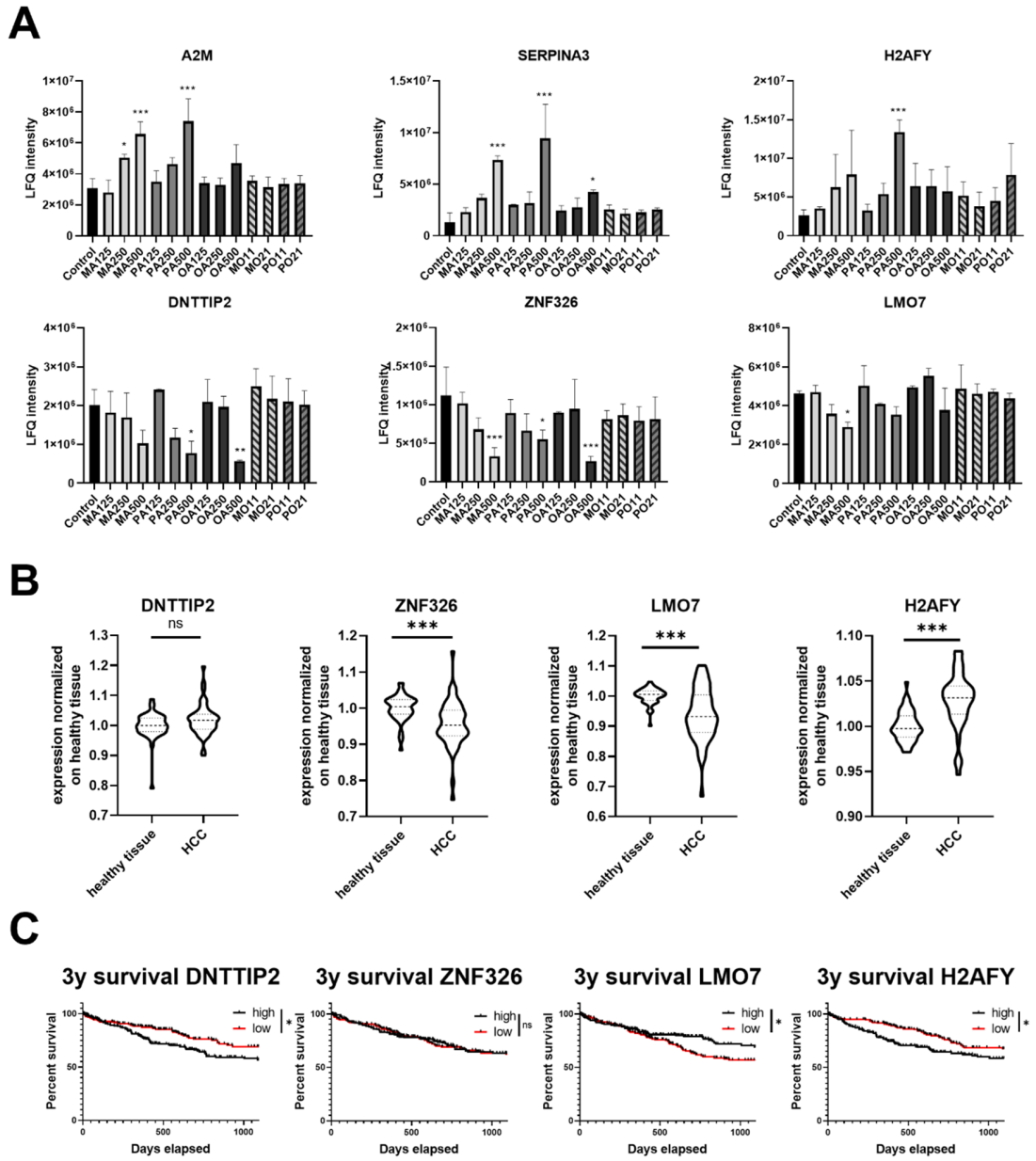

Figure 20 Proteins regulated by saturated fatty acids, their gene expression and correlation with survival in hepatocellular carcinoma. Conditions are labelled as FA and concentration used in µM (MA myristic acid; PA palmitic acid; OA oleic acid) The PTs indicate both fatty acids and the ratio (MO myristic and oleic acid; PO palmitic and oleic acid; 11 125:125 µM; 21 250:125 µM). A) The six proteins which were found to show a dose dependency between protein expression levels and the impact on viability as well as a regression to control levels in the prevention treatments B) mRNA expression levels of healthy tissue compared to HCC samples for the four proteins involved in transcription C) Kaplan Meier plots of the 3-year survival rate of HCC patients p < 0.05 (*); p < 0.01 (**); p < 0.001 (***). Figure adapted from Gindlhuber et al. 2022 with permission from the publisher.

being differentially expressed in HCC, thus carrying no prognostic value (Fig. 20 C). LMO7 was the only protein next to the previously described H2AFY found to display changes on protein level following FA treatment as well as being differentially expressed on mRNA level in HCC patients and exhibiting a significant difference in the survival rate (although in opposite direction).

3.6. Fatty acid specific changes to the lipidome

To determine the impact of the added FAs on the lipidome we monitored different lipid species in the cell utilizing a reversed phase LC-MS/MS approach. 24 hours after the lipid loading, the cells were harvested and the organic phase from the Folch extraction was used for MS measurement. The protein content of each sample was determined and used as a second normalization step to account for the variations in cell density at the point of harvest especially following PA treatment. Both saturated FAs led to a dose-depended increase in CER, SL, DG and PL, represented by PC and PE (Fig 21 A, B, C, E, F). Of all the groups, only DGs proved to be also elevated following OA treatment. OA almost exclusively led to elevated TG levels (Fig 21 D). TGs were also the group which exhibited a completely different trend between the two saturated FA. Whilst myristic acid exposure exhibited a significant increase in measured TG content after surpassing 125 µM, no change compared to the control ratios could be found for PA at any concentration tested. PTs reduced the levels of CER, SL as well as PC and PE so that they were again comparable to the control or OA treatments (Fig. 22 A, B, E, F). DG levels proved ameliorated but were on average still three times higher than control. However, these levels were now in range of what could be observed following OA treatments (Fig. 22 C). TG levels for PTs with PA displayed a fourfold increase, however the further increase of PT with MA was less pronounced (Fig. 22 D). Heat maps breaking down alterations of the lipid classes on individual species level can be found in the appendix.

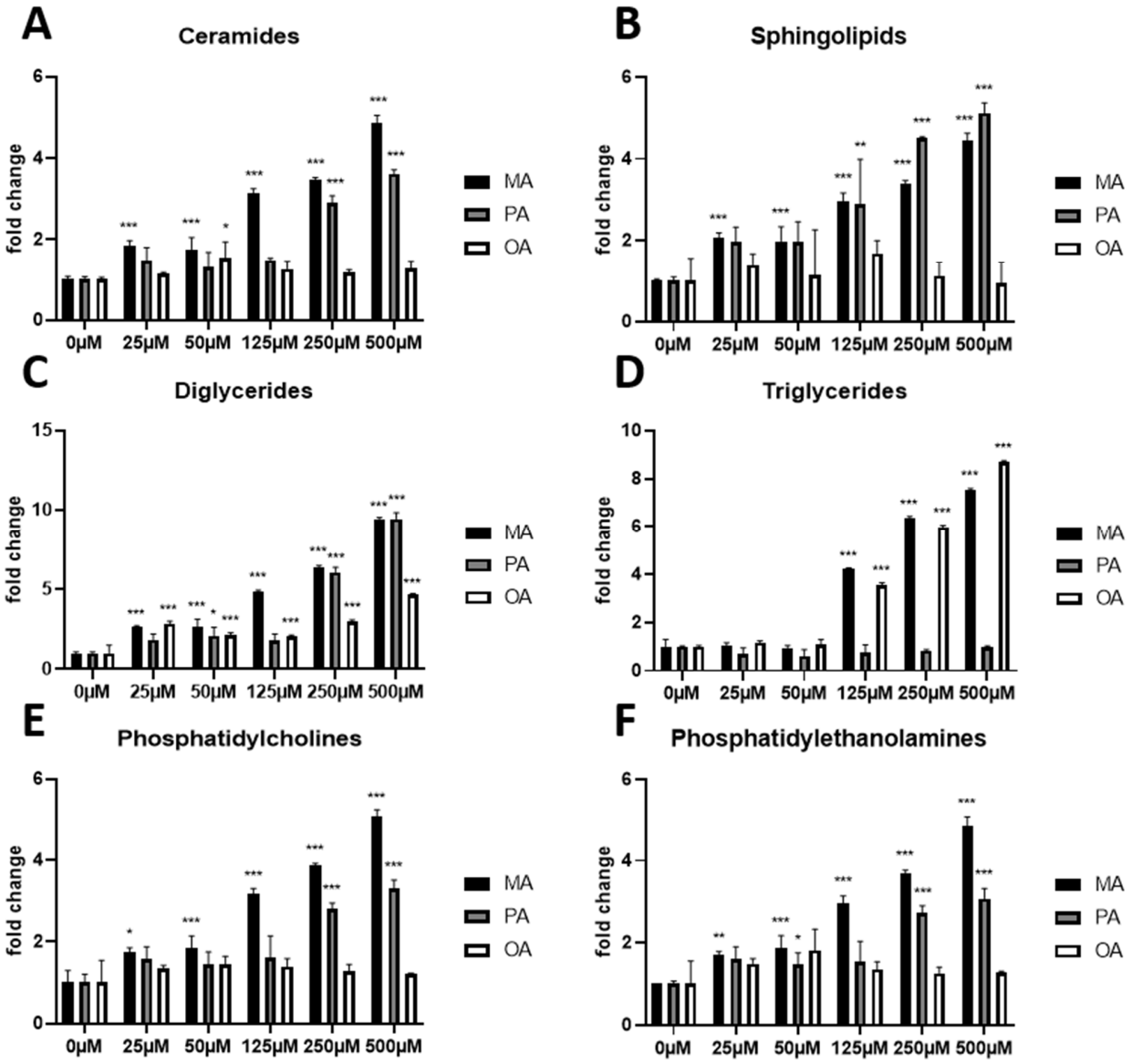

Figure 21 Alterations in the abundance of lipid classes following 24 hours of FA treatment. Results were normalized on internal standard and protein content of the individual sample. A) Ceramides display an immediate response to saturated fatty acid supplementation. B) Sphingolipids display a dose dependent increase in direct correlation to the saturated fatty dose. C) The accumulation of diglycerides intermediates is more pronounced following saturated fatty acid treatment. D) An increase in triglyceride levels was only observed following treatment with either myristic or oleic acid. Palmitic acid did not influence triglyceride levels. E, F) The phospholipids phosphatidylserine and phosphatidylcholine displayed a dose dependent increase in direct correlation to the amount of saturated fatty acid supplemented, in both cases it was however less pronounced in the case of palmitic acid supplementation. ($p < 0.05$ (*); $p < 0.01$ (**); $p < 0.001$ (***) compared to control)

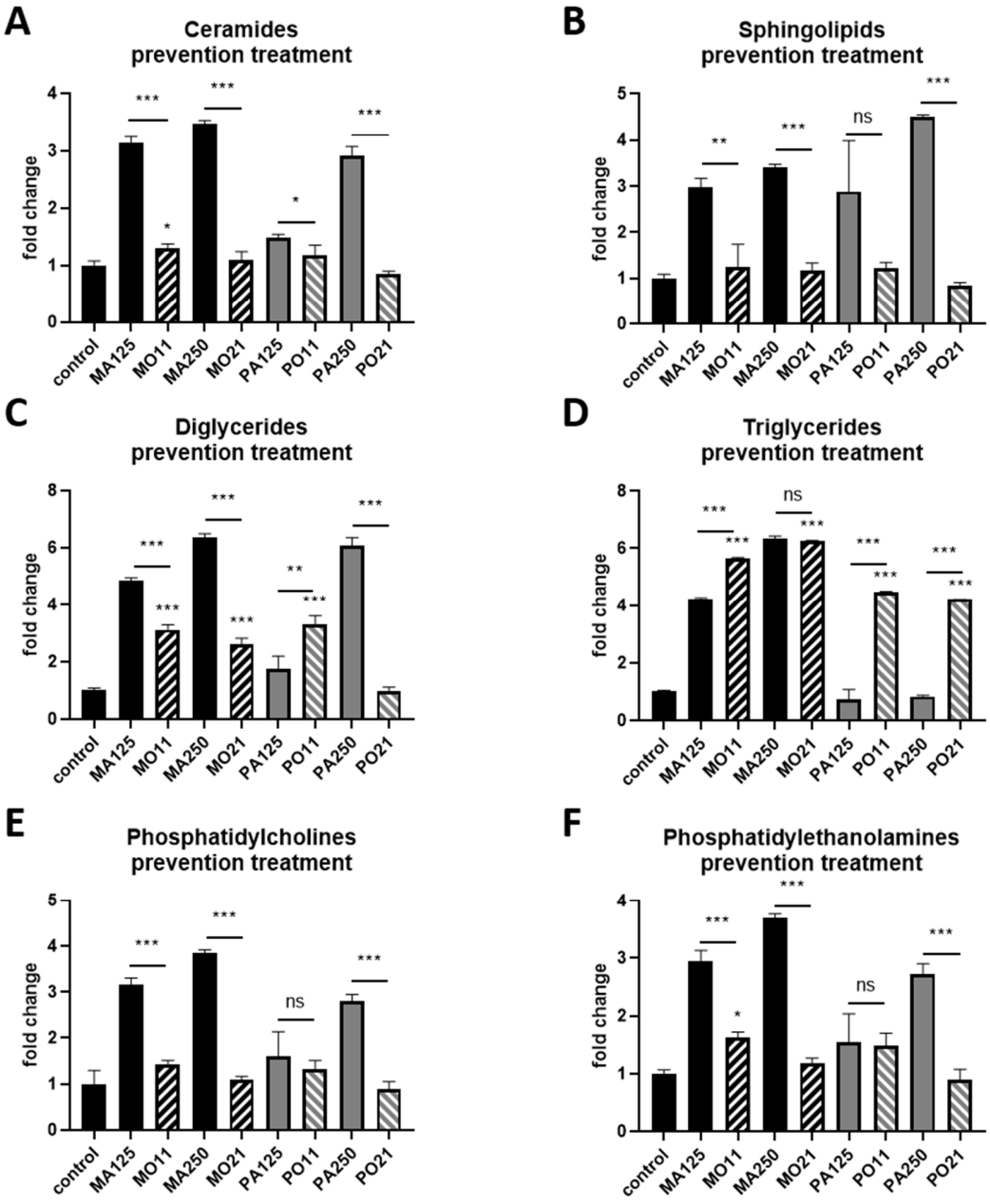

Figure 22 Alterations in the abundance of lipid classes following 24 hours of prevention treatments. For the sake of comparison, the results of the saturated fatty acids were put ahead of the corresponding prevention treatment. Results were normalized on internal standard and protein content of the individual sample. Stars directly over the treatment refer to statistically significant differences between the individual treatments compared to control group, whilst dashes refer to results in-between the two connected groups. A, B) the levels of ceramides as well as sphingolipids return to basal conditions in prevention treatments. C) Diglycerides levels overall seem reduced in prevention treatments compared to the treatments with saturated fatty acids alone but on average do not return to control levels. D) Triglycerides increase 4-fold in the prevention treatments with palmitic acid, however the increase in prevention treatments including myristic acid is minor. E, F) The elevated levels of phospholipids return to control levels in prevention treatments for both saturated fatty acids. Conditions are labelled as FA and concentration used in µM (MA myristic acid; PA palmitic acid; OA oleic acid). The PTs indicate both fatty acids and the ratio (MO myristic and oleic acid; PO palmitic and oleic acid; 11 125:125 µM; 21 250:125 µM; $p < 0.05$ (*); $p < 0.01$ (**); $p < 0.001$ (***); not statistically significant (ns)).

3.7. Fatty acid uptake

Media aliquots were taken during the 24-hour time period of the lipid treatment (at 0h, 3h, 6h, 12h and 24h) to determine the amount and rate of the individual FA uptake. The base level concentration of MA in the media was determined to be below 0.3 µg/ml with a maximum measured uptake of 3.02 µg/ml/h per 100.000 cells (Fig. 23 A). The uptake dynamics of MA changed with increasing concentrations as the 25, 50 and 125 µM treatment resulted in almost no uptake during the first 3 h with an increase after 6 h while 250 and 500 µM led to an immediate uptake of MA by the cells. The base level PA concentration in the media was determined to be 67.2 µg/ml with a measured maximum hourly uptake of 13.3 µg/ml/hour per 100,000 cells (Fig. 23 B). All PA treatments show a dose dependent decline of uptake over time indicating an immediate import without the delay phase as seen for the lower MA concentrations. With a basal concentration of 28.3 µg/ml OA was right in between the two saturated FAs tested and a maximum measured uptake of 5.3 µg/ml/h per 100,000 cells (Fig. 23 C). While the higher concentrations of OA treatment exhibited the same delay as the lower MA concentrations, the 25 and 50 µM treatment experienced their highest uptake already within the first 3 hours of the experiment. All plates were around 80% confluent at the time the uptake assay began, equaling around 300.000 cells. MO PTs did not exhibit altered uptake dynamics for MA but displayed an increase of maximum OA uptake after 6h to twice the level observed in the 125 µM OA treatment (Fig. 24 A, B, C). PO PTs did exhibit altered uptake dynamics for PA as well as OA (Fig. 25 A, B, C). While PA uptake came to an arrest at the 6h time point OA was taken up by the cells immediately, without the otherwise observed delay.

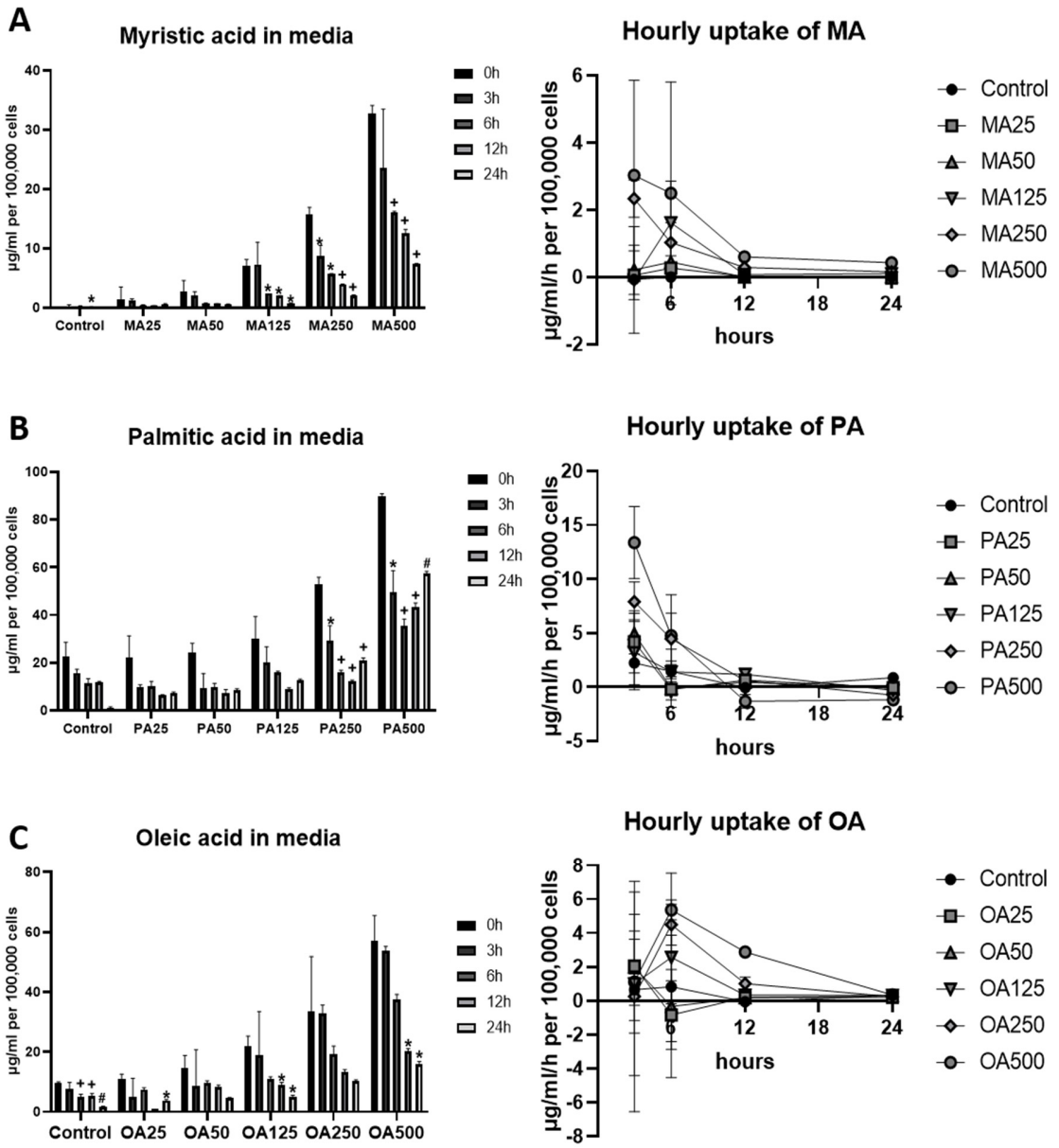

Figure 23 Analysis of individual FA levels in the medium of respective treatment conditions with GC-MS. Absolute quantification was performed with comparison to a Supelco 37-Component Fame Mix dilution series. Columns represent means of 3 biological replicates. XY plots show FA uptake per hour depending on concentration, dots represent means of 3 biological replicates. A) Cells treated with myristic acid display a continous time dependent uptake with a maximum of 3.02 µg/ml/100.000 cells following MA500 treatment. The uptake dynamics depend on the concentration, with concentrations up to 125 µM exhibiting a delay with the maximum uptake only being observed after 6 hours. B) Cells treated with PA acid did not exhibit a uniform uptake. Following an initial decrease due to cellular uptake, high dosage treatments such as 125, 250 and 500 µM show an increase of PA in the media at later timepoints, most likely as a result of increased apoptosis. Uptake dynamics show the same trend in all treatments with the highest hourly rate of 13.3 µg/ml/100.000 cells in PA 500 s. C) OA levels in the media deplete continously over time. However uptake dynamics reveal a general delay of oleic acid uptake with a maximum of 5.3 µg/ml/100.000 cells observed after 6 hours in OA500 treatment. Conditions are labelled as FA and concentration used in µM (MA myristic acid; PA palmitic acid; OA oleic acid; 2way ANOVA results indicated as p < 0.05 (*); p < 0.01 (+); p < 0.001 (#) compared to time point 0h within group).

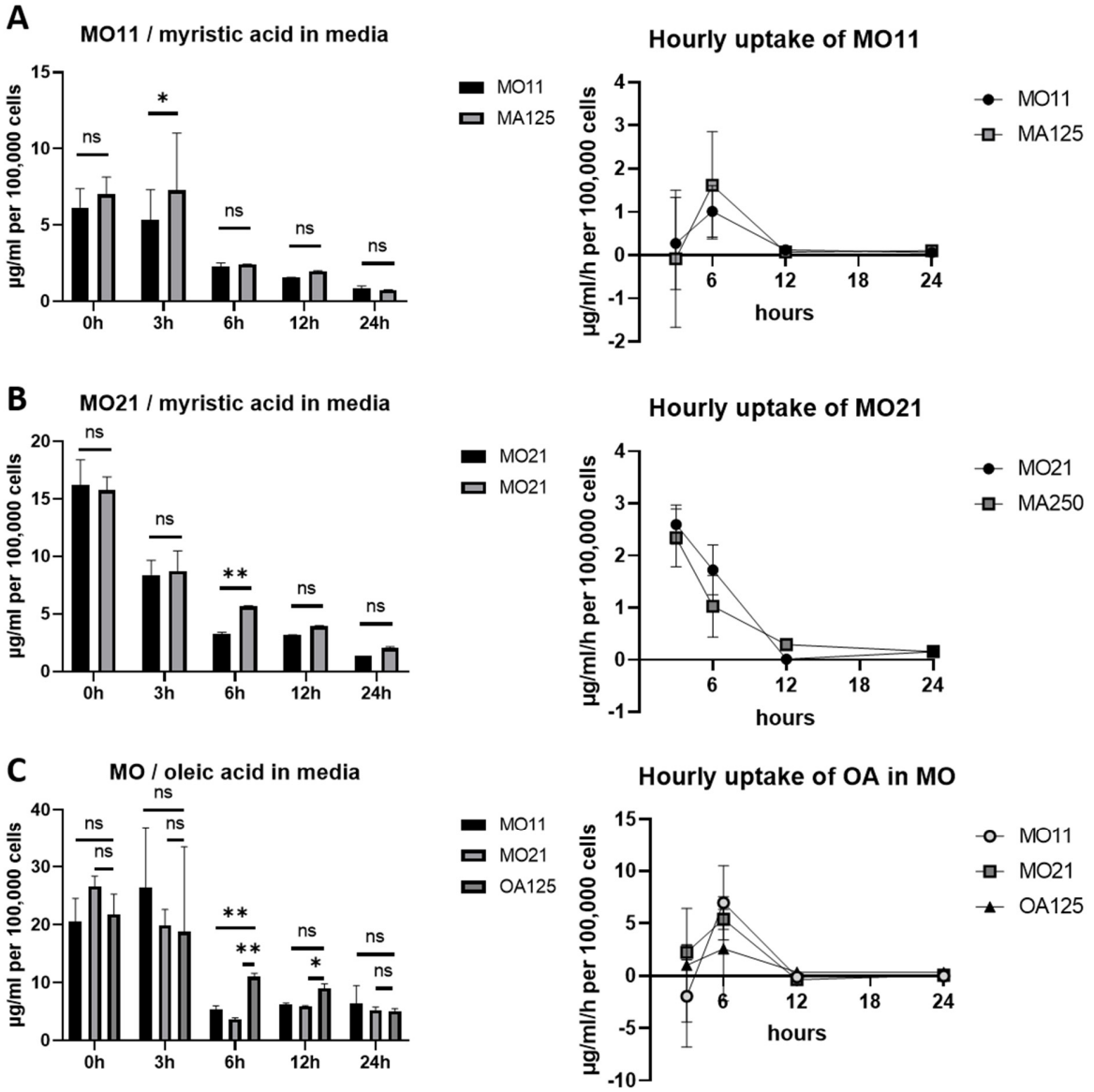

Figure 24 Analysis of individual FA levels in the medium of respective treatment conditions with GC-MS. Conditions are labelled as FA and concentration used in µM (MA myristic acid; OA oleic acid). The PTs indicate both fatty acids and the ratio (MO myristic and oleic acid; 11 125:125 µM; 21 250:125 µM). Columns represent mean of 3 biological replicates. XY plots show FA uptake per hour depending on concentration, dots represent means of 3 biological replicates. A) Comparison of MA levels in 1:1 PT compared to the uptake of single 125 µM FA treatment. B) Comparison of MA levels in 2:1 PT compared to the uptake of single 250 µM FA treatment. C) Comparison of OA levels in 1:1 and 2:1 PTs compared to the uptake of single 125 µM OA treatment. The uptake dynamics of MA in the PTs presents largely unchanged in A and B. For OA the observed maximum uptake was still delayed at 6 hours but doubled compared to single FA treatment. (2way ANOVA results indicated as p < 0.05 (*); p < 0.01 (**); p < 0.001 (***); not statistically significant (ns); compared groups within each time point are indicated with a dash)

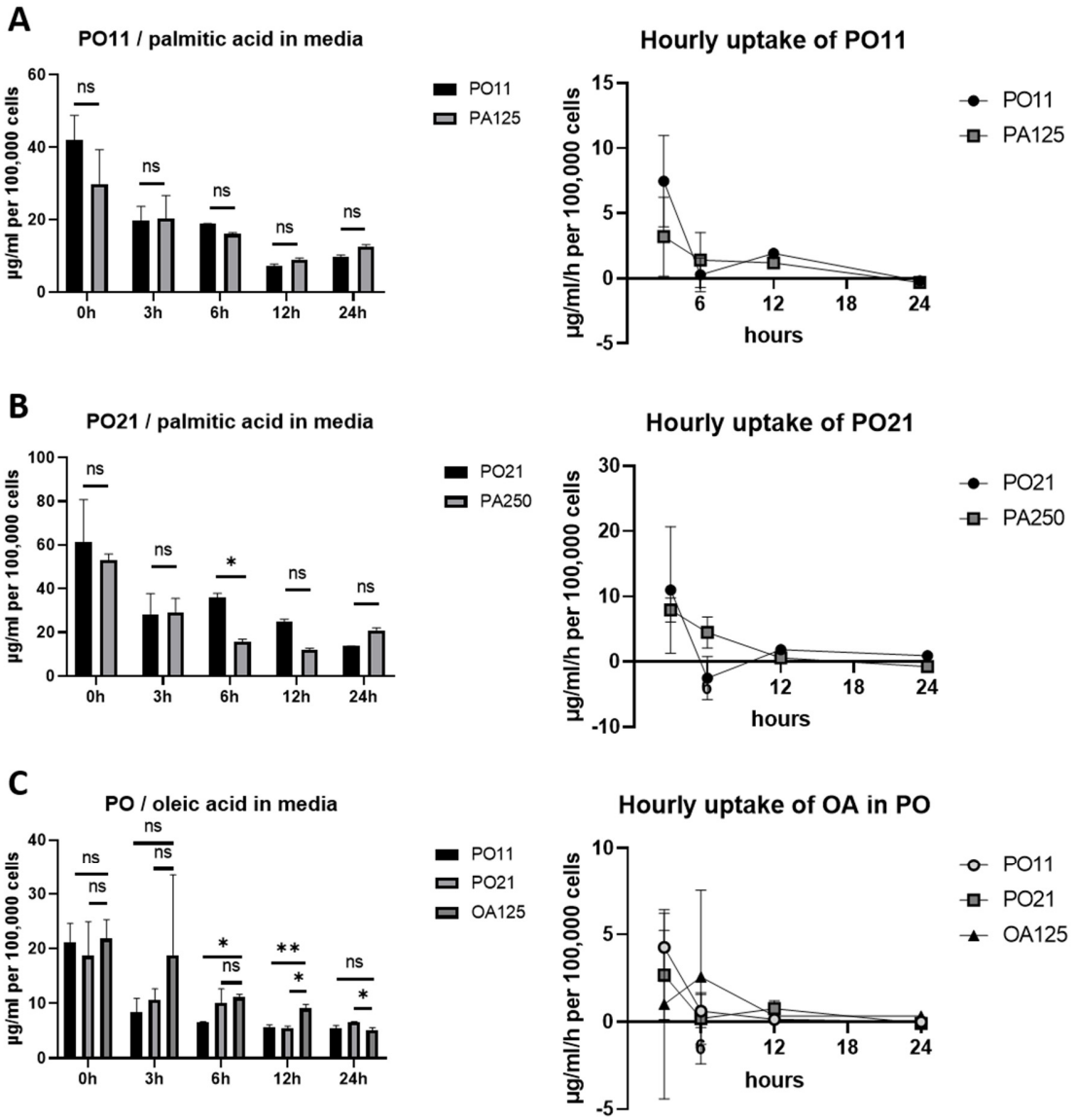

Figure 25 Analysis of individual FA levels in the medium of respective treatment conditions with GC-MS. Conditions are labelled as FA and concentration used in µM (PA palmitic acid; OA oleic acid). The PTs indicate both fatty acids and the ratio (PO palmitic and oleic acid; 11 125:125 µM; 21 250:125 µM). Columns represent means of 3 biological replicates. XY plots show FA uptake per hour depending on concentration, dots represent means of 3 biological replicates. A) Comparison of PA levels in 1:1 PT compared to the uptake of single 125 µM FA treatment. B) Comparison of PA levels in 2:1 PT compared to the uptake of single 250 µM FA treatment. C) Comparison of OA levels in 1:1 and 2:1 PTs compared to the uptake of single 125 µM OA treatment. The Uptake dynamics of PA in the PTs is changed slightly in A and prominently in B with uptake coming to a halt at the 6 h time point. For OA the observed maximum uptake was now already at the 3 h, implicating a complete change to the otherwise delayed uptake kinetics of OA. (2way ANOVA results indicated as $p < 0.05$ (*); $p < 0.01$ (**); $p < 0.001$ (***); not statistically significant (ns); compared groups within each time point are indicated with a dash)

4. Discussion

To establish a baseline for the lipid treatment regime HepG2 cells were incubated with increasing concentrations of the three common FAs individually. The following five concentrations 25 µM, 50 µM, 125 µM, 250 µM and 500 µM were chosen to be used in further experiments, based on the rationale that at the 500 µM concentration no further growth was detected for both saturated FAs while also the unsaturated OA started to exhibit adverse growth effects in our assays, and the treatment parameters were still within reported human serum concentrations (145).

In the growth analysis the two saturated FAs, MA and PA, presented with an almost identical, strictly dose dependent decline of growth rates, culminating at the highest dose of 500 µM where no further growth could be detected (Fig. 15). The treatment with 25 µM of PA was the only outlier, by inducing a significant increase of cellular growth rates out of all the concentrations and combinations tested. For OA no such trend could be observed except a decline of about 50% at the highest concentration. Previous research in CHO cells by Listenberger et al. had indicated, that the observed lipotoxicity of saturated FA could be ameliorated via a co-treatment with an unsaturated FA allowing for safe TG accumulation (157). In consideration of our growth results we decided to structure the PTs following two assumptions: first as TGs are made from glycerol and three FAs a 2:1 ratio of saturated to unsaturated FA should not be exceeded; second at 500 µM also OA was negatively impacting cellular growth rates thus the total concentration used should remain below this threshold. As both saturated FAs displayed significantly reduced growth rates already at 125 µM and 250 µM we decided to employ these in combination with a constant co-treatment dose of 125 µM OA resulting in a 1:1 PT with a total added FFA concentration of 250 µM and a 2:1 ratio PT with a total concentration of 375 µM FFAs added, respectively. Growth experiments for the PTs revealed that also in liver cells the observed adverse impact of saturated FAs was abolished when unsaturated FAs were administered in combination. To confirm if this observed rescue of the cellular proliferation rates is linked to triglyceride accumulation within the cell, we performed a LD stain with subsequent volume quantification. The fluorescent labelling of the LDs allowed for their acquisition via the use of a confocal laser scanning microscope, resulting in a very accurate representation of the LDs not only in x/y axis but also in the z dimension. Thus, we were not limited to an image analysis based on the area of a maximum intensity projection but could adopt a voxel

based volumetric approach. This allowed us to circumvent the problem of many tiny LDs resulting in the same area fraction as a single bigger LD despite them having a completely different total lipid content. Both saturated FA acids exhibited an initial increase in the number of LDs formed but did fail to impact the LD volume in any significant way (Fig.16, App. 1). OA on the other hand showed a very clear dose dependent increase in LD volume over 24 hours forming fewer larger LDs. A similar difference in lipid accumulation following treatments with PA and OA was described by Ricchi et al. for various hepatic cell models (158). Examining the PTs revealed that the prevention of reduced growth rates indeed was accompanied by an increase in intracellular TG content. The 1:1 combination of MA and OA, MO11, with a total lipid concentration of 250 µM rose to a level comparable to the OA250 treatment, but what came as a surprise was that for the MO21 treatment no further increase in LD content could be observed. The PTs containing PA on the other hand did not show an initial TG increase in PO11, which resulted in an average LD volume per cell of 47.37 μm^3 compared to OA125's 45.08 μm^3. However, LD content was increased in PO21 and was then also comparable to levels found in OA250.

Combining the results from these first two experiments our data supports the hypothesis that lipotoxicity is inversely correlated with the cell's ability to store surplus FFAs safely as TGs. The only exception to this rule found is PO11 which did not exhibit any adverse effects on cellular growth but the measured LD volume did not correspond to the amount administered to the cell, raising the question about the cellular fate of PA.

To gain further insight into the alterations in our cell model in response to FA treatment, we performed a comprehensive proteomics analysis using LC-MS/MS. FA treatment caused a plethora of changes to the proteome, ranging from 350 up to 512 proteins exhibiting a fold change of $\leq \pm$ 1.5, thus the challenge lay in determining which of them correlated simply to lipid uptake and which of them could be considered a indicators for lipotoxicity. Initial statistical analysis of the data set resulted in a list of only 38 proteins that were significantly altered in at least one treatment condition after multitesting correction. And only one out of these 38 was found to be upregulated following treatment with every single FFA, namely PRKDC (Fig. 17A). PRKDC is reported to be a sensor for DNA damage and essential for double strand break repair, being a mediator of rRNA biogenesis, a regulator of apoptosis and a housekeeper of hepatic mitochondrial homeostasis (159–

163). Nevertheless, PRKDC was found to be upregulated following FFA treatment in a dose dependent manner, and also was upregulated in PTs, so it is more likely linked to lipid uptake in general, as reported previously, rather than being a specific readout of lipotoxicity (160). Another protein which displayed an interesting change was GRSF1, as it was differentially regulated in both saturated FAs. Cells treated with MA exhibited a dose dependent increase in GRSF1 abundance culminating at a 3.6-fold increase compared to control while cells following PA treatment started with a 2.8-fold increase compared to control dropping down to 0.86-fold at 500 μM. All other concentrations were on average elevated about 2.7 times of the control levels Fig. 17B). GRSF1 is a regulator of mitochondrial gene expression, making the fact that it is differentially regulated in-between the two saturated fatty acids even more intriguing.(164,165). In addition, we found two proteins, HDGF and ROCK2, which displayed a significant down regulation following MA treatment (Fig 17 B, C) (166,167). These proteins have been associated with cell cycle progression and led to the question if MA, despite its almost identical performance in the growth assay, might result in a completely different cellular fate than PA, which has been shown to induce apoptosis in hepatocytes (168).

To visualize proteomic changes introduced by the FA treatment Venn diagrams were created including all proteins which displayed a ± 1.5-fold change compared to control (Fig. 18). Despite all the differently expressed proteins in each condition the actual overlap in between the different FAs was surprisingly low with a tendency to increase at higher concentration treatments. Even more striking was the fact that the PTs had many unique alterations making them quite distinct from each of their FA constituents.

Proteins of the high concentration treatments displaying a ± 1.5-fold change compared to control were also used in a cluster and GO analysis, to highlight biological processes which were affected by these treatments. The GO enrichment reflected the reduced cellular growth rates in the form of prominent cytosolic translation clusters being downregulated in all high FFA conditions. As well as all treatments displaying signs of increased mitochondrial biogenesis, which is most likely due to FA induced activation of peroxisome proliferation- activated receptors (169). However, clusters indicating enhanced FA oxidation were only found following MA and PTs (APP. 2-11).

With the dedicated aim to identify proteins which only exhibited alteration as a response to treatments with toxic levels of FAs, we correlated the information from the growth assay with our proteomics data. Individual proteins were examined for dose dependent abundance changes correlating with their impact on cellular growth rates, meaning changes needed to be present in the saturated FAs and OA500 treatments in contrast to treatments not affecting growth. In addition, we discarded all proteins still exhibiting an altered expression in the PTs, suggesting that they are not specific for a distinct FA, resulting in a final list of 6 proteins, A2M, SERPINA3, H2AFY, DNTTIP2, ZNF326 and LMO7 (Fig 20 A). The first two proteins, A2M and SERPINA3, we identified as potential indicators of lipotoxicity, are considered modulators of the immune system (170–173). They are of special interest as inflammation is one of the key processes in the development and progression of NAFLD and linked to the intake and metabolization of FAs (174–176). Both act as protease inhibitors, A2M as abroad spectrum inhibitor and SERPINs are specific serine protease inhibitors thus are also connected to extracellular matrix remodelling. A2M was already found to be upregulated in a previous study of our laboratory focusing exclusively on alterations in HepG2 following MA treatment. It also has previously been used as a serum marker for patients suffering from moderate or advanced hepatic fibrosis. Our results indicate that A2M might be of clinical interest even during early stages of pathogenesis (177,178). Elevated SERPINA3 protein levels have been studied for many years in the context of neurodegenerative diseases like Alzheimer's, glioblastoma and multiple sclerosis (179,180). Only recently, it was shown that elevated SERPINA3 protein levels result in a poor prognosis for HCC patients despite its overall mRNA levels in liver tumours have been reported to be lower than in healthy tissue (181). It has been suggested that this observed difference of transcriptional and protein levels might be due to a stabilizing effect of posttranslational modification induced through ROS. The oxidised form of SERPINA3 has been shown to modulate hnRNP-K's transcriptional activity by forming a SERPINA3-HNRP-K complex leading to telomere elongation and an increased malignant phenotype in HCC (182). Our results thus suggest that hepatocytes themselves are able to affect the immune response following FFA treatment, which may thus not solely be dictated by specialised immune cells and their pattern recognition receptors (183).

The four remaining proteins which fitted our profile search for specific lipotoxicity markers are all involved in transcription. Of those, H2AFY has recently been described as a possible biomarker for HCC progression via a data mining approach. Our data corroborates that the changes in expression indeed may be due to FA uptake as hypothesized by the authors (184). As HCC is a possible late stage of NAFLD, we used data of the cancer genome atlas liver hepatocellular carcinoma (LIHC) project to test also DNTTIP2, ZNF326 and LMO7 for their potential as biomarkers (Fig. 20 A, B, C). The LHIC project contains gene expression and survival data and is the same dataset which was used in the discovery of H2AFY. We used data of the 50 patients for whom also data of healthy adjacent liver tissue was available. Our measurements of DNTTIP2 protein levels showed their reduction following FA treatment, which is not reflected on mRNA level expression between healthy and cancerous tissue. The 3-year survival rate displays even a significant increase in survival rates correlating with lower expression which does not correlate to our observation of a reduction upon fatty acid treatment. For ZNF326 we observed a reduction in protein levels which was also reflected in the cancer mRNA expression data. Nevertheless, no significant correlation between ZNF326 expression levels and the patients' survival was found. Only for LMO7 the reduction in protein levels post FFA treatment was also reflected in the expression levels and correlated with a statistical influence on survival rates, making it an excellent candidate for further research as a biomarker. However, the potential prognostic value of DNTTIP2 and ZNF326 should also not be disregarded as firstly HCC is only one possible end stage pathology of NAFLD, secondly the expression data in the LIHC dataset is based on mRNA levels which can differ significantly from protein abundance and thirdly no meta-data of the individuals' prior alcohol intake was available. A way to investigate and evaluate these proteins' correlation with NAFLD development would be a clinical study of patients before the advanced fibrosis has set in, thus consisting preferably of the staging point of a NASH with a fibrosis level of F1.

To corroborate the proteomics result, of the cell cycle proteins ROCK2 and HDGF being impacted following specifically MA treatment a cell cycle and apoptosis/necrosis assay was performed. And whilst for every FA at the 500 µM treatment concentration a significant reduction of cells in G2 phase was detected, only MA influenced the cell cycle at lower concentrations. Already at 125 µM, MA reduced the number of cells in G2 phase by 40% (Fig. 19 A). The apoptosis/necrosis assay on

the other hand only showed elevated levels of apoptotic cells following PA treatment. No change in the number of necrotic cells was found following treatments with FFAs (Fig. 19 B). This revealed that despite Ma and PA almost having identical results in the growth assay, the type of impairment fundamental for their growth decline was completely different; and to the best of our knowledge, this differential effect on apoptosis and cell cycle progression between two saturated FFAs within one cell system has not been reported so far. Results of the discussion upon this point are summarised in Fig. 26.

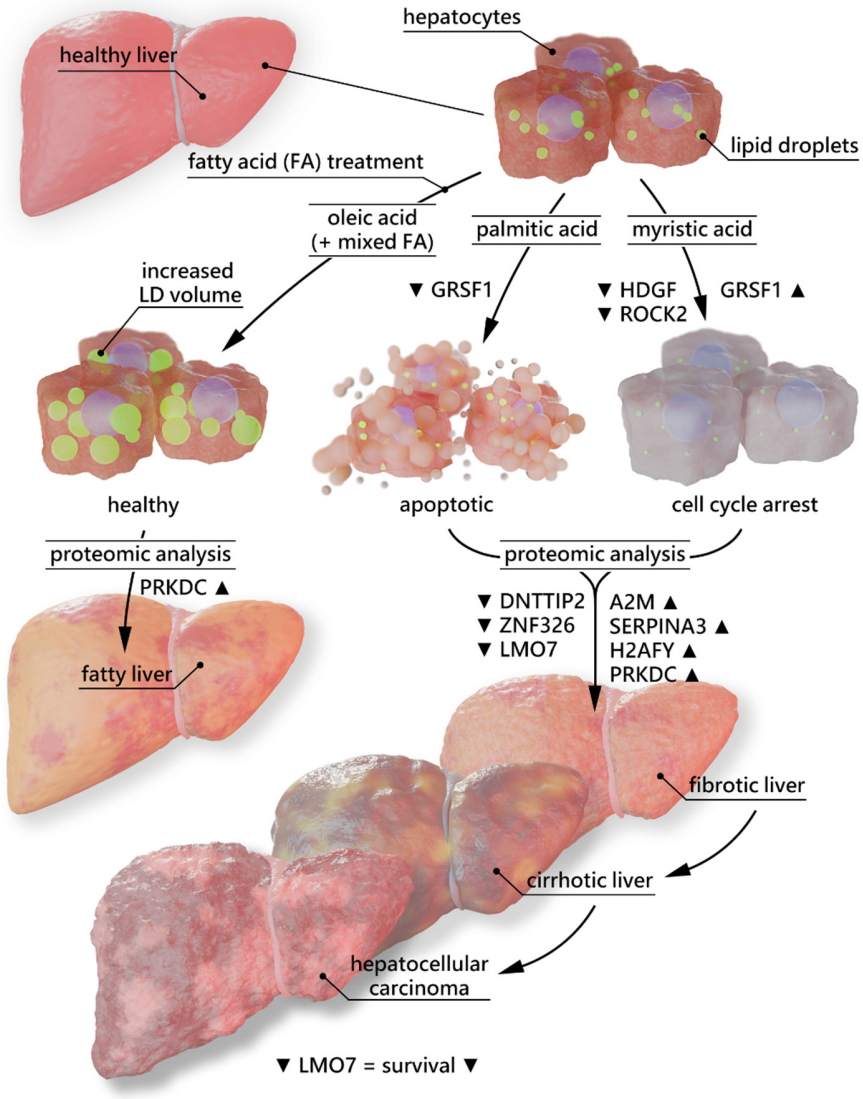

Figure 26 Summary figure of the proteomics study. Figure adapted from Gindlhuber et al. 2022 with permission from the publisher.

Moving further, the examination of the lipidome via LC/MS showed that following the FA supplementation of the media several changes in the abundance of different lipid classes could be observed. A dose dependent increase of CERs was caused by both saturated FAs, but was more pronounced following MA treatment (Fig. 21 A). Indeed, a 3-fold increase above control levels could be observed in 125 µM MA treatment condition, which is the same level that led to a reduction in cellular growth rates. The CER levels increased in PA treatments only at 250 µM or higher while OA did not influence the CER levels at all. As CERs are the precursor for SLs it is not surprising to see a similar dynamic in both, however now the impact of PA was visible immediately (Fig. 21 B). This could be explained by a faster synthesis and turnover of CER 16:0 and metabolization into a safer SL, as especially CER 16:0 has been attributed with cytotoxic effects (Fig. 21. A, B; App. 12, 13). Similarly, DGs should only be present transiently inside of the cell and their accumulation is associated with a lipotoxic phenotype such as lipid induced insulin resistance. For MA a 5-fold increase of DGs over control levels was detected at the 125 µM concentration, with PA again only matching this increase at higher concentrations (Fig. 21 C). According to our lipid droplet quantification we would have only expected to observe an increase in TG levels following treatment with OA and not with PA and MA (Fig. 21 D). To our surprise we detected an equal increase following MA treatment, with the increase in TG levels being dominantly present in the form of trimyristin (TG42:0) and closely related forms (App.15). As this result contradicted not only our LD volume measurements but also the hypothesis that TG accumulation protects from lipotoxic effects, the mass spectrometry results were validated with a trimyristin standard and matched on MS/MS level as well as on specific retention time. A dose dependent increase could also be observed in the PL levels following saturated FA treatment (Fig. 21 E, F). An explanation for this observed increase in membrane lipids despite an overall reduction of cell numbers might be found in the cells´ attempt to form new lysosomes, overburdening the system and leading to a downstream suppression of autophagy (185). Taken together, the lipidomics measurements exhibited many intriguing differences between MA and PA. While CERs, DGs, PCs and PEs exhibit an increase following saturated acid treatment all of them show so a concentration earlier and, with the exception of DGs, were more pronounced following MA treatment. We would have expected a similar trend by both FAs and changes predominantly

occurring from the treatment dose of 125 µM, at which a negative impact on cell growth, cell cycle progression and apoptosis was observed.

Referring to the results of the PTs for additional information on how the dysregulation in lipid composition might be indicative of a lipotoxic effect did not prove as successful as for the proteomics analysis. All measured lipid species reverted to control levels, with the only exception being DGs and TGs. However, the rise of TG levels was expected and confirmed previous LD quantification; and the DG levels, despite being elevated, were still comparable to the OA250 treatment. Whilst for MO11 and MO21 no increase in LD volume was detected, TG levels according to the MS data did rose. This discrepancy between LD volume and measured TG content following MA treatment necessitates further investigation but could be due to different staining efficiencies of TGs containing saturated fatty acids as compared to unsaturated fatty acids.

To follow up on the findings from the LC-MS/MS lipidomics approach we performed a FAME based uptake assay to investigate if different uptake kinetics were the cause for the differences observed between both saturated FFAs. Measuring the basal media conditions made it obvious that individual FFA concentrations introduced via the FBS are quite different: While MA's concentration was only 7.24 µM and OA's basal level was 24.43 µM, the measured concentration of PA was 181.28 µM (Fig. 23 A, B, C). Overlaying this information with the observed effects might explain why alterations following PA treatment seemingly only appear at higher doses as the 125 µM treatment represents a 15-fold increase for MA and only a 1.7-fold increase for PA. Investigating the uptake over time for the different concentrations returned in most cases a linear decline for the FA in question in the medium over time with the exception of PA500. For PA500 the concentration in the growth medium declined up to the 6 h time point until reaching a minimum of 35.39 µg/ml per 100.000 cells after which levels rose again. This effect might be attributed to cells dying from the treatment and/or the FAs being released back into the media. The highest measured uptake over 24 hours was relatively comparable in between the 3 FFAs with 25,35 µg/ml per 100.000 cells for MA500, 41,05 µg/ml per 100.000 cells for OA500 and 32,32 µg/ml per 100.000 cells for PA500, respectively; whilst remaining concentrations in the medium varied. The resulting question was, with the maximum uptake of the individual FAs being so similar, if there were differences in the individual kinetics and whether the PTs influenced the individual uptake a

particular way. Thus, we plotted the individual uptake over time, for all the concentrations as an average per hour and could indeed discern to different uptake forms. An immediate uptake dependent only on the dose of FA administered as can be observed for all PA treatments (Fig. 23 B). The other was a delayed uptake type as is observable for all OA treatments where independent of the dose for the first 3 hours all exhibit a similar uptake rate, with distinct concentration dependent maxima only being observable at a later time point (Fig. 23 C). MA exhibited a mix of both observed types with 25 µM,50 µM and 125 µM assigned to the delayed and 250 µM and 500 µM to the immediate uptake type. Regarding changes introduced with the PTs: MA uptake was not altered but the maximum hourly uptake of oleic acid was doubled in the PTs compared to the OA125 treatment. (Fig. 24 A, B, C). In PTs with PA the uptake kinetics of both PA and oleic acid were found to be altered (Fig. 25 A, B, C). PA uptake was found to be almost halted after the 3h time point and oleic acid uptake changed from the delayed to the immediate uptake type. In both treatments OA uptake was either increased or sped up, implicating the need of unsaturated FAs for TG synthesis and LD formation.

Conclusion

In conclusion, this study revealed a regulatory difference between two saturated FFAs within the same cell system which has not been described so far. We were able to contextualize the proteome alterations introduced with the FA treatments via the help of PTs to differentiate between generalized lipid induced responses and specific lipotoxic alterations. All together 6 proteins were identified as potential markers for lipotoxicity of which LMO7 was successfully identified as a potential biomarker for HCC progression with data from the LIHC cancer genome atlas project. Two other proteins, A2M and SERPINA3, could play a role not only in modulating the inflammatory process on tissue level but, as protease inhibitors, in extracellular matrix remodelling and thus possibly also in the development of fibrosis during the progression from NAFL to NASH. The assumption that TG accumulation is a protective mechanism has to be re-evaluated as MA treatment led to a dose dependent increase in TG levels without lipid droplets being visible. However, no TG accumulation was found following PA treatment highlighting again how different the effects of these two FAs on the cell are, emphasizing the need for more FAs being studied than the major FAs PA and OA. As the explanation of how the PT work was linked to TG formation we investigated the possibility of alterations in the individual FFA uptake. In both cases alterations resulting in increased OA uptake could be observed coinciding with elevated TG levels. Leading us to form the hypothesis that the important step is the formation of LDs and not TGs alone. Altered biophysical properties of TGs only consisting from “rigid” saturated FAs might prevent the LD from budding off from the ER, thus leading to downstream complications of protein synthesis etc. Experiments trying to investigate this hypothesis were conceptualised but couldn’t be finished in a timely fashion. In addition, the results originating from the proteomics experiments need further validation for their use as biomarkers with patient data preferably from patients at an early stage of NASH.

Study limitations

This study is solely comprised of cell culture data of employing a cancer cell line, which has definite limitations on how much results obtained from it will relate to in vivo data. Recently, a research group around Tatsuya Shimizu from Tokyo has published a 3D cell culture model based around primary human hepatocytes in co-culture with dermal fibroblasts in which ballooning could be observed for the first time (186). Thus, a change to a more natural model might be considered.

We examine changes to the cells that happen within 24 hours after lipid treatment whilst in humans the estimated development time of NAFLD is months if not years. However, keeping a cell in culture for this extended period will induce changes and is against common good laboratory practice.

The impact of the saturated FAs on the mitochondrial system has not been investigated in depth and no comprehensive experiment about the FAs being used as fuel in beta oxidation has been performed so far.

Specific supplementation of certain lipid species in correlation to the lipidomics results need to be performed to determine with certainty which of them are causal with the observed lipotoxic effects.

The proteomics experiment included a few hundred measurements and thus stretched beyond half a year of consecutive machine use with only an n number of 3. The coherency of a data set of this size might be impaired due to machine performance drift.

5. References

1. Gindlhuber J, Schinagl M, Liesinger L, Darnhofer B, Tomin T, Schittmayer M, et al. Hepatocyte Proteome Alterations Induced by Individual and Combinations of Common Free Fatty Acids. Int J Mol Sci. 2022 Mar 20;23(6):3356.
2. Miller SL. A Production of Amino Acids Under Possible Primitive Earth Conditions. Science (1979). 1953 May 15;117(3046):528–9.
3. Miller SL, Urey HC. Organic Compound Synthesis on the Primitive Earth. Science (1979). 1959 Jul 31;130(3370):245–51.
4. Johnson AP, Cleaves HJ, Dworkin JP, Glavin DP, Lazcano A, Bada JL. The Miller Volcanic Spark Discharge Experiment. Science (1979). 2008 Oct 17;322(5900):404–404.
5. Oró J, Kimball AP. Synthesis of purines under possible primitive earth conditions. I. Adenine from hydrogen cyanide. Arch Biochem Biophys. 1961 Aug;94(2):217–27.
6. Brooks DJ, Fresco JR, Lesk AM, Singh M. Evolution of Amino Acid Frequencies in Proteins Over Deep Time: Inferred Order of Introduction of Amino Acids into the Genetic Code. Mol Biol Evol. 2002 Oct 1;19(10):1645–55.
7. Trevors JT, Psenner R. From self-assembly of life to present-day bacteria: a possible role for nanocells. FEMS Microbiol Rev. 2001 Dec;25(5):573–82.
8. Keeling PJ, Archibald JM. Organelle Evolution: What's in a Name? Current Biology. 2008 Apr;18(8):R345–7.
9. Segré D, Ben-Eli D, Deamer DW, Lancet D. The Lipid World. Origins of Life and Evolution of the Biosphere. 2001;31(1/2):119–45.
10. Fahy E, Subramaniam S, Murphy RC, Nishijima M, Raetz CRH, Shimizu T, et al. Update of the LIPID MAPS comprehensive classification system for lipids. J Lipid Res. 2009 Apr;50:S9–14.
11. Crown SB, Marze N, Antoniewicz MR. Catabolism of Branched Chain Amino Acids Contributes Significantly to Synthesis of Odd-Chain and Even-Chain Fatty Acids in 3T3-L1 Adipocytes. PLoS One. 2015 Dec 28;10(12):e0145850.
12. Walther TC, Chung J, Farese R v. Lipid Droplet Biogenesis. Annu Rev Cell Dev Biol. 2017 Oct 6;33(1):491–510.
13. Buhman KK, Chen HC, Farese R v. The Enzymes of Neutral Lipid Synthesis. Journal of Biological Chemistry. 2001 Nov;276(44):40369–72.
14. WEISS SB, KENNEDY EP, KIYASU JY. The enzymatic synthesis of triglycerides. J Biol Chem. 1960 Jan;235:40–4.
15. Wang H, Becuwe M, Housden BE, Chitraju C, Porras AJ, Graham MM, et al. Seipin is required for converting nascent to mature lipid droplets. Elife. 2016 Aug 26;5.

16. Frühbeck G, Méndez-Giménez L, Fernández-Formoso JA, Fernández S, Rodríguez A. Regulation of adipocyte lipolysis. Nutr Res Rev. 2014 Jun 28;27(1):63–93.

17. Vance JE, Tasseva G. Formation and function of phosphatidylserine and phosphatidylethanolamine in mammalian cells. Biochimica et Biophysica Acta (BBA) - Molecular and Cell Biology of Lipids. 2013 Mar;1831(3):543–54.

18. Emoto K, Kobayashi T, Yamaji A, Aizawa H, Yahara I, Inoue K, et al. Redistribution of phosphatidylethanolamine at the cleavage furrow of dividing cells during cytokinesis. Proceedings of the National Academy of Sciences. 1996 Nov 12;93(23):12867–72.

19. Blunsom NJ, Cockcroft S. Phosphatidylinositol synthesis at the endoplasmic reticulum. Biochimica et Biophysica Acta (BBA) - Molecular and Cell Biology of Lipids. 2020 Jan;1865(1):158471.

20. Shulga Y v., Topham MK, Epand RM. Substrate specificity of diacylglycerol kinase-epsilon and the phosphatidylinositol cycle. FEBS Lett. 2011 Dec 15;585(24):4025–8.

21. Burke JE. Structural Basis for Regulation of Phosphoinositide Kinases and Their Involvement in Human Disease. Mol Cell. 2018 Sep;71(5):653–73.

22. Wood R, Harlow RD. Structural analyses of rat liver phosphoglycerides. Arch Biochem Biophys. 1969;135:272–81.

23. de Craene JO, Bertazzi D, Bär S, Friant S. Phosphoinositides, Major Actors in Membrane Trafficking and Lipid Signaling Pathways. Int J Mol Sci. 2017 Mar 15;18(3):634.

24. Bartke N, Hannun YA. Bioactive sphingolipids: metabolism and function. J Lipid Res. 2009 Apr;50:S91–6.

25. Garidel P, Fölting B, Schaller I, Kerth A. The microstructure of the stratum corneum lipid barrier: Mid-infrared spectroscopic studies of hydrated ceramide:palmitic acid:cholesterol model systems. Biophys Chem. 2010 Aug;150(1–3):144–56.

26. Dbaibo GS, El-Assaad W, Krikorian A, Liu B, Diab K, Idriss NZ, et al. Ceramide generation by two distinct pathways in tumor necrosis factor α-induced cell death. FEBS Lett. 2001 Aug 10;503(1):7–12.

27. Haimovitz-Friedman A, Kan CC, Ehleiter D, Persaud RS, McLoughlin M, Fuks Z, et al. Ionizing radiation acts on cellular membranes to generate ceramide and initiate apoptosis. Journal of Experimental Medicine. 1994 Aug 1;180(2):525–35.

28. Dbaibo GS, Pushkareva MY, Rachid RA, Alter N, Smyth MJ, Obeid LM, et al. p53-dependent ceramide response to genotoxic stress. Journal of Clinical Investigation. 1998 Jul 15;102(2):329–39.

29. Rotolo JA, Zhang J, Donepudi M, Lee H, Fuks Z, Kolesnick R. Caspase-dependent and -independent Activation of Acid Sphingomyelinase Signaling. Journal of Biological Chemistry. 2005 Jul;280(28):26425–34.

30. Tafesse FG, Ternes P, Holthuis JCM. The Multigenic Sphingomyelin Synthase Family. Journal of Biological Chemistry. 2006 Oct;281(40):29421–5.

31. TESTI R. Sphingomyelin breakdown and cell fate. Trends Biochem Sci. 1996 Dec;21(12):468–71.

32. Bach D, Wachtel E. Phospholipid/cholesterol model membranes: formation of cholesterol crystallites. Biochimica et Biophysica Acta (BBA) - Biomembranes. 2003 Mar;1610(2):187–97.

33. Hofmann AF, Hagey LR, Krasowski MD. Bile salts of vertebrates: structural variation and possible evolutionary significance. J Lipid Res. 2010 Feb;51(2):226–46.

34. Chiang JYL. Bile Acid Metabolism and Signaling. In: Comprehensive Physiology. Wiley; 2013. p. 1191–212.

35. Djurhuus CB, Gravholt CH, Nielsen S, Mengel A, Christiansen JS, Schmitz OE, et al. Effects of cortisol on lipolysis and regional interstitial glycerol levels in humans. American Journal of Physiology-Endocrinology and Metabolism. 2002 Jul 1;283(1):E172–7.

36. Coderre L, Srivastava AK, Chiasson JL. Role of glucocorticoid in the regulation of glycogen metabolism in skeletal muscle. American Journal of Physiology-Endocrinology and Metabolism. 1991 Jun 1;260(6):E927–32.

37. Belizário JE, Brandão W, Rossato C, Peron JP. Thymic and Postthymic Regulation of Naïve CD4 $^{+}$ T-Cell Lineage Fates in Humans and Mice Models. Mediators Inflamm. 2016;2016:1–16.

38. PALACIOS R, SUGAWARA I. Hydrocortisone Abrogates Proliferation of T Cells in Autologous Mixed Lymphocyte Reaction by Rendering the Interleukin-2 Producer T Cells Unresponsive to Interleukin-1 and Unable to Synthesize the T-Cell Growth Factor. Scand J Immunol. 1982 Jan;15(1):25–31.

39. ELENKOV IJ. Glucocorticoids and the Th1/Th2 Balance. Ann N Y Acad Sci. 2004 Jun;1024(1):138–46.

40. Kuzuyama T, Seto H. Diversity of the biosynthesis of the isoprene units. Nat Prod Rep. 2003 Mar 25;20(2):171–83.

41. Breitmaier E. Terpenes. Wiley; 2006.

42. Raetz CRH, Guan Z, Ingram BO, Six DA, Song F, Wang X, et al. Discovery of new biosynthetic pathways: the lipid A story. J Lipid Res. 2009 Apr;50:S103–8.

43. Smith S, Tsai SC. The type I fatty acid and polyketide synthases: a tale of two megasynthases. Nat Prod Rep. 2007;24(5):1041.

44. Payushina O v. Hematopoietic Microenvironment in the Fetal Liver: Roles of Different Cell Populations. ISRN Cell Biol. 2012 Oct 23;2012:1–7.

45. Tsolaki E, Athanasiou E, Gounari E, Zogas N, Siotou E, Yiangou M, et al. Hematopoietic stem cells and liver regeneration: Differentially acting hematopoietic stem cell mobilization agents reverse induced chronic liver injury. Blood Cells Mol Dis. 2014;53(3):124–32.

46. Collardeau-Frachon S, Scoazec JY. Vascular Development and Differentiation During Human Liver Organogenesis. The Anatomical Record: Advances in Integrative Anatomy and Evolutionary Biology. 2008 Jun;291(6):614–27.

47. Lautt WW. Hepatic Circulation. Colloquium Series on Integrated Systems Physiology: From Molecule to Function. 2009 Jan;1(1):1–174.

48. Burr GO, Burr MM. ON THE NATURE AND RÔLE OF THE FATTY ACIDS ESSENTIAL IN NUTRITION. Journal of Biological Chemistry. 1930 Apr;86(2):587–621.

49. Burr GO, Burr MM, Miller ES. ON THE FATTY ACIDS ESSENTIAL IN NUTRITION. III. Journal of Biological Chemistry. 1932 Jul;97(1):1–9.

50. Whelan J, Fritsche K. Linoleic Acid. Advances in Nutrition. 2013 May 1;4(3):311–2.

51. Calder PC. Eicosanoids. Essays Biochem. 2020 Sep 23;64(3):423–41.

52. Burdge GC, Calder PC. Conversion of alpha-linolenic acid to longer-chain polyunsaturated fatty acids in human adults. Reprod Nutr Dev. 2005 Sep;45(5):581–97.

53. Yue H, Qiu B, Jia M, Liu W, Guo X fei, Li N, et al. Effects of α-linolenic acid intake on blood lipid profiles：a systematic review and meta-analysis of randomized controlled trials. Crit Rev Food Sci Nutr. 2021 Sep 25;61(17):2894–910.

54. Naghshi S, Aune D, Beyene J, Mobarak S, Asadi M, Sadeghi O. Dietary intake and biomarkers of alpha linolenic acid and risk of all cause, cardiovascular, and cancer mortality: systematic review and dose-response meta-analysis of cohort studies. BMJ. 2021 Oct 13;n2213.

55. Schittmayer M, Vujic N, Darnhofer B, Korbelius M, Honeder S, Kratky D, et al. Spatially Resolved Activity-based Proteomic Profiles of the Murine Small Intestinal Lipases. Molecular & Cellular Proteomics. 2020 Dec;19(12):2104–15.

56. Hamosh M, Scow RO. Lingual Lipase and Its Role in the Digestion of Dietary Lipid. Journal of Clinical Investigation. 1973 Jan 1;52(1):88–95.

57. Abrams CK, Hamosh M, Hubbard VS, Dutta SK, Hamosh P. Lingual lipase in cystic fibrosis. Quantitation of enzyme activity in the upper small intestine of patients with exocrine pancreatic insufficiency. Journal of Clinical Investigation. 1984 Feb 1;73(2):374–82.

58. Sams L, Paume J, Giallo J, Carrière F. Relevant pH and lipase for in vitro models of gastric digestion. Food Funct. 2016;7(1):30–45.

59. Bourlieu C, Mahdoueni W, Paboeuf G, Gicquel E, Ménard O, Pezennec S, et al. Physico-chemical behaviors of human and bovine milk membrane extracts and their influence on gastric lipase adsorption. Biochimie. 2020 Feb;169:95–105.

60. Pafumi Y, Lairon D, de la Porte PL, Juhel C, Storch J, Hamosh M, et al. Mechanisms of Inhibition of Triacylglycerol Hydrolysis by Human Gastric Lipase. Journal of Biological Chemistry. 2002 Aug;277(31):28070–9.

61. Borgström B. The action of bile salts and other detergents on pancreatic lipase and the interaction with colipase. Biochimica et Biophysica Acta (BBA) - Lipids and Lipid Metabolism. 1977 Sep;488(3):381–91.

62. Lombardo D. Bile salt-dependent lipase: its pathophysiological implications. Biochimica et Biophysica Acta (BBA) - Molecular and Cell Biology of Lipids. 2001 Aug;1533(1):1–28.

63. Chapus C, Rovery M, Sarda L, Verger R. Minireview on pancreatic lipase and colipase. Biochimie. 1988 Sep;70(9):1223–33.

64. Jo Y, Okazaki H, Moon YA, Zhao T. Regulation of Lipid Metabolism and Beyond. Int J Endocrinol. 2016;2016:1–2.

65. Julve J, Martín-Campos JM, Escolà-Gil JC, Blanco-Vaca F. Chylomicrons: Advances in biology, pathology, laboratory testing, and therapeutics. Clinica Chimica Acta. 2016 Apr;455:134–48.

66. Kersten S. Physiological regulation of lipoprotein lipase. Biochimica et Biophysica Acta (BBA) - Molecular and Cell Biology of Lipids. 2014 Jul;1841(7):919–33.

67. Basu D, Goldberg IJ. Regulation of lipoprotein lipase-mediated lipolysis of triglycerides. Curr Opin Lipidol. 2020 Jun;31(3):154–60.

68. César TB, Oliveira MRM, Mesquita CH, Maranhão RC. High Cholesterol Intake Modifies Chylomicron Metabolism in Normolipidemic Young Men. J Nutr. 2006 Apr 1;136(4):971–6.

69. Gibbons GF, Wiggins D, Brown AM, Hebbachi AM. Synthesis and function of hepatic very-low-density lipoprotein. Biochem Soc Trans. 2004 Feb 1;32(1):59–64.

70. Ossoli A, Simonelli S, Vitali C, Franceschini G, Calabresi L. Role of LCAT in Atherosclerosis. J Atheroscler Thromb. 2016;23(2):119–27.

71. Huang CX, Zhang YL. The Target of Regulating The ATP-binding Cassette A1 Protein (ABCA1): Promoting ABCA1-Mediated Cholesterol Efflux in Different Cells. Curr Pharm Biotechnol. 2013 Nov 31;14(6):623–31.

72. März W, Kleber ME, Scharnagl H, Speer T, Zewinger S, Ritsch A, et al. HDL cholesterol: reappraisal of its clinical relevance. Clinical Research in Cardiology. 2017 Sep 24;106(9):663–75.

73. Mei S, Ni HM, Manley S, Bockus A, Kassel KM, Luyendyk JP, et al. Differential Roles of Unsaturated and Saturated Fatty Acids on Autophagy and Apoptosis in Hepatocytes. Journal of Pharmacology and Experimental Therapeutics. 2011 Nov;339(2):487–98.

74. Harris JJ, Attwell D. The Energetics of CNS White Matter. Journal of Neuroscience. 2012 Jan 4;32(1):356–71.

75. Schönfeld P, Reiser G. Why does Brain Metabolism not Favor Burning of Fatty Acids to Provide Energy? - Reflections on Disadvantages of the Use of Free Fatty Acids as Fuel for Brain. Journal of Cerebral Blood Flow & Metabolism. 2013 Oct 7;33(10):1493–9.

76. Panov A, Orynbayeva Z, Vavilin V, Lyakhovich V. Fatty Acids in Energy Metabolism of the Central Nervous System. Biomed Res Int. 2014;2014:1–22.

77. Verkhratsky A, Nedergaard M. Physiology of Astroglia. Physiol Rev. 2018 Jan 1;98(1):239–389.

78. Hsiao YH, Lin CI, Liao H, Chen YH, Lin SH. Palmitic Acid-Induced Neuron Cell Cycle G2/M Arrest and Endoplasmic Reticular Stress through Protein Palmitoylation in SH-SY5Y Human Neuroblastoma Cells. Int J Mol Sci. 2014 Nov 13;15(11):20876–99.

79. Little JP, Madeira JM, Klegeris A. The Saturated Fatty Acid Palmitate Induces Human Monocytic Cell Toxicity Toward Neuronal Cells: Exploring a Possible Link Between Obesity-Related Metabolic Impairments and Neuroinflammation. Journal of Alzheimer's Disease. 2012 Jun 8;30(s2):S179–83.

80. Smolič T, Zorec R, Vardjan N. Pathophysiology of Lipid Droplets in Neuroglia. Antioxidants. 2021 Dec 23;11(1):22.

81. Goodwin GW, Taylor CS, Taegtmeyer H. Regulation of Energy Metabolism of the Heart during Acute Increase in Heart Work. Journal of Biological Chemistry. 1998 Nov;273(45):29530–9.

82. Harmancey R, Wilson CR, Taegtmeyer H. Adaptation and Maladaptation of the Heart in Obesity. Hypertension. 2008 Aug;52(2):181–7.

83. Hammer S, van der Meer RW, Lamb HJ, Schär M, de Roos A, Smit JWA, et al. Progressive Caloric Restriction Induces Dose-Dependent Changes in Myocardial Triglyceride Content and Diastolic Function in Healthy Men. J Clin Endocrinol Metab. 2008 Feb 1;93(2):497–503.

84. Wende AR, Abel ED. Lipotoxicity in the heart. Biochimica et Biophysica Acta (BBA) - Molecular and Cell Biology of Lipids. 2010 Mar;1801(3):311–9.

85. Tsushima K, Bugger H, Wende AR, Soto J, Jenson GA, Tor AR, et al. Mitochondrial Reactive Oxygen Species in Lipotoxic Hearts Induce Post-Translational Modifications of AKAP121, DRP1, and OPA1 That Promote Mitochondrial Fission. Circ Res. 2018 Jan 5;122(1):58–73.

86. Symons JD, Abel ED. Lipotoxicity contributes to endothelial dysfunction: A focus on the contribution from ceramide. Rev Endocr Metab Disord. 2013 Mar 5;14(1):59–68.

87. Triggle CR, Ding H. A review of endothelial dysfunction in diabetes: a focus on the contribution of a dysfunctional eNOS. Journal of the American Society of Hypertension. 2010 May;4(3):102–15.

88. Sessa WC. eNOS at a glance. J Cell Sci. 2004 May 15;117(12):2427–9.

89. Holland WL, Summers SA. Sphingolipids, Insulin Resistance, and Metabolic Disease: New Insights from in Vivo Manipulation of Sphingolipid Metabolism. Endocr Rev. 2008 Jun 1;29(4):381–402.

90. Chavez JA, Summers SA. Lipid oversupply, selective insulin resistance, and lipotoxicity: Molecular mechanisms. Biochimica et Biophysica Acta (BBA) - Molecular and Cell Biology of Lipids. 2010 Mar;1801(3):252–65.

91. Wu Y, Song P, Xu J, Zhang M, Zou MH. Activation of Protein Phosphatase 2A by Palmitate Inhibits AMP-activated Protein Kinase. Journal of Biological Chemistry. 2007 Mar;282(13):9777–88.

92. Zhang DX, Zou AP, Li PL. Ceramide-induced activation of NADPH oxidase and endothelial dysfunction in small coronary arteries. American Journal of Physiology-Heart and Circulatory Physiology. 2003 Feb 1;284(2):H605–12.

93. Li H, Junk P, Huwiler A, Burkhardt C, Wallerath T, Pfeilschifter J, et al. Dual Effect of Ceramide on Human Endothelial Cells. Circulation. 2002 Oct 22;106(17):2250–6.

94. Zheng T, Li W, Wang J, Altura BT, Altura BM. Sphingomyelinase and ceramide analogs induce contraction and rises in $[Ca^{2+}]_i$ in canine cerebral vascular muscle. American Journal of Physiology-Heart and Circulatory Physiology. 2000 May 1;278(5):H1421–8.

95. Zajac J, Shrestha A, Patel P, Poretsky L. The Main Events in the History of Diabetes Mellitus. In: Principles of Diabetes Mellitus. Boston, MA: Springer US; 2010. p. 3–16.

96. Lytrivi M, Castell AL, Poitout V, Cnop M. Recent Insights Into Mechanisms of β-Cell Lipo- and Glucolipotoxicity in Type 2 Diabetes. J Mol Biol. 2020 Mar;432(5):1514–34.

97. Vilas-Boas EA, Almeida DC, Roma LP, Ortis F, Carpinelli AR. Lipotoxicity and β-Cell Failure in Type 2 Diabetes: Oxidative Stress Linked to NADPH Oxidase and ER Stress. Cells. 2021 Nov 26;10(12):3328.

98. El-Assaad W, Buteau J, Peyot ML, Nolan C, Roduit R, Hardy S, et al. Saturated Fatty Acids Synergize with Elevated Glucose to Cause Pancreatic β-Cell Death. Endocrinology. 2003 Sep 1;144(9):4154–63.

99. Maris M, Robert S, Waelkens E, Derua R, Hernangomez MH, D'Hertog W, et al. Role of the Saturated Nonesterified Fatty Acid Palmitate in Beta Cell Dysfunction. J Proteome Res. 2013 Jan 4;12(1):347–62.

100. Hagman DK, Hays LB, Parazzoli SD, Poitout V. Palmitate Inhibits Insulin Gene Expression by Altering PDX-1 Nuclear Localization and Reducing MafA Expression in Isolated Rat Islets of Langerhans. Journal of Biological Chemistry. 2005 Sep;280(37):32413–8.

101. Samuel VT, Petersen KF, Shulman GI. Lipid-induced insulin resistance: unravelling the mechanism. The Lancet. 2010 Jun;375(9733):2267–77.

102. Watson RT, Pessin JE. GLUT4 translocation: The last 200 nanometers. Cell Signal. 2007 Nov;19(11):2209–17.

103. Lewis RE, Cao L, Perregaux D, Czech MP. Threonine 1336 of the human insulin receptor is a major target for phosphorylation by protein kinase C. Biochemistry. 1990 Feb 20;29(7):1807–13.

104. Baron AD, Brechtel G, Wallace P, Edelman S v. Rates and tissue sites of non-insulin- and insulin-mediated glucose uptake in humans. American Journal of Physiology-Endocrinology and Metabolism. 1988 Dec 1;255(6):E769–74.

105. Lamsfuss J, Bargmann S. Skeletal muscle: Modeling the mechanical behavior by taking the hierarchical microstructure into account. J Mech Behav Biomed Mater. 2021 Oct;122:104670.

106. Coen PM, Dubé JJ, Amati F, Stefanovic-Racic M, Ferrell RE, Toledo FGS, et al. Insulin Resistance Is Associated With Higher Intramyocellular Triglycerides in Type I but Not Type II Myocytes Concomitant With Higher Ceramide Content. Diabetes. 2010 Jan 1;59(1):80–8.

107. Goodpaster BH, He J, Watkins S, Kelley DE. Skeletal Muscle Lipid Content and Insulin Resistance: Evidence for a Paradox in Endurance-Trained Athletes. J Clin Endocrinol Metab. 2001 Dec 1;86(12):5755–61.

108. van Loon LJC. Use of intramuscular triacylglycerol as a substrate source during exercise in humans. J Appl Physiol. 2004 Oct;97(4):1170–87.

109. Irrcher I, Ljubicic V, Hood DA. Interactions between ROS and AMP kinase activity in the regulation of PGC-1α transcription in skeletal muscle cells. American Journal of Physiology-Cell Physiology. 2009 Jan;296(1):C116–23.

110. Tadaishi M, Miura S, Kai Y, Kano Y, Oishi Y, Ezaki O. Skeletal Muscle-Specific Expression of PGC-1α-b, an Exercise-Responsive Isoform, Increases Exercise Capacity and Peak Oxygen Uptake. PLoS One. 2011 Dec 8;6(12):e28290.

111. López-Lluch G, Hunt N, Jones B, Zhu M, Jamieson H, Hilmer S, et al. Calorie restriction induces mitochondrial biogenesis and bioenergetic efficiency. Proceedings of the National Academy of Sciences. 2006 Feb 7;103(6):1768–73.

112. Turpin SM, Lancaster GI, Darby I, Febbraio MA, Watt MJ. Apoptosis in skeletal muscle myotubes is induced by ceramides and is positively related to insulin resistance. American Journal of Physiology-Endocrinology and Metabolism. 2006 Dec;291(6):E1341–50.

113. Neuschwander-Tetri B. Nonalcoholic steatohepatitis: Summary of an AASLD Single Topic Conference. Hepatology. 2003 May;37(5):1202–19.

114. Eslam M, Newsome PN, Sarin SK, Anstee QM, Targher G, Romero-Gomez M, et al. A new definition for metabolic dysfunction-associated fatty liver disease: An international expert consensus statement. J Hepatol. 2020 Jul;73(1):202–9.

115. Fouad Y, Waked I, Bollipo S, Gomaa A, Ajlouni Y, Attia D. What's in a name? Renaming 'NAFLD' to 'MAFLD.' Liver International. 2020 Jun 28;40(6):1254–61.

116. Bianco C, Romeo S, Petta S, Long MT, Valenti L. MAFLD vs NAFLD: Let the contest begin! Liver International. 2020 Sep 12;40(9):2079–81.

117. Younossi ZM, Koenig AB, Abdelatif D, Fazel Y, Henry L, Wymer M. Global epidemiology of nonalcoholic fatty liver disease-Meta-analytic assessment of prevalence, incidence, and outcomes. Hepatology. 2016 Jul;64(1):73–84.

118. Estes C, Razavi H, Loomba R, Younossi Z, Sanyal AJ. Modeling the epidemic of nonalcoholic fatty liver disease demonstrates an exponential increase in burden of disease. Hepatology. 2018 Jan;67(1):123–33.

119. Byrne CD, Targher G. NAFLD: A multisystem disease. J Hepatol. 2015 Apr;62(1):S47–64.

120. Friedman SL, Neuschwander-Tetri BA, Rinella M, Sanyal AJ. Mechanisms of NAFLD development and therapeutic strategies. Nat Med. 2018 Jul 2;24(7):908–22.

121. Muthiah MD, Sanyal AJ. Current management of non-alcoholic steatohepatitis. Liver International. 2020 Feb 20;40(S1):89–95.

122. Sumida Y. Limitations of liver biopsy and non-invasive diagnostic tests for the diagnosis of nonalcoholic fatty liver disease/nonalcoholic steatohepatitis. World J Gastroenterol. 2014;20(2):475.

123. Ekstedt M, Franzén LE, Mathiesen UL, Thorelius L, Holmqvist M, Bodemar G, et al. Long-term follow-up of patients with NAFLD and elevated liver enzymes. Hepatology. 2006 Oct;44(4):865–73.

124. Hyysalo J, Männistö VT, Zhou Y, Arola J, Kärjä V, Leivonen M, et al. A population-based study on the prevalence of NASH using scores validated against liver histology. J Hepatol. 2014 Apr;60(4):839–46.

125. Anstee QM, Targher G, Day CP. Progression of NAFLD to diabetes mellitus, cardiovascular disease or cirrhosis. Nat Rev Gastroenterol Hepatol. 2013 Jun 19;10(6):330–44.

126. Romeo S, Kozlitina J, Xing C, Pertsemlidis A, Cox D, Pennacchio LA, et al. Genetic variation in PNPLA3 confers susceptibility to nonalcoholic fatty liver disease. Nat Genet. 2008 Dec 25;40(12):1461–5.

127. Loomba R, Sanyal AJ. The global NAFLD epidemic. Nat Rev Gastroenterol Hepatol. 2013 Nov 17;10(11):686–90.

128. Hodson L, Rosqvist F, Parry SA. The influence of dietary fatty acids on liver fat content and metabolism. Proceedings of the Nutrition Society. 2020 Feb 3;79(1):30–41.

129. Geisler CE, Renquist BJ. Hepatic lipid accumulation: cause and consequence of dysregulated glucoregulatory hormones. Journal of Endocrinology. 2017 Jul;234(1):R1–21.

130. Joshi-Barve S, Barve SS, Amancherla K, Gobejishvili L, Hill D, Cave M, et al. Palmitic acid induces production of proinflammatory cytokine interleukin-8 from hepatocytes. Hepatology. 2007 Sep;46(3):823–30.

131. Ramadori G, Armbrust T. Cytokines in the liver. Eur J Gastroenterol Hepatol. 2001 Jul;13(7):777–84.

132. Anderson N, Borlak J. Molecular Mechanisms and Therapeutic Targets in Steatosis and Steatohepatitis. Pharmacol Rev. 2008 Sep;60(3):311–57.

133. Carter JK, Friedman SL. Hepatic Stellate Cell-Immune Interactions in NASH. Front Endocrinol (Lausanne). 2022 Jun 9;13.

134. Karagiannides I, Abdou R, Tzortzopoulou A, Voshol PJ, Kypreos KE. Apolipoprotein E predisposes to obesity and related metabolic dysfunctions in mice. FEBS Journal. 2008 Oct;275(19):4796–809.

135. Sahai A, Malladi P, Pan X, Paul R, Melin-Aldana H, Green RM, et al. Obese and diabetic db / db mice develop marked liver fibrosis in a model of nonalcoholic steatohepatitis: role of short-form leptin receptors and osteopontin. American Journal of Physiology-Gastrointestinal and Liver Physiology. 2004 Nov;287(5):G1035–43.

136. Trevaskis JL, Griffin PS, Wittmer C, Neuschwander-Tetri BA, Brunt EM, Dolman CS, et al. Glucagon-like peptide-1 receptor agonism improves metabolic, biochemical, and histopathological indices of nonalcoholic steatohepatitis in mice. American Journal of Physiology-Gastrointestinal and Liver Physiology. 2012 Apr 15;302(8):G762–72.

137. Bieghs V, van Gorp PJ, Wouters K, Hendrikx T, Gijbels MJ, van Bilsen M, et al. LDL Receptor Knock-Out Mice Are a Physiological Model Particularly Vulnerable to Study the Onset of Inflammation in Non-Alcoholic Fatty Liver Disease. PLoS One. 2012 Jan 25;7(1):e30668.

138. Schierwagen R, Maybüchen L, Zimmer S, Hittatiya K, Bäck C, Klein S, et al. Seven weeks of Western diet in apolipoprotein-E-deficient mice induce metabolic syndrome and non-alcoholic steatohepatitis with liver fibrosis. Sci Rep. 2015 Oct 11;5(1):12931.

139. Kristiansen MNB, Veidal SS, Rigbolt KTG, Tølbøl KS, Roth JD, Jelsing J, et al. Obese diet-induced mouse models of nonalcoholic steatohepatitis-tracking disease by liver biopsy. World J Hepatol. 2016;8(16):673.

140. Charlton M, Krishnan A, Viker K, Sanderson S, Cazanave S, McConico A, et al. Fast food diet mouse: novel small animal model of NASH with ballooning, progressive fibrosis, and high physiological fidelity to the human condition. American Journal of Physiology-Gastrointestinal and Liver Physiology. 2011 Nov;301(5):G825–34.

141. Jahn D, Kircher S, Hermanns HM, Geier A. Animal models of NAFLD from a hepatologist's point of view. Biochimica et Biophysica Acta (BBA) - Molecular Basis of Disease. 2019 May;1865(5):943–53.

142. Lackner C. Hepatocellular ballooning in nonalcoholic steatohepatitis: the pathologist's perspective. Expert Rev Gastroenterol Hepatol. 2011 Apr 10;5(2):223–31.

143. Rangwala F, Guy CD, Lu J, Suzuki A, Burchette JL, Abdelmalek MF, et al. Increased production of sonic hedgehog by ballooned hepatocytes. J Pathol. 2011 Jul;224(3):401–10.

144. Caldwell S, Lackner C. Perspectives on NASH Histology: Cellular Ballooning. Ann Hepatol. 2017 Mar;16(2):182–4.

145. Abdelmagid SA, Clarke SE, Nielsen DE, Badawi A, El-Sohemy A, Mutch DM, et al. Comprehensive Profiling of Plasma Fatty Acid Concentrations in Young Healthy Canadian Adults. PLoS One. 2015 Feb 12;10(2):e0116195.

146. Schindelin J, Arganda-Carreras I, Frise E, Kaynig V, Longair M, Pietzsch T, et al. Fiji: an open-source platform for biological-image analysis. Nat Methods. 2012 Jul 28;9(7):676–82.

147. Kapur JN, Sahoo PK, Wong AKC. A new method for gray-level picture thresholding using the entropy of the histogram. Comput Vis Graph Image Process. 1985 Mar;29(3):273–85.

148. Kulak NA, Geyer PE, Mann M. Loss-less Nano-fractionator for High Sensitivity, High Coverage Proteomics. Molecular & Cellular Proteomics. 2017 Apr;16(4):694–705.

149. Tyanova S, Temu T, Cox J. The MaxQuant computational platform for mass spectrometry-based shotgun proteomics. Nat Protoc. 2016 Dec 27;11(12):2301–19.

150. Tyanova S, Temu T, Sinitcyn P, Carlson A, Hein MY, Geiger T, et al. The Perseus computational platform for comprehensive analysis of (prote)omics data. Nat Methods. 2016 Sep 27;13(9):731–40.

151. Hulsen T, de Vlieg J, Alkema W. BioVenn – a web application for the comparison and visualization of biological lists using area-proportional Venn diagrams. BMC Genomics. 2008;9(1):488.

152. Folch J, Lees M, Stanley GHS. A SIMPLE METHOD FOR THE ISOLATION AND PURIFICATION OF TOTAL LIPIDES FROM ANIMAL TISSUES. Journal of Biological Chemistry. 1957 May;226(1):497–509.

153. Iverson SJ, Lang SLC, Cooper MH. Comparison of the bligh and dyer and folch methods for total lipid determination in a broad range of marine tissue. Lipids. 2001 Nov;36(11):1283–7.

154. Züllig T, Trötzmüller M, Köfeler HC. Lipidomics from sample preparation to data analysis: a primer. Anal Bioanal Chem. 2020 Apr 10;412(10):2191–209.

155. Hartler J, Trötzmüller M, Chitraju C, Spener F, Köfeler HC, Thallinger GG. Lipid Data Analyzer: unattended identification and quantitation of lipids in LC-MS data. Bioinformatics. 2011 Feb 15;27(4):572–7.

156. Pino LK, Searle BC, Bollinger JG, Nunn B, MacLean B, MacCoss MJ. The Skyline ecosystem: Informatics for quantitative mass spectrometry proteomics. Mass Spectrom Rev. 2020 May;39(3):229–44.

157. Listenberger LL, Han X, Lewis SE, Cases S, Farese R v., Ory DS, et al. Triglyceride accumulation protects against fatty acid-induced lipotoxicity. Proceedings of the National Academy of Sciences. 2003 Mar 18;100(6):3077–82.

158. Ricchi M, Odoardi MR, Carulli L, Anzivino C, Ballestri S, Pinetti A, et al. Differential effect of oleic and palmitic acid on lipid accumulation and apoptosis in cultured hepatocytes. J Gastroenterol Hepatol. 2009 May;24(5):830–40.

159. Anderson CW. DNA damage and the DNA-activated protein kinase. Trends Biochem Sci. 1993 Nov;18(11):433–7.

160. Kwan HY, Fong WF, Yang Z, Yu ZL, Hsiao WLW. Inhibition of DNA-dependent protein kinase reduced palmitate and oleate-induced lipid accumulation in HepG2 cells. Eur J Nutr. 2013 Sep 27;52(6):1621–30.

161. Wong RHF, Chang I, Hudak CSS, Hyun S, Kwan HY, Sul HS. A Role of DNA-PK for the Metabolic Gene Regulation in Response to Insulin. Cell. 2009 Mar;136(6):1056–72.

162. Zhou H, Zhu P, Wang J, Toan S, Ren J. DNA-PKcs promotes alcohol-related liver disease by activating Drp1-related mitochondrial fission and repressing FUNDC1-required mitophagy. Signal Transduct Target Ther. 2019 Dec 6;4(1):56.

163. Shao Z, Flynn RA, Crowe JL, Zhu Y, Liang J, Jiang W, et al. DNA-PKcs has KU-dependent function in rRNA processing and haematopoiesis. Nature. 2020 Mar 12;579(7798):291–6.

164. Antonicka H, Sasarman F, Nishimura T, Paupe V, Shoubridge EA. The Mitochondrial RNA-Binding Protein GRSF1 Localizes to RNA Granules and Is Required for Posttranscriptional Mitochondrial Gene Expression. Cell Metab. 2013 Mar;17(3):386–98.

165. Jourdain AA, Koppen M, Wydro M, Rodley CD, Lightowlers RN, Chrzanowska-Lightowlers ZM, et al. GRSF1 Regulates RNA Processing in Mitochondrial RNA Granules. Cell Metab. 2013 Mar;17(3):399–410.

166. Enomoto H, Nakamura H, Liu W, Nishiguchi S. Hepatoma-Derived Growth Factor: Its Possible Involvement in the Progression of Hepatocellular Carcinoma. Int J Mol Sci. 2015 Jun 19;16(12):14086–97.

167. Kümper S, Mardakheh FK, McCarthy A, Yeo M, Stamp GW, Paul A, et al. Rho-associated kinase (ROCK) function is essential for cell cycle progression, senescence and tumorigenesis. Elife. 2016 Jan 14;5.

168. Ji J, Zhang L, Wang P, Mu YM, Zhu XY, Wu YY, et al. Saturated free fatty acid, palmitic acid, induces apoptosis in fetal hepatocytes in culture. Experimental and Toxicologic Pathology. 2005 Apr;56(6):369–76.

169. Hong F, Pan S, Guo Y, Xu P, Zhai Y. PPARs as Nuclear Receptors for Nutrient and Energy Metabolism. Molecules. 2019 Jul 12;24(14):2545.

170. Armstrong PB, Quigley JP. α 2 -macroglobulin: an evolutionarily conserved arm of the innate immune system. Dev Comp Immunol. 1999 Jun;23(4–5):375–90.

171. Gourine A v., Gourine VN, Tesfaigzi Y, Caluwaerts N, van Leuven F, Kluger MJ. Role of α 2 - macroglobulin in fever and cytokine responses induced by lipopolysaccharide in mice. American Journal of Physiology-Regulatory, Integrative and Comparative Physiology. 2002 Jul 1;283(1):R218–26.

172. Kalsheker NA. α1-antichymotrypsin. Int J Biochem Cell Biol. 1996 Sep;28(9):961–4.

173. Silverman GA, Bird PI, Carrell RW, Church FC, Coughlin PB, Gettins PGW, et al. The Serpins Are an Expanding Superfamily of Structurally Similar but Functionally Diverse Proteins. Journal of Biological Chemistry. 2001 Sep;276(36):33293–6.

174. Echeverría F, Valenzuela R, Espinosa A, Bustamante A, Álvarez D, Gonzalez-Mañan D, et al. Reduction of high-fat diet-induced liver proinflammatory state by eicosapentaenoic acid plus hydroxytyrosol supplementation: involvement of resolvins RvE1/2 and RvD1/2. J Nutr Biochem. 2019 Jan;63:35–43.

175. Korbecki J, Bajdak-Rusinek K. The effect of palmitic acid on inflammatory response in macrophages: an overview of molecular mechanisms. Inflammation Research. 2019 Nov 30;68(11):915–32.

176. Andreyev AYu, Kushnareva YuE, Starkov AA. Mitochondrial metabolism of reactive oxygen species. Biochemistry (Moscow). 2005 Feb;70(2):200–14.

177. Loomba R, Jain A, Diehl AM, Guy CD, Portenier D, Sudan R, et al. Validation of Serum Test for Advanced Liver Fibrosis in Patients With Nonalcoholic Steatohepatitis. Clinical Gastroenterology and Hepatology. 2019 Aug;17(9):1867-1876.e3.

178. Speziali G, Liesinger L, Gindlhuber J, Leopold C, Pucher B, Brandi J, et al. Myristic acid induces proteomic and secretomic changes associated with steatosis, cytoskeleton remodeling, endoplasmic reticulum stress, protein turnover and exosome release in HepG2 cells. J Proteomics. 2018 Jun;181:118–30.

179. Fissolo N, Matute-Blanch C, Osman M, Costa C, Pinteac R, Miró B, et al. CSF SERPINA3 Levels Are Elevated in Patients With Progressive MS. Neurology - Neuroimmunology Neuroinflammation. 2021 Mar 12;8(2):e941.

180. Norton ES, da Mesquita S, Guerrero-Cazares H. SERPINA3 in glioblastoma and Alzheimer's disease. Aging. 2021 Sep 30;13(18):21812–3.

181. Ko E, Kim JS, Bae JW, Kim J, Park SG, Jung G. SERPINA3 is a key modulator of HNRNP-K transcriptional activity against oxidative stress in HCC. Redox Biol. 2019 Jun;24:101217.

182. Gallardo M, Hornbaker MJ, Zhang X, Hu P, Bueso-Ramos C, Post SM. Aberrant hnRNP K expression: All roads lead to cancer. Cell Cycle. 2016 Jun 17;15(12):1552–7.

183. Rocha DM, Caldas AP, Oliveira LL, Bressan J, Hermsdorff HH. Saturated fatty acids trigger TLR4-mediated inflammatory response. Atherosclerosis. 2016 Jan;244:211–5.

184. Ma X, Ding Y, Zeng L. The diagnostic and prognostic value of H2AFY in hepatocellular carcinoma. BMC Cancer. 2021 Dec 15;21(1):418.

185. Yamamoto T, Takabatake Y, Minami S, Sakai S, Fujimura R, Takahashi A, et al. Eicosapentaenoic acid attenuates renal lipotoxicity by restoring autophagic flux. Autophagy. 2021 Jul 3;17(7):1700–13.

186. Gao B, Sakaguchi K, Matsuura K, Ogawa T, Kagawa Y, Kubo H, et al. In Vitro Production of Human Ballooned Hepatocytes in a Cell Sheet-based Three-dimensional Model. Tissue Eng Part A. 2020 Jan 1;26(1–2):93–101.

6. Appendix

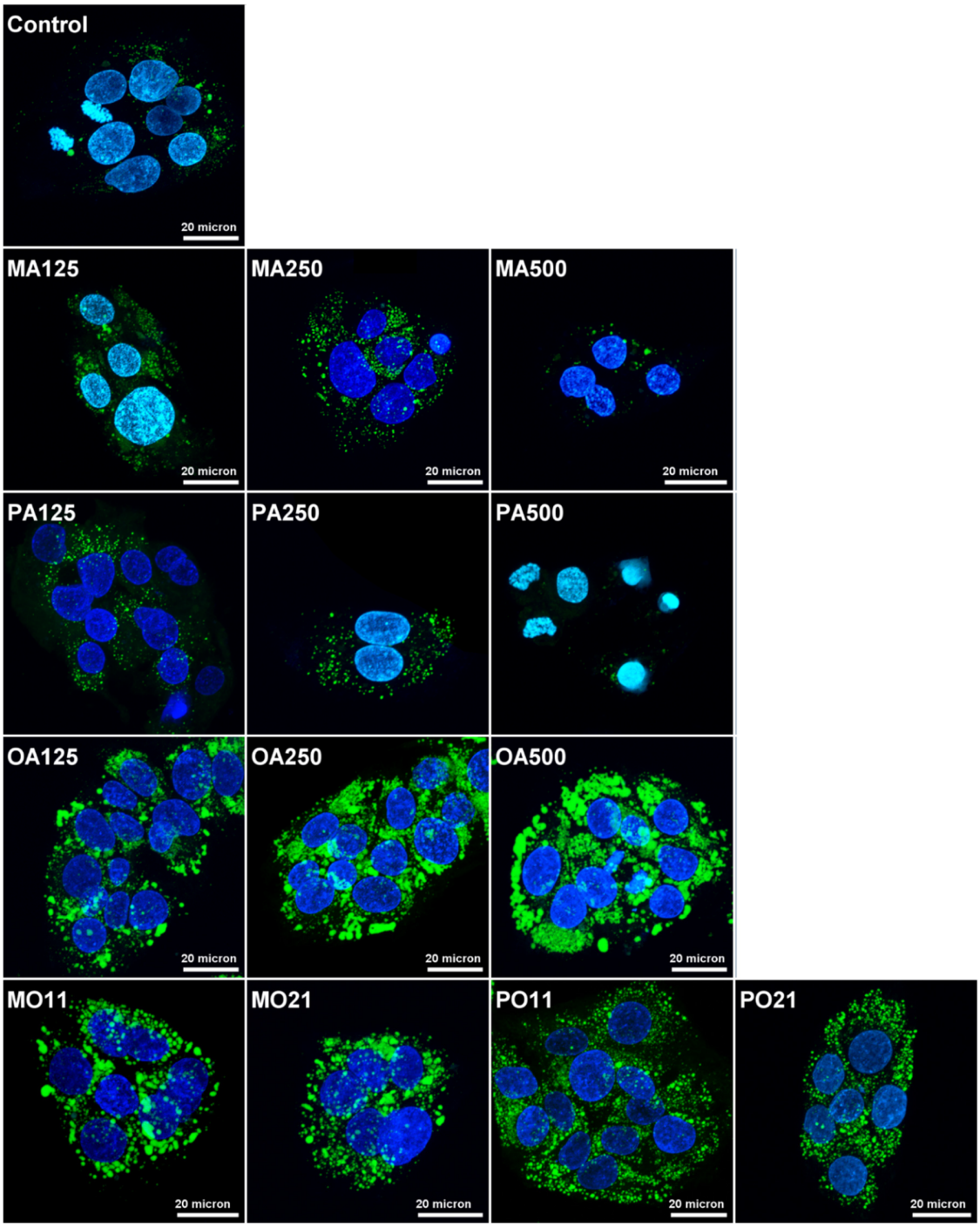

Appendix 1 Representative images of HepG2 cells after 24 hours of lipid loading. Lipid droples have been stained with BODIPY™ 493/503 and nuclei with DAPI (lipid droplets= green; nuclei= blue). MA: myristic acid; PA: palmitic acid; OA: oleic acid; MO: myristic: oleic acid; PO: palmitic: oleic acid; 125: 125µM; 250: 250µM; 500: 500µM;11: 125µM: 125 µM; 21: 250 µM: 125 µM. Figure adapted from Gindlhuber et al. 2022 with permission from the publisher.

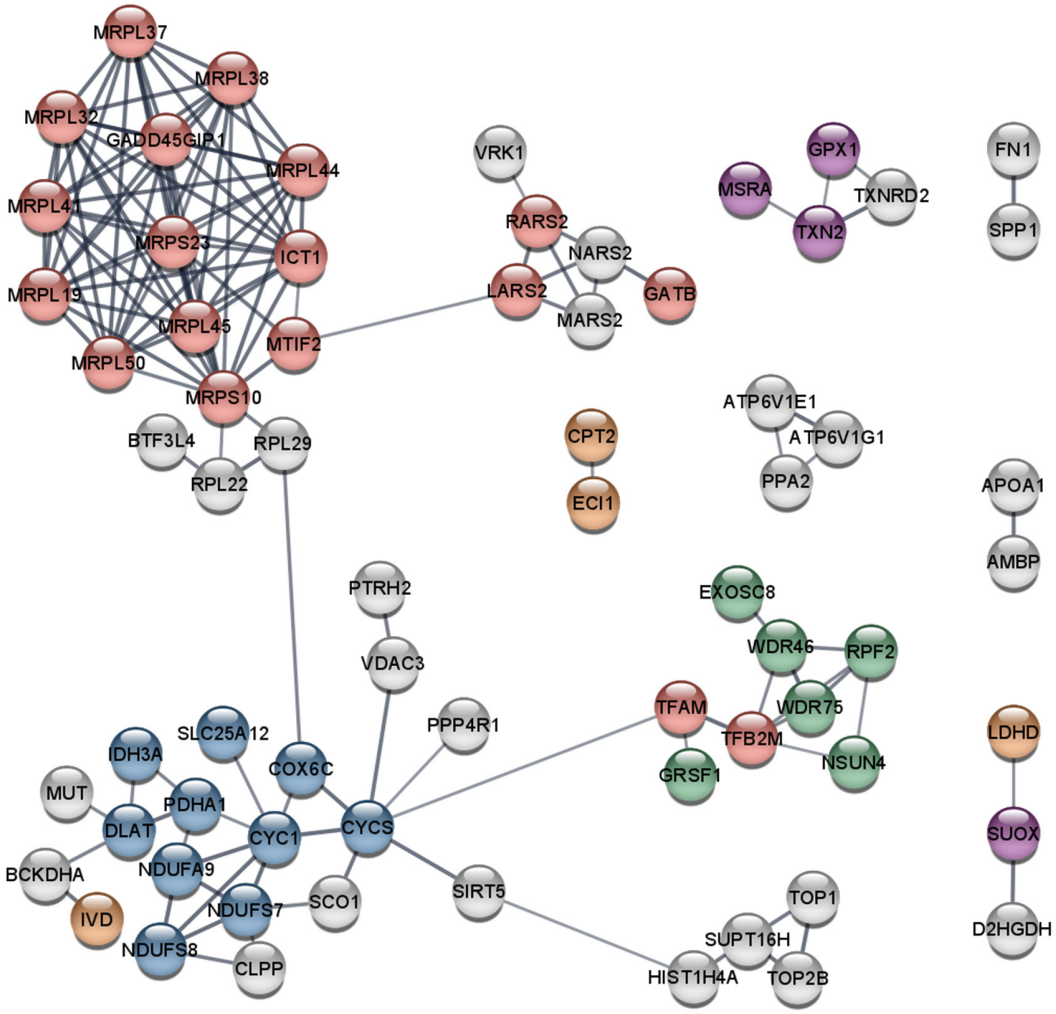

	GO-term	strength	FDR
	Mitochondrial gene expression	1.33	4.94e-15
	Cellular respiration	1.05	4.59e-06
	Monocarboxylic acid catabolic process	0.91	0.0317
	ncRNA metabolic process	0.69	0.00058
	Sulfur compound metabolic process	0.66	0.0237

Appendix 2 String analysis of proteins exhibiting a ≥1.5-fold change following MA500 treatment. The minimum required interaction score was set to 0.7 (high confidence) and disconnected nodes were excluded from the display. Nodes were colored correspondingly to selected GO biological process search results. MA treatment resulted in an upregulation of proteins associated with mitochondrial protein synthesis as well as oxidative phosphorylation. MA500: 500 µM myristic acid for 24 h. Figure adapted from Gindlhuber et al. 2022 with permission from the publisher.

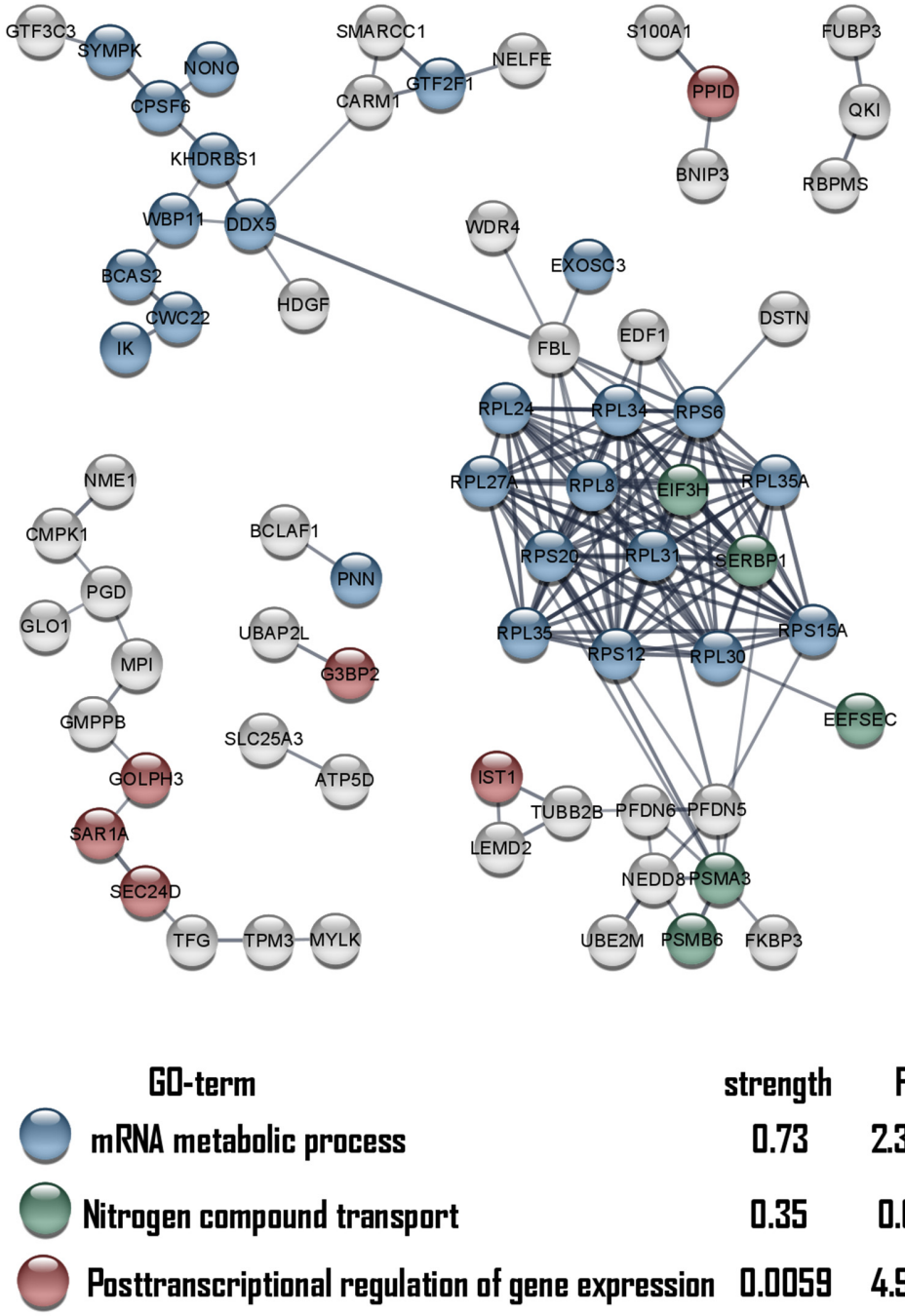

Appendix 3 String analysis of proteins exhibiting a ≥-1.5-fold change following MA500 treatment. The minimum required interaction score was set to 0.7 (high confidence) and disconnected nodes were excluded from the display. Nodes were colored corresponding to selected GO biological process search. MA treatment resulted in a downregulation of ribosomal proteins indicating a reduction in cellular growth. MA500: 500 µM myristic acid for 24 h. Figure adapted from Gindlhuber et al. 2022 with permission from the publisher.

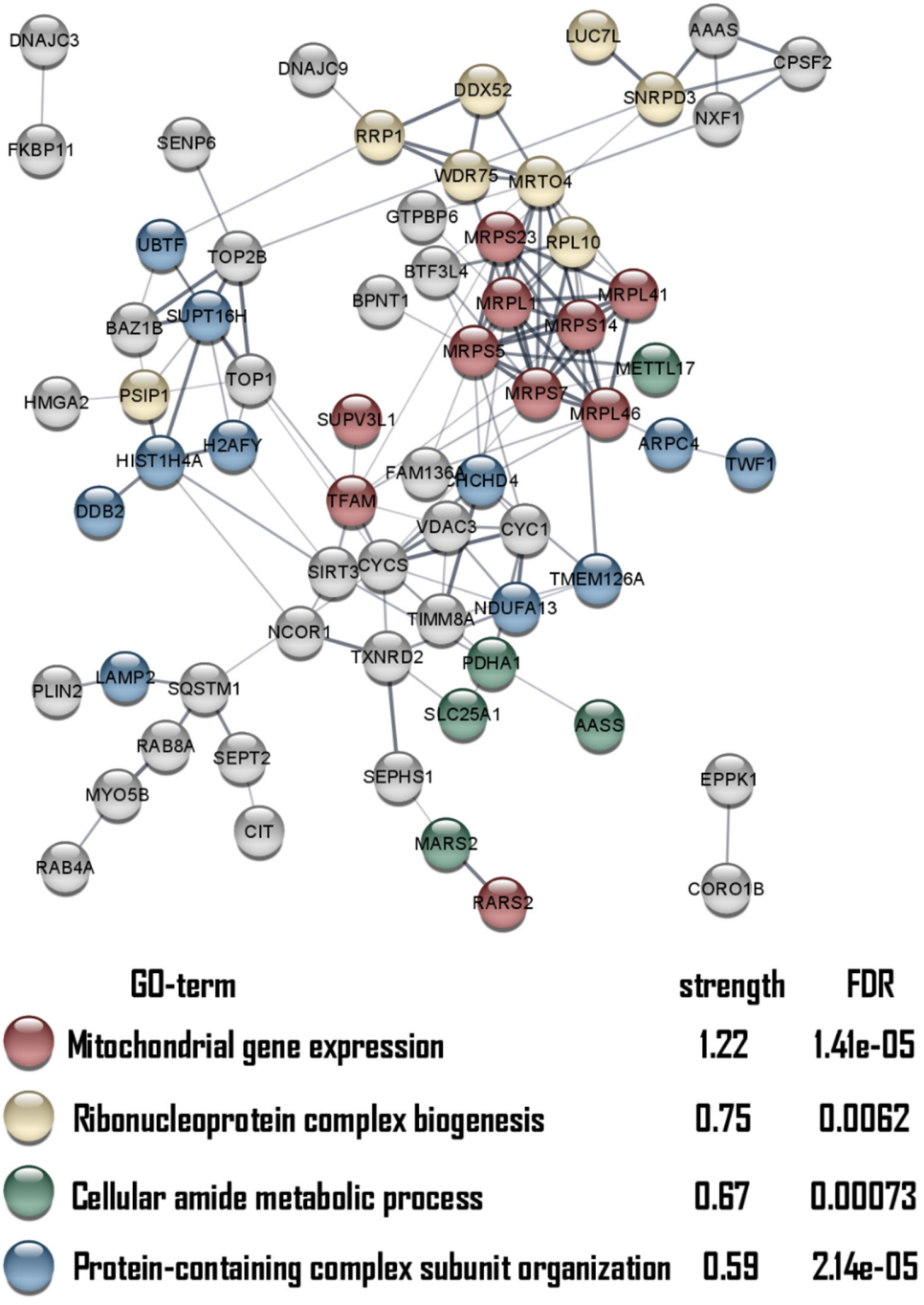

Appendix 4 String analysis of proteins exhibiting a ≥1.5-fold change following PA500 treatment. The minimum required interaction score was set to 0.7 (high confidence) and disconnected nodes were excluded from the display. Nodes were colored correspondingly to selected GO biological process search results. PA treatment resulted in an upregulation of proteins associated with mitochondrial protein synthesis.PA500: 500 µM palmitic acid for 24 h. Figure adapted from Gindlhuber et al. 2022 with permission from the publisher. Figure adapted from Gindlhuber et al. 2022 with permission from the publisher.

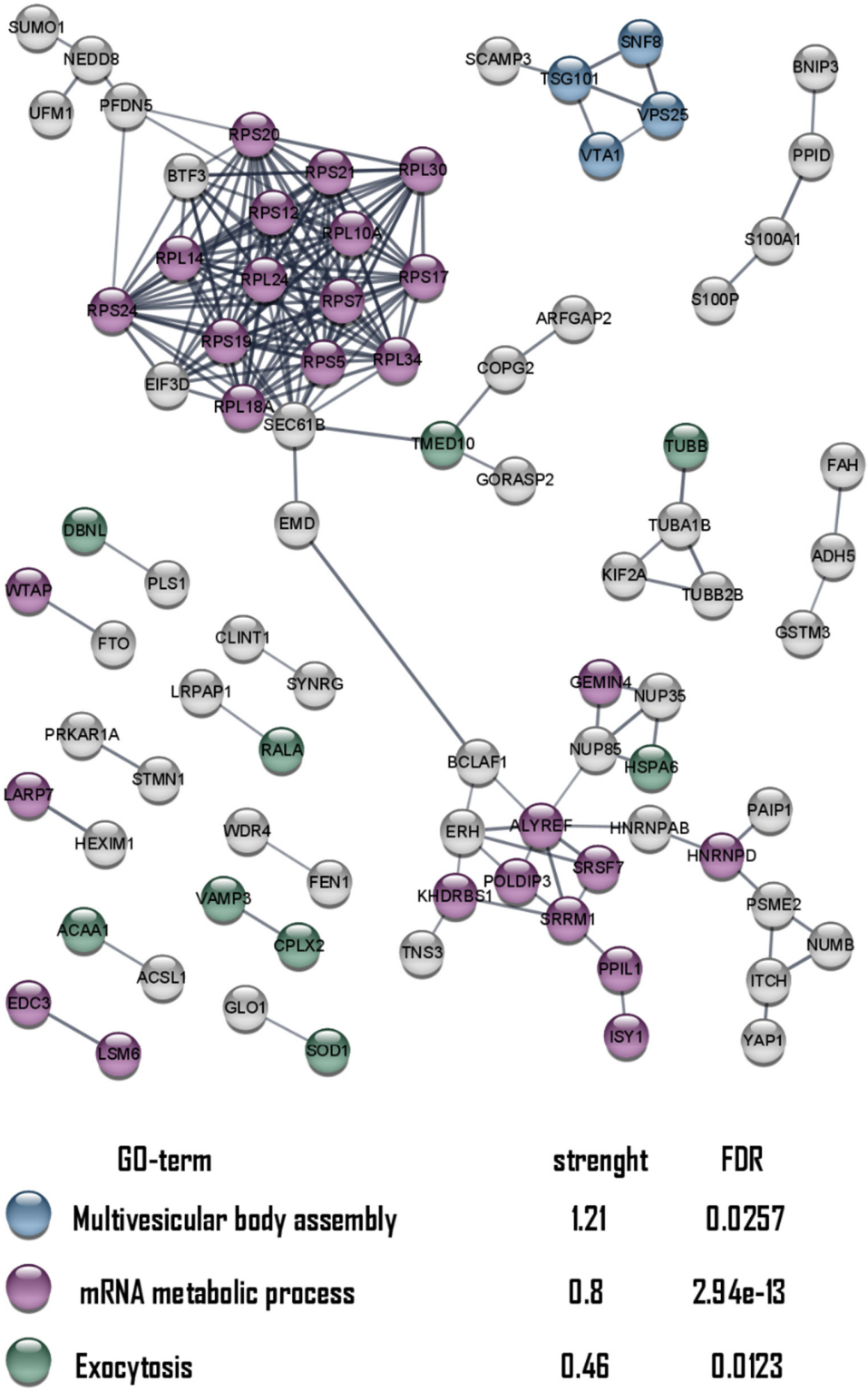

Appendix 5 String analysis of proteins exhibiting a ≥-1.5-fold change following PA500 treatment. The minimum required interaction score was set to 0.7 (high confidence) and disconnected nodes were excluded from the display. Nodes were colored correspondingly to selected GO biological process search. PA treatment resulted in a downregulation of ribosomal proteins indicating a reduction of cellular growth. PA500: 500 µM palmitic acid for 24 h. Figure adapted from Gindlhuber et al. 2022 with permission from the publisher.

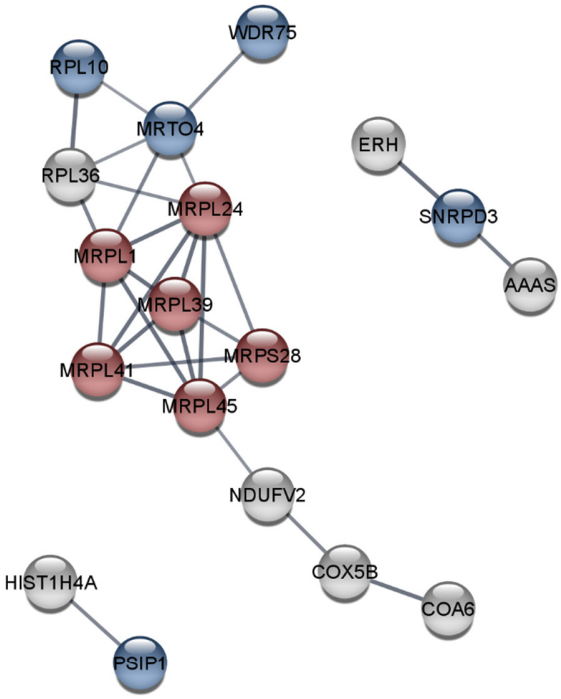

GO-term	strength	FDR
Mitochondrial gene expression	1.3	5.34e-05
Ribonucleoprotein complex biogenesis	0.83	0.0124

Appendix 6 String analysis of proteins exhibiting a ≥1.5-fold change following OA500 treatment. The minimum required interaction score was set to 0.7 (high confidence) and disconnected nodes were excluded from the display. Nodes were colored correspondingly to selected GO biological process search results. Treatment with OA led to an increase of proteins associated with mitochondrial protein synthesis. OA500: 500 µM oleic acid for 24 h. Figure adapted from Gindlhuber et al. 2022 with permission from the publisher.

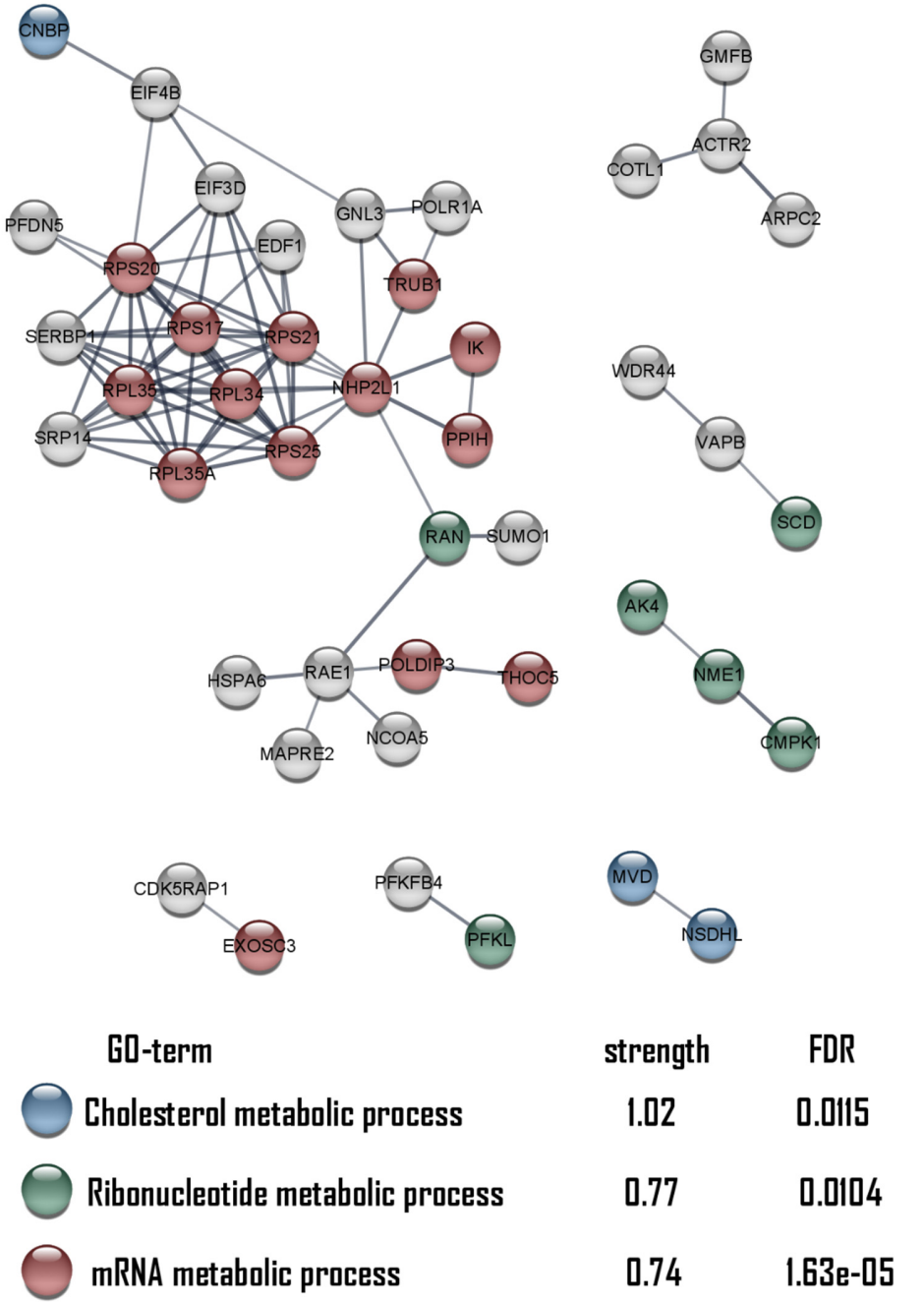

Appendix 7 String analysis of proteins exhibiting a ≥-1.5-fold change following OA500 treatment. The minimum required interaction score was set to 0.7 (high confidence) and disconnected nodes were excluded from the display. Nodes were colored correspondingly to selected GO biological process search results. OA treatment resulted in a downregulation of ribosomal proteins indicating a reduction of cellular growth. OA500: 500 µM oleic acid for 24 h. Figure adapted from Gindlhuber et al. 2022 with permission from the publisher.

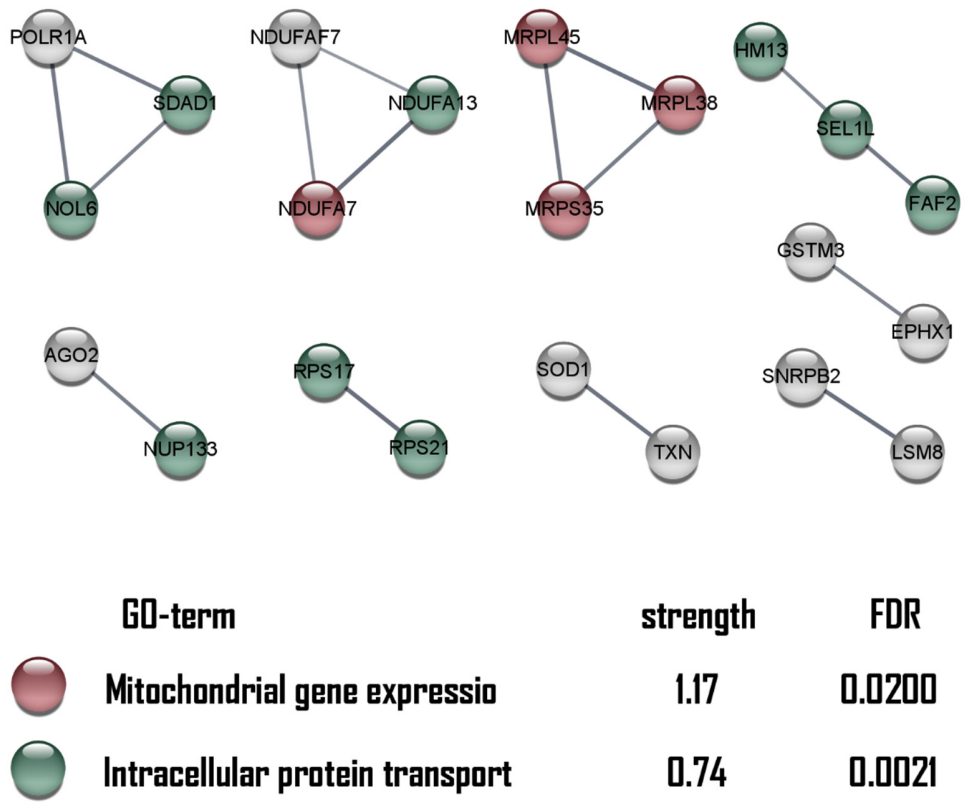

Appendix 8 String analysis of proteins exhibiting a ≥1.5-fold change comparing MA250 treatment to MO21. The minimum required interaction score was set to 0.7 (high confidence) and disconnected nodes were excluded from the display. Nodes were colored correspondingly to selected GO biological process search results. Compared to the prevention treatment, MA250 presented with an upregulation of proteins associated with mitochondrial and cytoplasmic protein synthesis. MA250: 250 µM myristic acid for 24 h. MO21: 250 µM myristic acid: 125 µM oleic acid for 24 h. Figure adapted from Gindlhuber et al. 2022 with permission from the publisher.

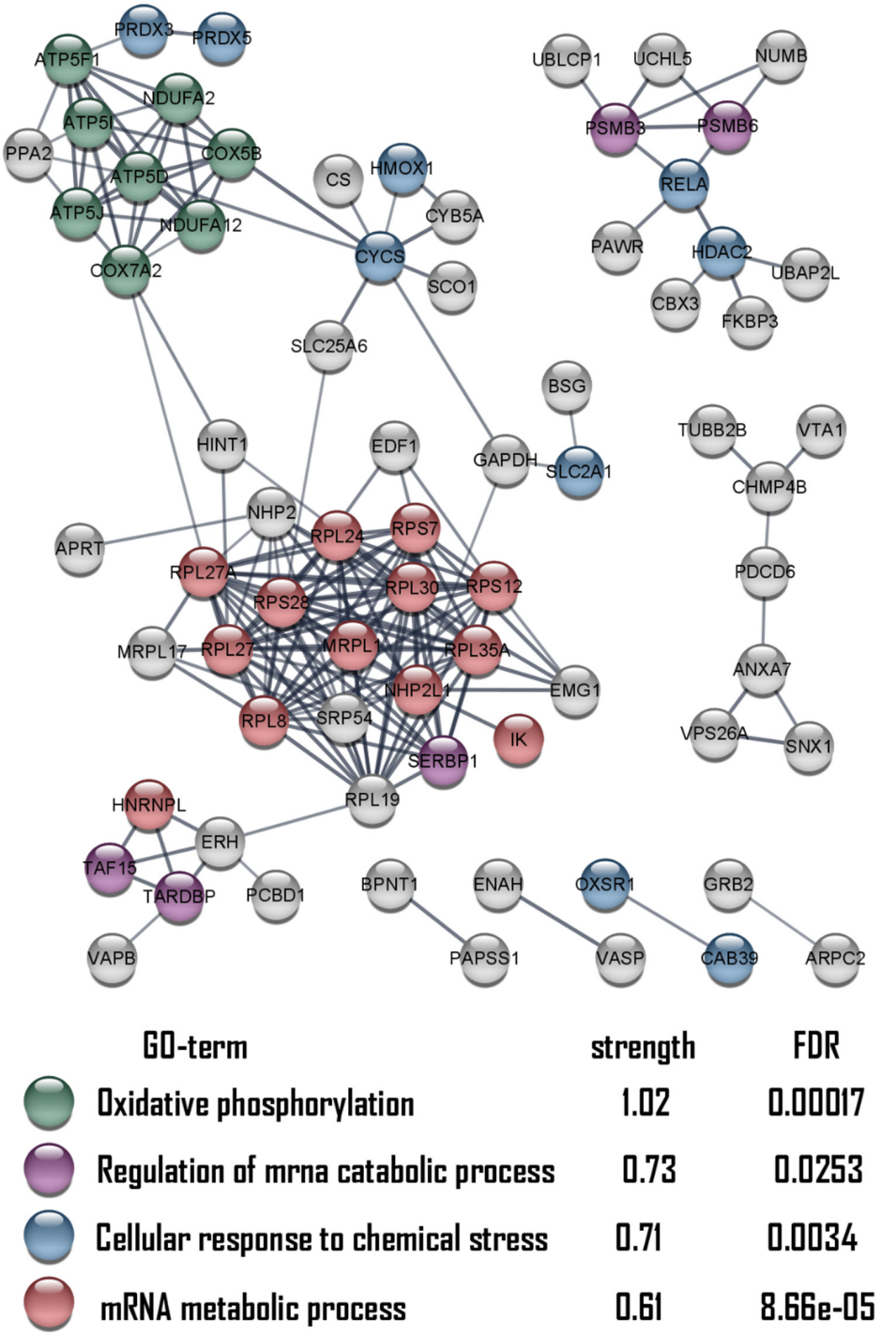

Appendix 9 String analysis of proteins exhibiting a ≥-1.5-fold change comparing MA250 treatment to MO21. The minimum required interaction score was set to 0.7 (high confidence) and disconnected nodes were excluded from the display. Nodes were colored correspondingly to selected GO biological process search results. In the prevention treatment proteins associated with oxidative phosphorylation and ribosomal proteins were found to be more abundant. The overabundance of ribosomal proteins corroborated the increase of proliferation rates back to control levels. MA250: 250 µM myristic acid for 24 h. MO21: 250 µM myristic acid: 125 µM oleic acid for 24 h. Figure adapted from Gindlhuber et al. 2022 with permission from the publisher.

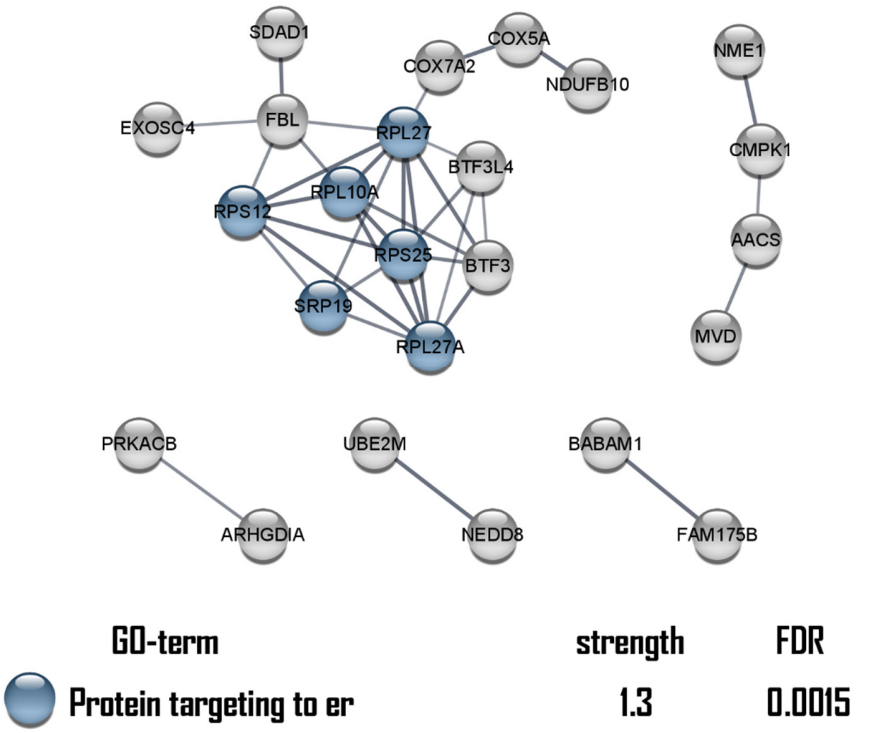

Appendix 10 String analysis of proteins exhibiting a ≥1.5-fold change comparing PA250 treatment to PO21. The minimum required interaction score was set to 0.7 (high confidence) and disconnected nodes were excluded from the display. Nodes were colored correspondingly to selected GO biological process search results. Compared to the prevention treatment, a subset of ribosomal proteins was found to be significantly enriched following PA treatment. PA250: 250 µM palmitic acid for 24 h. PO21: 250 µM palmitic acid: 125 µM oleic acid for 24 h Figure adapted from Gindlhuber et al. 2022 with permission from the publisher.

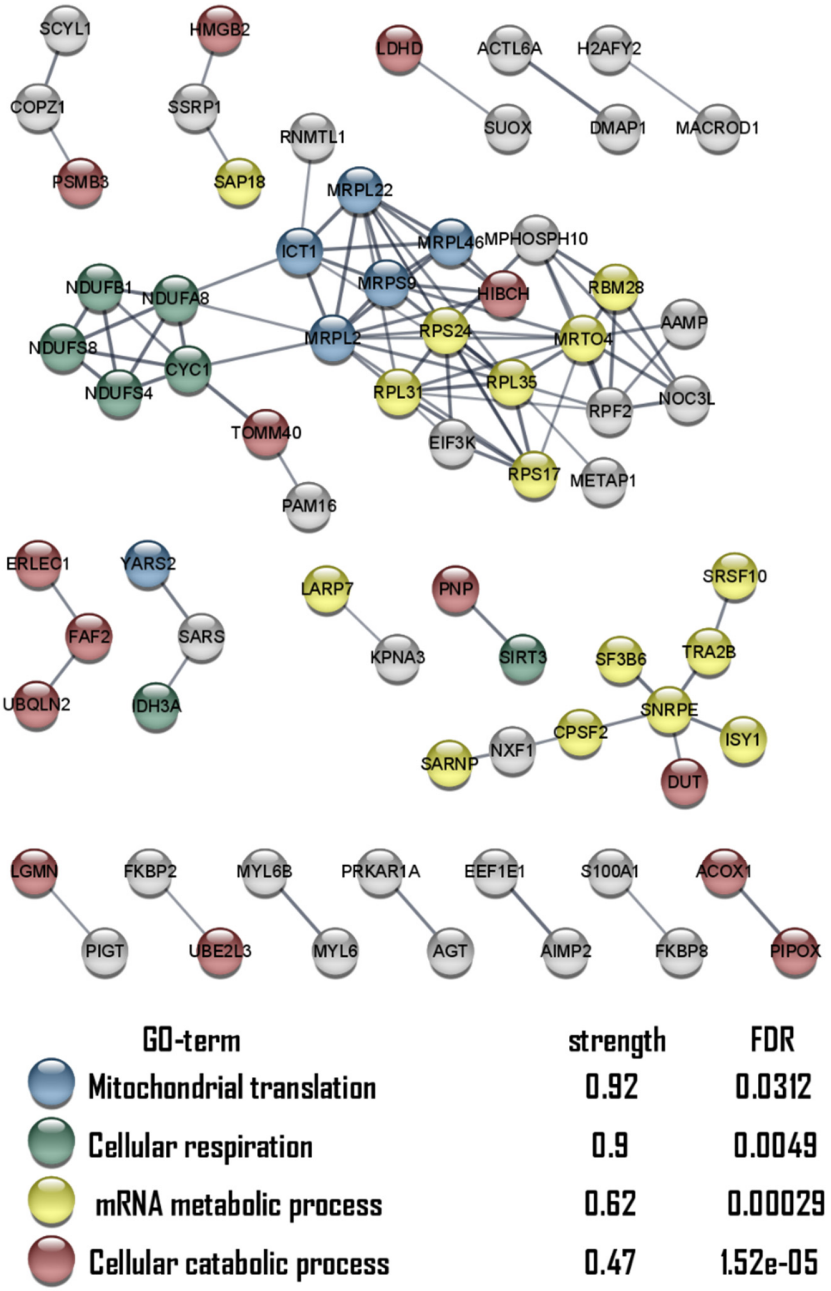

Appendix 11 String analysis of proteins exhibiting a ≥-1.5-fold change comparing PA250 treatment to PO21. The minimum required interaction score was set to 0.7 (high confidence) and disconnected nodes were excluded from the display. Nodes were colored correspondingly to selected GO biological process search results. Proteins associated with mitochondrial protein synthesis and oxidative phosphorylation, as well as a subset of ribosomal proteins was found to be significantly enriched in the prevention treatment. PA250: 250 µM palmitic acid for 24 h. PO21: 250 µM palmitic acid: 125 µM oleic acid for 24 h. Figure adapted from Gindlhuber et al. 2022 with permission from the publisher.

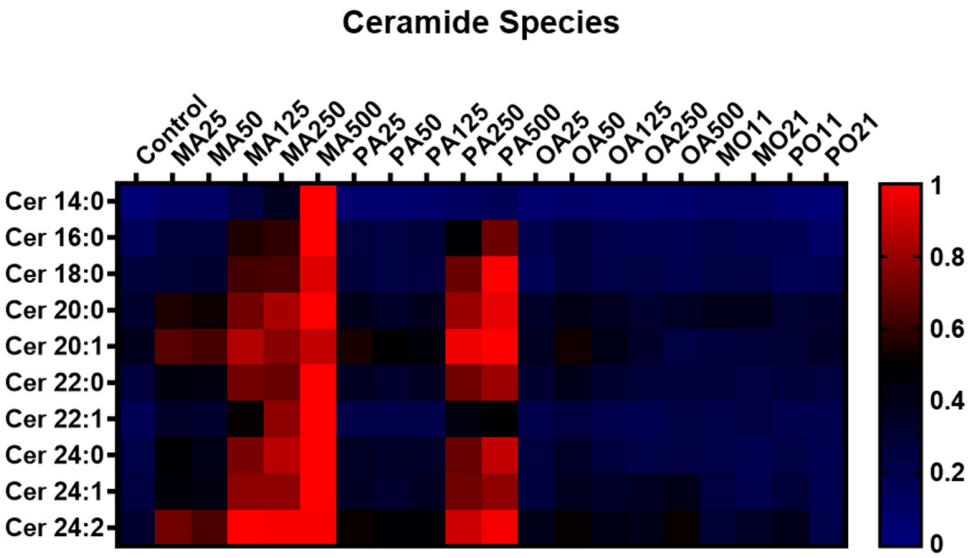

Appendix 12 Heatmap of measured ceramide species. Chain length indicates the second fatty acyl CoA chain added to a C18 sphingosine body. Results are normalized on the maximum within each row. All measured species are elevated following saturated FA treatment. C14:0 is only observable following MA supplementation. Surprisingly also C16:0 levels proved to be higher following MA supplementation rather than in PA treated samples.

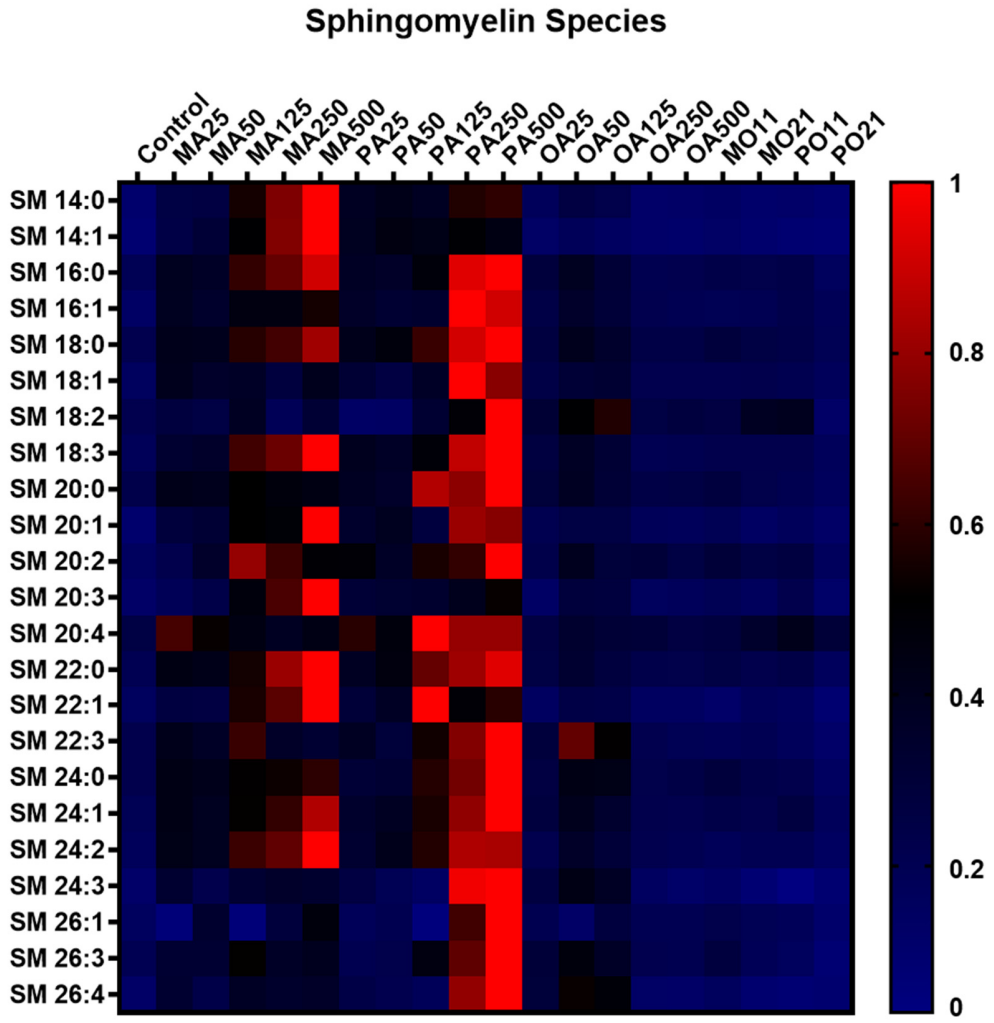

Appendix 13 Heatmap of measured sphingomyelin species. Chain length indicates the second fatty acyl CoA chain added to a sphingosine body with either a phosphocholine or phosphoethanolamine group. Results are normalized on the maximum within each row. All measured species are elevated following saturated FA treatment. 14:0 FA is only observable following MA supplementation as well as its mono unsaturated form 14:1. 16:0 sphingomyelin levels are the highest following PA treatment, indicating an upregulation of sphingomyelin synthesis specifically following PA treatment.

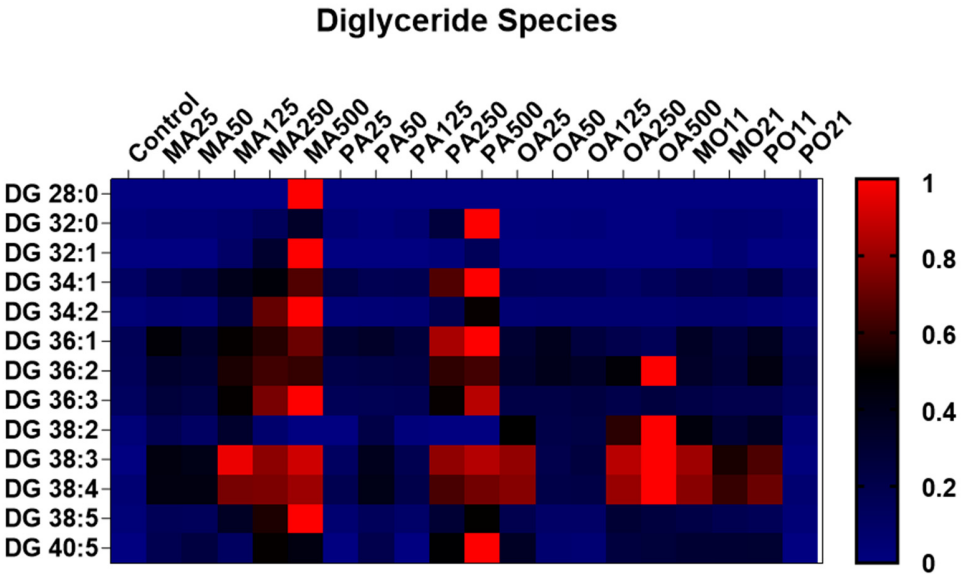

Appendix 14 Heatmap of measured diglyceride species. Chain length indicates the sum of both fatty acyl CoA chains added to a glycerin body. Results are normalized on the maximum within each row. Levels are found to be elevated following high concentrations of FA treatment with the main corresponding DG exhibiting maxima following treatment with its corresponding FA. (MA DG 28:0; PA DG 32:0; OA DG 36:2)

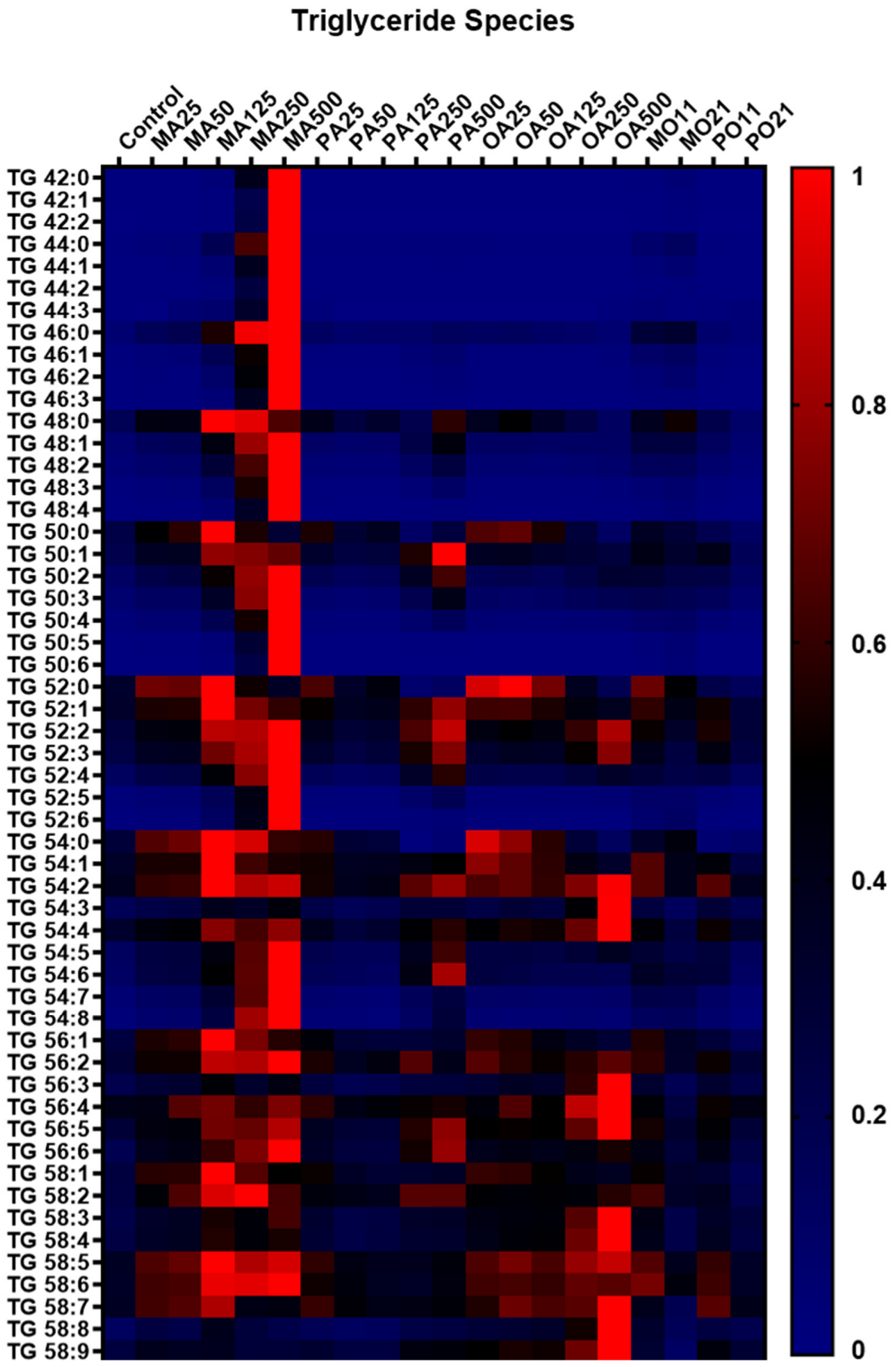
Triglyceride Species
Control
MA25
MA50
MA125
MA250
MA500
PA25
PA50
PA125
PA250
PA500
OA25
OA50
OA125
OA250
OA500
MO11
MO21
PO11
PO21
TG 42:0
TG 42:1
TG 42:2
TG 44:0
TG 44:1
TG 44:2
TG 44:3
TG 46:0
TG 46:1
TG 46:2
TG 46:3
TG 48:0
TG 48:1
TG 48:2
TG 48:3
TG 48:4
TG 50:0
TG 50:1
TG 50:2
TG 50:3
TG 50:4
TG 50:5
TG 50:6
TG 52:0
TG 52:1
TG 52:2
TG 52:3
TG 52:4
TG 52:5
TG 52:6
TG 54:0
TG 54:1
TG 54:2
TG 54:3
TG 54:4
TG 54:5
TG 54:6
TG 54:7
TG 54:8
TG 56:1
TG 56:2
TG 56:3
TG 56:4
TG 56:5
TG 56:6
TG 58:1
TG 58:2
TG 58:3
TG 58:4
TG 58:5
TG 58:6
TG 58:7
TG 58:8
TG 58:9
1
0.8
0.6
0.4
0.2
0

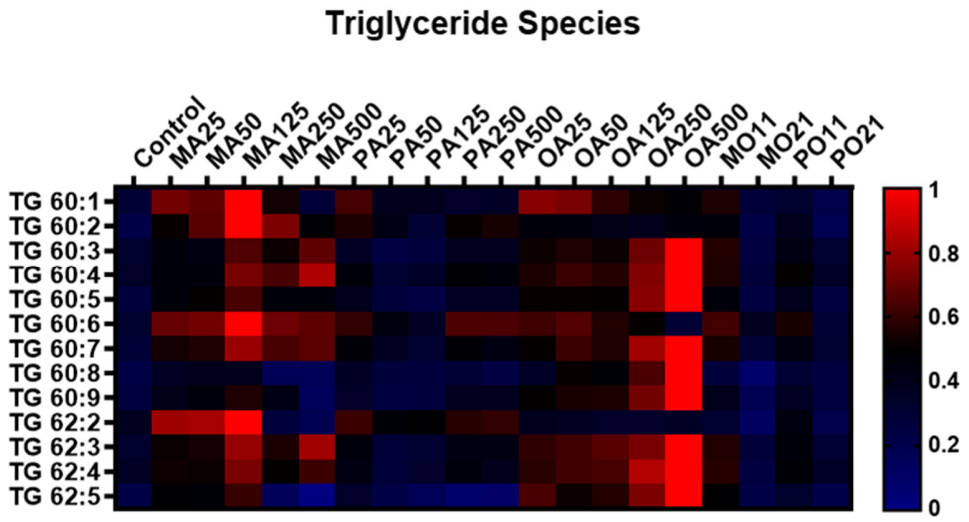

Appendix 15 Heatmap of measured triglyceride species. Chain length indicates the sum of the three fatty acyl CoA chains added to a glycerin body. Results are normalized on the maximum within each row. Levels are found to be elevated following high concentrations of FA treatment with the exception of PA. Following MA treatment to the formation of TG 42:0 trimyristin could be observed which was thought not to be dominantly present in mammalian cells. OA induced the predominantly the formation of triolein, TG 54:3 and in general impacted more the abundance of TGs with longer chain length and higher grade of desaturation compared to MA.

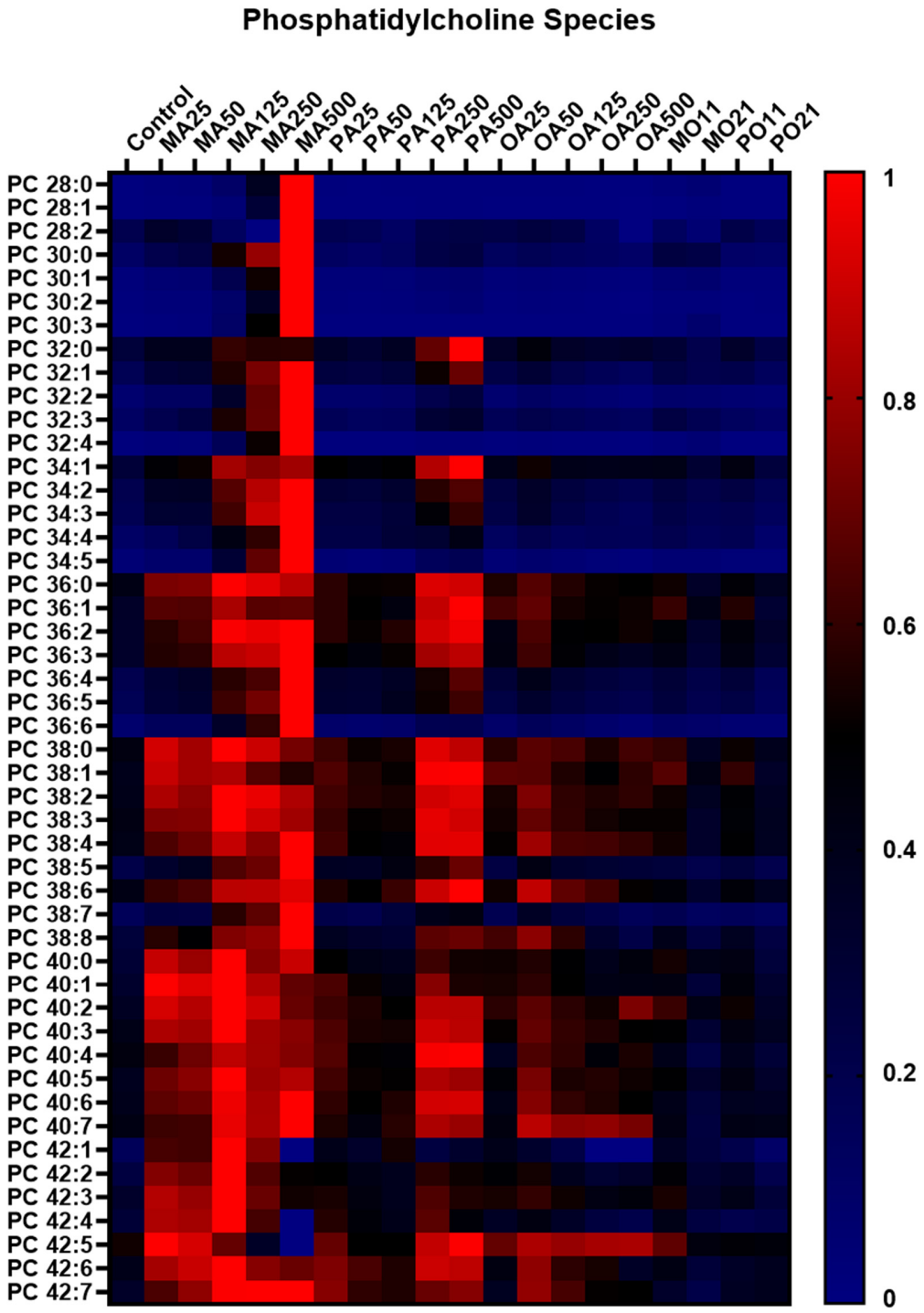

Appendix 16 Heatmap of measured phosphatidylcholine species. Chain length indicates the sum of both fatty acyl CoA chain added to a glycerin with a phosphatidylcholine head group. Results are normalized on the maximum within each row. In general levels seamed to only be elevated following saturated FA treatment.

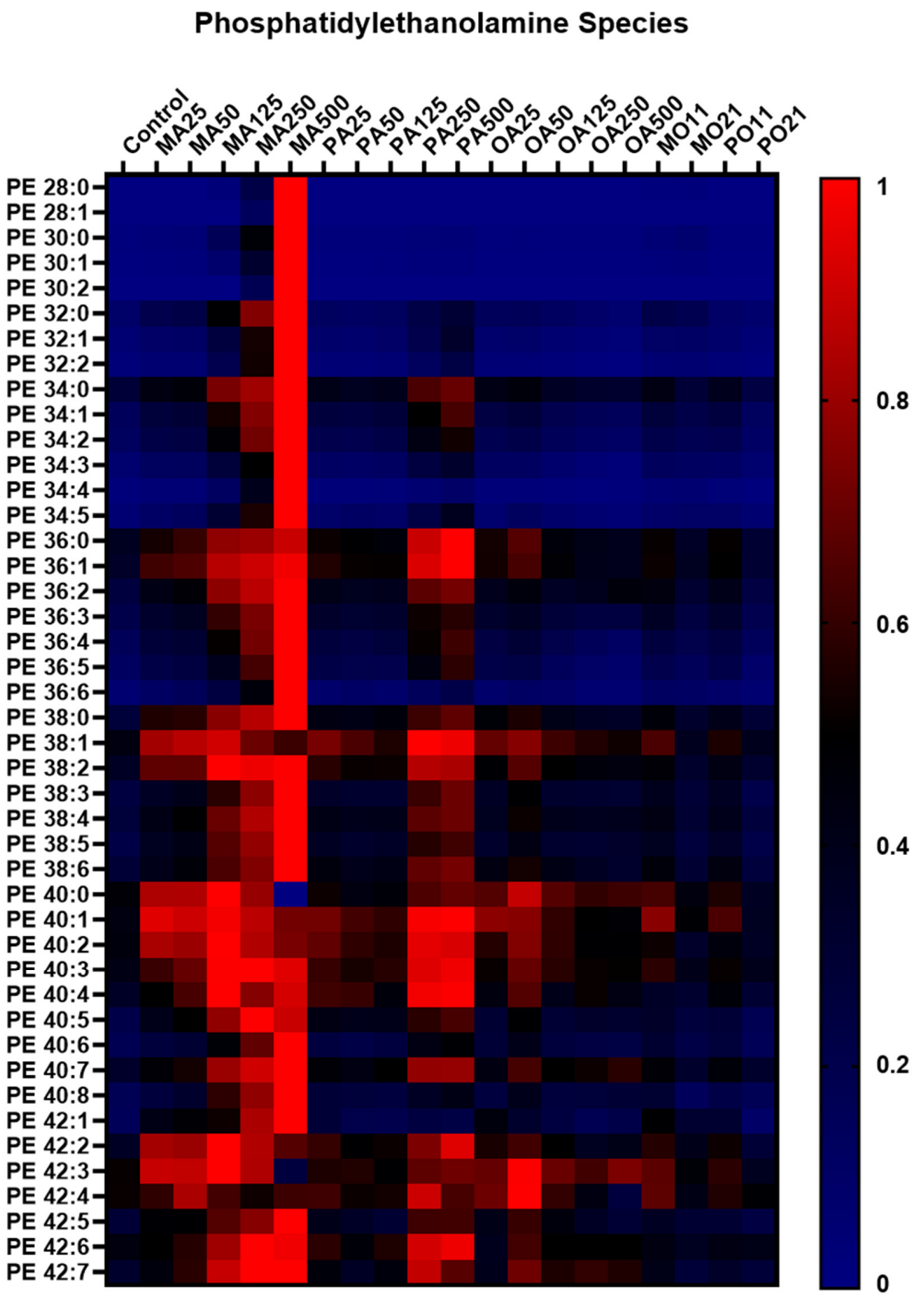

Appendix 17 Heatmap of measured phosphatidylethanolamine species. Chain length indicates the sum of both fatty acyl CoA chain added to a glycerin with a phosphatidylethanolamine head group. Results are normalized on the maximum within each row. In general levels seamed to only be elevated following saturated FA treatment.